A

THEORETICAL AND EXPERIMENTAL HEAT TRANSFER STUDIES OF THE RAT TAIL WITH APPLICATION TO THE HUMAN DIGIT

by

YULONG WU

A dissertation submitted to the Graduate Faculty
in Engineering in partial fulfillment of the
requirements for the degree
of Doctor of Philosophy

The City University of New York

1995

This manuscript has been read and accepted for the Graduate Faculty in Engineering in satisfaction of the dissertation requirement for degree of Doctor of Philosophy.

4/25/95
Date

Professor Sheldon Weinbaum
Chair of Examining Committee

4/25/95
Date

Professor Gerard G. Lowen
Executive Officer

Professor Sheldon Weinbaum

Professor Latif. M. Jiji

Professor Daniel E. Lemons

Professor Lisa X. Xu

Professor Jim W. Baish
Supervisory Committee

The City University of New York

Abstract

THEORETICAL AND EXPERIMENTAL HEAT TRANSFER STUDIES OF THE RAT TAIL WITH APPLICATION TO THE HUMAN DIGIT

by

Yulong Wu

Advisers: Professor Sheldon Weinbaum

Professor Latif M. Jiji

Professor Daniel Lemons

In this dissertation an experimental study is conducted to investigate the thermoregulatory function of the rat tail blood flow and the tail heat transfer. A non-uniform three-dimensional perfusion model of the tail heat transfer is presented to predict the heat transfer and temperature profile of the tail. The tail is the primary heat transfer organ in the rat and under conditions of heat stress can account for up to 40 % of the rat's total energy exchange. The rat tail is believed to be a good model for heat exchange in the human fingers.

A brief introduction to the thermoregulatory and heat transfer mechanisms in the human limb, digit and rat tail is given in chapter 1. In chapter 2 a new approximate analytic solution technique is developed for treating the heat exchange between two or more axially interacting vessels which are arbitrarily positioned in the cross-section of a tissue cylinder. The cylinder exchanges heat by convection with the environment and has a non-uniform

surface temperature due to the vessel eccentricity. The solution to this fundamental configuration can be used as a building block for modeling heat transfer in the rat tail, human digit and limb.

In chapter 3 the tail vascular anatomy is first examined experimentally and the crucial vascular elements in the tail blood flow regulation and heat transfer are identified. This anatomical study is then used to construct a simplified model of the rat tail heat transfer. The rat tail blood flow regulation and heat transfer in response to variant local and central temperatures are then investigated experimentally. The blood flow at the tail base and middle are measured by strain gauge plethysmography. The blood flow at the tail tip is measured by a new computerized balance technique. The tail surface temperature profile and the rat rectal temperature are measured by infra-red thermography and calibrated thermocouples. Experimental results show that the tail volumetric blood perfusion is highly non-uniform along its length. The primary mechanism for rat thermoregulation is the change in tail blood flow. The blood flow increases in an on-off manner in the tail middle and tip regions, and in a proportional manner with the rat core temperature in the base region for rats under body heating.

Based on the experimental studies in chapter 3, a new three-dimensional model is developed in chapter 4 to determine the heat transfer function of the rat tail at different local and central temperatures. This model takes into account the axial variation in tail anatomy and our experimental measurements of the axial blood flow distribution. Good agreement between the model predictions and the experimental measurements is obtained for the axial surface temperature distribution in the tail.

To My Wife

Xuhong

Acknowledgments

The author wishes to express his deepest gratitude and appreciation to Professor Sheldon Weinbaum, Professor Latif M. Jiji and Professor Daniel E. Lemons for their constant support, encouragement and guidance which made it possible for the author to enter the frontier of this promising and challenging field of research.

The author would also like to thank Professor Lisa X. Xu for many helpful discussions and to thank Ms. Ji Song, Mr. Peter Butler and Ms. Liang Zhu for their help and cooperation during the course of experimental study of this research.

The author is grateful to Professor Gerard G. Lowen for handling administrative details in such a warm and friendly manner.

This research was supported by NIH grant HL 26090 and a CUNY Robert Grilleece Fellowship for the author.

Table of Contents

List of Symbols

a	vessel radius (a,v)
a_0, a_n	coefficients for single vessel non-conformal mapping solution, defined by equation (2.13) in chapter 2 and for tail cutaneous layer temperature solution, defined by equation (4.12) in chapter 4
A_{ij}, Ap_{ij}	numerical coefficients for multi-vessel solution in equations (4.19)
A_n,B_n,C_n	numerical coefficients for bicylindrical solution in equations (2.31) and (2.32)
A_{tip}	tail tip surface area in (4.23)
b_0, b_n	coefficients for countercurrent solutions defined by equation (2.45) in chapter 2 and for tail cutaneous layer temperature solution, defined by (4.12) in chapter 4
Bi	Biot number, hR/k_t
c	specific heat
c_0, c_n	coefficients for countercurrent solutions defined by equation (2.45) in chapter 2 and for tail tendon layer solution, defined by equations (4.11) in chapter 4
c_{0l}, c_0*, c_n*	coefficients for tail tendon layer solution, defined by equations (4.21) and (B10)
d_n, d_n*	coefficients for tail tendon layer solution, defined by equations (4.11) and (B11)
e_0, e_n	coefficients for tail bone region solution, defined by equations (4.13)
G_c	cross-sectional area of the tail cutaneous layer in chapter 4

h	heat transfer coefficient
I_n, K_n	modified bessel functions
k	thermal conductivity
$\overline{k}$	ratio of fluid to embedding medium thermal conductivities
k_1	ratio of tendon to cutaneous thermal conductivities.
k_2	ratio of tendon to bone thermal conductivities.
M_i	blood flow rate in vessel *I*
N	number of blood vessels
Nu	Nusselt number of vessel
Pe	Peclet number of vessel, $2\rho_f c_f a_a V_0/k_f$
q	heat flow rate per unit length of the vessel
r	radial coordinate, Fig.2 and Fig.22
R	radius of embedding cylinder in Fig.2 and rat tail in Fig.22
s	distance from origin to vessel axis, Fig.2 and Fig. 22
sp	axis-to-axis distance between vessels, Fig.2 and Fig.22
T	temperature
T_0	artery bulk temperature at z=0
T_∞	ambient temperature
x,y	Cartesian coordinate, Fig.3
V	mean fluid flow velocity
V_0	artery mean fluid flow velocity at z=0
$\overline{V}$	ratio of V to V_0

V_{tip}	tail tip cutaneous volume in (4.23) in chapter 4
W	blood perfusion rate
W_{tip}	blood perfusion rate in tail tip
z	dimensionless axial coordinate
Z	axial coordinate

Greek Symbols

α,β	bicylindrical coordinates, Fig.3
Δ_0	constant defined by equations (B9)
Δ_n	constant defined by equations (B15)
Δ_{1n}	constant defined by equations (B16)
θ	dimensionless temperature
θ_{tm}	dimensionless tissue mean temperature
$\theta_{s,j}$	dimensionless temperature solution of single vessel j (4.14) in chapter 4
λ_i	eigenvalue defined by equation (2.54) in chapter 2
η, ξ	defined by equations (2.55) and (2.56) in chapter 2
ρ	dimensionless radial coordinate
ρ_f	density of fluid in vessels
ρ_b	dimensionless radius of bone
ρ_t	dimensionless radius of tendon for rat tail model
ρ_R	dimensionless radius of embedding cylinder
σ_a	shape factor for single vessel case defined by equation (2.19)

σ_{av}	shape factor between vessels, defined by equation (2.57)
σ_m	shape factor between vessel pair and environment, defined by equation (2.58)
ϕ	polar angle in cylindrical coordinate shown in Fig.2 and Fig.22
$\phi_{v,j}$	polar angle of vessel j in cylindrical coordinate shown in Fig.22
χ_i	constant defined by equations (2.52) and (2.53)
ω_{ij}	component of eigenvector,defined by equations (2.52) and (2.53)

Superscript

-	dimensionless

Subscripts

a	artery in chapter 2 and artery at z=0 in chapter 4
b	bulk in chapter 2 and bone region in chapter 4
f	fluid in vessels
h	homogeneous temperature
ib	bulk (for vessel i, i=1,2,3) in chapter 4
i, j	vessel (i, j=1 artery, i, j=2,3 vein) in chapter 4
m	matrix value for vessels and embedding cylinder in chapter 2
p	particular temperature
t	tissue in chapter 2 and tendon layer in chapter 4
v	vein
w	wall

List of Figures

Chapter 1. Introduction

The hand (or extremity) has been long thought to be an important heat transfer site, and changes in blood flow to the hand are related to the thermal state of the body core and to the skin temperature [1-7]. Our understanding of the heat transfer in the human extremity and human digit requires experimental work in a suitable animal model where the key parameters can be directly measured. Fortunately, the rat tail is such a model, having both a similar function to the human digit, and a comparable vascular architecture and physiology. Both the finger and the rat tail are tapered cylindrical structures with large bony cores and little soft tissue. Both have a high density of arteriovenous anastomoses, AVA's, at their tips [8,9] and blood flows which are often far in excess of the nutritional requirements of the tissue. These similarities make the rat tail a good model for studying the vasomotor effector responses to heat or cold stress, and the relationship of blood flow to heat transfer for the human digit.

The rat tail itself has proved a useful model for studying the vasomotor effector responses to heat or cold stress, and the relationship of tail blood flow, TBF, to tail heat transfer, THT. The tail can either conserve or reject up to 40% of the rat's heat production through the regulation of the tail blood flow. Some of the concepts of the rat tail thermoregulation and the approach of the tail heat transfer modeling are related to the studies in the heat transfer of the human limb and human digit. Bazett and co-workers[10-12] experimentally investigated the axial temperature variation in the human limb. Temperature profiles were measured in the major arteries and veins along the limb under

various ambient temperature conditions. They advanced the concept of shunting venous blood as a key effector serving temperature regulation. They classified veins as superficial (near the skin) and deep. The deep veins are accompanied by the major arteries in a countercurrent flow arrangement, whereas the superficial veins are not accompanied by arteries since there are no superficial arteries in the human limb. Bazett et al. suggested that at high ambient temperatures blood returns via the superficial veins, presumably to increase heat loss to the environment. At low ambient temperatures, the blood returns via the deep veins. The cool deep venous blood exchanges heat with the warm arterial blood which flows in the opposite direction. In this manner, the rewarmed venous blood returns to the body core at a higher temperature than it would have without the heat transfer between the artery and vein. As a result the heat loss from the limb to the environment is decreased. A similar shunting of venous blood was also proposed to take place in the human extremity and rat tail, by Raman and co-workers [13,14] in their mathematical models for the human extremity and the rat tail. They introduced three conduction shape factors and a blood flow distribution parameter that divided the venous return circulation between a deep vessel and a superficial vessel. These four parametric constants were determined by curve fitting their experimental data [15, 16]. Thus their model did not provide theoretical predictions of the heat transfer and temperature distribution in the rat tail and the human extremity based on fundamental principles.

The validation of the hypothesis that the shunting of the venous blood is a major mechanism in the limb thermoregulation is based on the assumption that there is a significant countercurrent heat exchange between the deep veins and arteries which

decreases the heat loss from the limb to the environment. To investigate the importance of the countercurrent heat exchange mechanism Scholander and Krog [17] developed a theoretical heat transfer model. They assumed that the axial temperature profiles in both the paired artery and vein were linear, with a constant temperature difference between the artery and the vein along their axes. This is the "perfect" countercurrent heat exchange assumption, whereby all heat that leaves the arterial blood enters the cool venous blood with no heat exchange with the surrounding. Two thin-walled copper tubes were used to simulate an artery-vein pair and verify their heat transfer model. Scholander and Krog show that for the special case when many arteries and veins are in close contact, such as the rete in the sloth limb, the countercurrent mechanism is significant. However, in the human limb, digit and rat tail, the major axial arteries and veins are not always in close proximity and the model developed by Scholander and Krog [17] may not be applicable.

The perfect countercurrent exchange assumption used in [17] is criticized by Mitchell and Myers[18] since it is not the general case for all artery-vein pairs and represents an idealization of their heat exchange. Also the use of copper tubes by Scholander and Krog added a significant axial heat transfer along the length of the tube wall that is not present in human and animal applications. The importance of the countercurrent heat exchange was further examined by Mitchell and Myers [18] in a more general manner than that presented by Scholander and Krog [17]. Mitchell and Myers developed a limb heat transfer model that treated the central artery and vein as a one-dimensional countercurrent heat exchanger with constant radius. The thermal conductances between the artery and vein, the vessels and the environment were assumed to be equal along the limb. The

perfusion or bleed-off was neglected and the heat loss from the extremity was not considered. Therefore the arterial and venous temperatures were assumed to be equal at the end of the limb. Mitchell and Myers found that the countercurrent heat exchange would only reduce the heat loss by 5% and that the countercurrent effect will be effective only when the blood flow rate is very small. This result suggests that changing the venous blood return path from superficial to deep veins is not a key effector in reducing the heat loss from the human limb. Such behavior would be in contradiction with the thermoregulation pattern in the human limb and extremity proposed by Bazzet et al. [10-12] and Roman et al. [13-16]. It is still not clear whether the shunting of venous blood is a major mechanism in the thermoregulation of the human limb and human digit. The basic difficulty in resolving this problem is that the previous models [18-21] have been too simple. They have either been based on a simple one-dimensional representation for countercurrent heat exchange [18,19] or on multi-layers using the Pennes bioheat equation [20,21]. The prototype of the former is the paper by Mitchell and Myers [18]. In the multi-layer models [20,21] , the limb was treated as concentric cylindrical layers. Each layer was modeled by a Pennes equation with a different blood perfusion rate. However, to properly model heat transfer in the human limb, digit or rat tail, one must take into consideration countercurrent blood flow through the major axial arteries and veins, blood perfusion in the microvascular network, axial variation in tissue anatomy and thermal interaction with the external environment. Major aspects of this complex, coupled, multi- domain, three dimensional problem were dealt with by Zhu and his co-workers [22,23]. In [22] a three-dimensional approximate analytic solution was

developed for treating unequal countercurrent heat transfer between parallel paired vessels of non-uniform temperature asymmetrically embedded in a constant radius cylinder of uniform thermal conductivity with surface convection. A perturbation solution was constructed for vessels embedded close to the cylinder's center, i.e. small eccentricity. This basic model was used to describe the unequal countercurrent heat exchange between the central artery and vein in the core region of the limb [23]. In the latter model the circular cross-section of the limb was divided into four regions: core, deep muscle layer, peripheral muscle layer and cutaneous layer with appropriate corresponding governing equations. The model allowed for an arbitrary variation of cross-sectional area and distribution of blood flow between the muscle and cutaneous tissue. The major limitation of [22,23] is that the models required small eccentricity of the blood vessels, whereas the major axial arteries and veins can be highly asymmetric in the limb and run close to the surface in the human digit and rat tail. A theory for treating two or more axially interacting vessels embedded arbitrarily in a cylinder with axially varying cross section needed to be developed. Another limitation of [23] is that the model for the limb incorporated empirically derived data on blood flow and heat transfer in the extremity, but did not attempt to model the heat transfer in the human extremity. Since the heat transfer and the blood flow in the human digit are related to the thermal state of the body core and the skin temperature [1-7], this is not an adequate model to describe heat transfer under a wide range of conditions. We thus need to develop a fundamental model of extremity heat transfer which can explain how the hand and digits function as heat exchangers.

The rat tail has frequently been used for the study of blood flow control with regard to central and local thermoregulation and as a model for the human digit because of the morphological similarities between the vascularity of the rat tail and that of the human digit [24,25]. The thermoregulatory function of the tail blood flow has been studied experimentally using blood flow measurements [15,26,27,28] and temperature measurements [29]. Hellström [26] investigated the vasomotor response of the tail of a rat under total-body heating with the tail at 25 °C. He found that the tail blood flow regulation is an effector response increasing gradually with an elevated rat core temperature. Raman et al. [15] have further suggested that (I) the tail blood flow is linearly related to core temperature when the rat is warmed and (ii) the venous blood shunting between the superficial lateral veins and the deep ventral vein plays a major role in the tail heat transfer. In contrast to Hellström and Roman et al., Rand et al. [27] investigated the change of the tail blood flow when rats were exposed to warm air. They found that an on-off system controlled the tail blood flow. Young and Dawson [29] measured the tail temperature difference between the ventral and lateral surface, and the tail heat transfer for a rat at varying temperatures between 25 and 35 °C . They concluded that the major mechanism for heat transfer regulation was heat-induced vasodilation or cold-induced vasoconstriction instead of shunting venous blood. They also suggested that the regulation of the tail blood flow is described by an on-off control, where the onset or offset is the abrupt increase or decrease of the tail cutaneous blood flow. Since the highest density of arteriovenous anastomoses (AVA's) occurs at the tip of the human digit and rat tail [9,10] and consequently a very high blood flow can be maintained there, it is possible that

increasing cutaneous blood flow by vasodilation or decreasing cutaneous blood flow by vasoconstriction may play a more significant role in heat transfer than shunting venous blood.

Despite the qualitatively obvious role of the regulation of TBF for the purpose of either conserving or rejecting up to 40% of the total heat generated by the rat [29], and the well established role of the sympathetic nervous system in its control [28], several fundamental questions remain. (1) What is the major mechanism of the rat tail thermoregulation for a rat at various local and central environment temperatures? Is it the change of the venous return path or the change of the blood flow through the cutaneous microcirculation? (2) Is the control pattern for the cutaneous blood flow response to the change of the rat core body temperature an on-off control or a proportional control? (3) Can we identify an easily measured parameter that describes the rat tail thermoregulation? (4) What is an adequate model to describe and predict the rat tail heat transfer? We shall address all these questions in the present research.

The primary objectives of this research are: (a) Develop an analytical approach which can treat two or more axially interacting countercurrent vessels which are arbitrarily embedded in a tissue cylinder with surface convection. The solution for this fundamental configuration can be used as the building block for modeling heat transfer in the rat tail, human digit and limb. (b) Examine the vascular anatomy of the rat tail experimentally to identify the crucial vascular elements that control blood flow distribution and local heat exchange in the rat tail. Conduct experimental studies on the rat tail to investigate the heat transfer and blood flow regulation corresponding to different thermal states of the rat

core and tail. (c) On the basis of above studies, develop a temperature and heat transfer model for rat tail. This dissertation is divided into three major chapters, one devoted to each of the three related principal objectives mentioned above.

Chapter 2. A New Analytic Technique for 3-D Heat Transfer from a Cylinder with Two or More Axially Interacting Eccentrically Embedded Vessels with Application to Countercurrent Blood Flow

In this chapter an analytical technique will be presented which can treat two or more axially interacting countercurrent vessels embedded arbitrarily in a cylinder with surface convection. In this theory, two solutions for the single vessel case are presented: an approximate non-conformal mapping analytic solution which is exact only when $\overline{k}$, the ratio of blood to tissue conductivities is unity, and a bicylindrical solution based on conformal mapping which is valid for all values of $\overline{k}$. The former will be used in a superposition scheme to construct the solution for two or more vessels while the latter, which precludes superposition, will be used to examine the accuracy of the approximate solution when $\overline{k} \neq 1$. Having demonstrated the accuracy of the approximate solution, we apply the single vessel non-conformal mapping analytic solution to construct by superposition a solution to the multiple embedded vessel problem. This basic technique can be used to modify the existing model [23] of the human limb by relaxing the restriction of small eccentricity of the blood vessels since the major arteries and veins can be highly asymmetric for the human limb. It can be also applied in the modeling of the rat tail and human digit where the major vessels run very close to the surface.

2.1. Introduction

This study was motivated by the need to describe the heat exchange between the

thermally significant countercurrent arteries and veins which occur throughout the macro and microvasculature of humans and animals. This three-way energy exchange occurs, for example, in the major axial arteries and veins that supply and drain the human limbs, fingers, and the rat's tail. A basic heat transfer model for such systems is a countercurrent artery-vein pair which is eccentrically embedded in a cylinder with surface convection to the environment (Fig.1). The eccentricity is arbitrary since the artery-vein pair may be close to the center of the tissue cylinder or the surface.

Although the motivation and focus in this study is the modeling of the biological systems described above, the analysis is equally applicable to heat transfer in engineering systems such as buried pipes and solar collectors.

Previous studies [22, 30-35] have analyzed heat transfer problems for one or two vessels embedded in infinite, semi-infinite or finite cylindrical media. Various boundary conditions on the vessels and cylinder surfaces were examined. Chato [30] considered two unequal vessels at uniform surface temperatures embedded in an infinite medium. Wissler [31] treated the same configuration with continuity of heat flux and non-uniform vessel wall temperature and was able to obtain an exact solution for the case of a linear thermal gradient with equal vessel and medium conductivities.

The problem of a single vessel in a semi-infinite medium was examined by Chato [30] and Bau and Sadhal [32]. The free surface exchanges heat by convection with the environment in [30] and is isothermal in [32].

Defelice and Bau [33] analyzed a single vessel which is eccentrically embedded in a cylinder using a conformal mapping method. The boundary conditions on the vessel and

cylinder surfaces were of the third kind, i.e., convective.

Recent interest in modeling countercurrent vessels in perfused tissue and limbs has motivated studies on two vessels embedded in a cylinder. Baish [34] considered two equal vessels symmetrically placed in a cylinder. Vessel boundary conditions were of the third kind, while the cylinder surface was at a uniform temperature. A similar problem was solved by Zhu et al. [35] using unequal vessels at uniform but unequal surface temperatures.

Since the major axial countercurrent artery-vein pairs in human limbs are eccentrically located, Zhu et al [22] investigated the effect of eccentricity of two unequal vessels which are asymmetrically embedded near the center of a cylinder. They imposed a convective condition on the cylinder surface and satisfied continuity of temperature and heat flux at the vessels' surfaces. A perturbation solution was obtained which is limited to small eccentricity of the artery-vein pair. This is a serious limitation in the biological applications mentioned earlier since the eccentricity can be significant with the major axial countercurrent artery-vein pairs running much closer to the surface than the center of the limb, finger or tail.

This paper removes this limitation by constructing a new approximate solution for a single vessel with arbitrary eccentricity. This solution is then applied to two unequal countercurrent vessels arbitrarily embedded in a cylinder which is subjected to the general boundary conditions treated in Zhu et al [22]. The solution is approximate because it exactly satisfies the continuity of heat flux condition at the vessel surface only when the ratio of fluid to the embedding material conductivity, $\overline{k}$, is unity.

A solution to the multiple embedded vessel problem may be obtained by the superposition of the single vessel solutions provided the basic solutions for each vessel

satisfy the continuity of temperature and flux at the surfaces of the other vessels and their superposition satisfies the surface boundary condition on the embedding cylinder. Although conformal mapping can be used to treat the single vessel case, as in [33], the form of the solution precludes superposition. The difficulty is traced to the nature of the boundary conditions considered, since solutions to two or more individual vessels in a cylinder cannot be transformed to common bicylindrical coordinates. An alternate approach is developed here in which a new non-conformal mapping solution for an individual vessel is constructed in which superposition methods can be applied.

The effect of not exactly satisfying the continuity of heat flux condition at the vessel's surface when $\overline{k} \neq 1$ is investigated by first obtaining a new exact solution for a single vessel in a cylinder with surface convection, which is valid for any value of $\overline{k}$, and comparing the predictions of this new exact solution with the approximate solution. The results show that the discrepancy is remarkably small over a wide range of the three governing parameters: the cylinder Biot number, the eccentricity and the cylinder-vessel diameter ratio.

2.2. Formulation

Consider two or more flow vessels embedded in a cylinder with surface convection. The geometry of the cross-sectional plane and the coordinate system used in the analysis are illustrated in Fig.2 in which two countercurrent vessels are shown. We assume that the flow in the vessels is laminar with a parabolic velocity profile with mean velocities V_a and V_v. The Peclet number is assumed to be very large and the cylinder is long. Thus axial conduction and end effects can be neglected.

The non-dimensional parameters and variables which are appropriate for both the single embedded vessel case and the countercurrent flow case illustrated in Fig.2 are defined as follows:

$$\bar{a}_v=\frac{a_v}{a_a} \qquad \bar{sp}=\frac{sp}{a_a} \qquad \bar{s}_a=\frac{s_a}{a_a} \qquad \bar{s}_v=\frac{s_v}{a_a}$$

$$\rho=\frac{r}{a_a} \qquad \rho_R=\frac{R}{a_a} \qquad \rho_a=\frac{r_a}{a_a} \qquad \rho_v=\frac{r_v}{a_v} \qquad B_i=\frac{hR}{k_t}$$

$$p_e=\frac{2\rho_f c_f a_a V_a}{k_f} \qquad \bar{k}=\frac{k_f}{k_t} \qquad \bar{V}=\frac{V_v}{V_a} \qquad z=\frac{Z}{a_a p_e} \qquad \theta=\frac{T-T_\infty}{T_0-T_\infty}$$

The subscripts a and v have been used here to denote an artery-vein pair that will be used as a simple model for the arm later in the paper. The technique, however, can be applied to any number of parallel vessels with flow in either direction. Based on the above assumptions and definitions the dimensionless energy equations for the artery and vein are:

$$\frac{1}{\rho}\frac{\partial}{\partial\rho}\left(\rho\frac{\partial\theta_a}{\partial\rho}\right)+\frac{1}{\rho^2}\frac{\partial^2\theta_a}{\partial\phi^2}=(1-\rho_a^2)\frac{\partial\theta_a}{\partial z} \qquad for \quad \rho_a<1 \tag{2.1}$$

$$\frac{1}{\rho}\frac{\partial}{\partial\rho}\left(\rho\frac{\partial\theta_v}{\partial\rho}\right)+\frac{1}{\rho^2}\frac{\partial^2\theta_v}{\partial\phi^2}=-\bar{V}(1-\rho_v^2)\frac{\partial\theta_v}{\partial z} \qquad for \quad \rho_v<1 \tag{2.2}$$

The minus sign in (2.2) is used to describe countercurrent flow for the biological application. The heat conduction equation in the surrounding tissue cylinder is

$$\frac{1}{\rho}\frac{\partial}{\partial\rho}\left(\rho\frac{\partial\theta_t}{\partial\rho}\right)+\frac{1}{\rho^2}\frac{\partial^2\theta_t}{\partial\phi^2}=0 \qquad for \quad \rho_a\geq 1, \quad \rho_v\geq 1 \tag{2.3}$$

The corresponding boundary conditions are

$$\theta_{a,v}=\theta_t \qquad for \quad \rho_{a,v}=1 \tag{2.4}$$

$$-k\frac{\partial\theta_{a,v}}{\partial\rho_{a,v}}=\frac{\partial\theta_t}{\partial\rho_{a,v}} \qquad for \quad \rho_{a,v}=1 \tag{2.5}$$

$$\frac{\partial\theta_t}{\partial\rho}=-\frac{Bi}{\rho_R}\theta_t \qquad for \quad \rho=\rho_R \tag{2.6}$$

In order to separate the variables in equations (2.1) and (2.2), we assume that the convection terms $\partial\theta_{a,v}/\partial z$ can be approximated by the axial gradient of the bulk temperatures in the vessels, $d\theta_{ab,vb}/dz$. Conservation of the axial energy flux in the vessels leads to the following expression for the vessel

$$\theta_{ab,vb}=\frac{2}{\pi}\int_0^{2\pi}\int_0^1 \theta_{a,v}(1-\rho_{a,v}^2)\rho_{a,v}d\rho_{a,v}d\phi_{a,v} \tag{2.7}$$

Introducing this approximation into equations (2.1)-(2.3), we obtain

$$\nabla^2\theta_a=(1-\rho_a^2)\frac{d\theta_{ab}}{dz} \qquad for \quad \rho_a<1 \tag{2.8}$$

$$\nabla^2 \theta_v = -\bar{V}(1-\rho_v^2)\frac{d\theta_{vb}}{dz} \qquad for \quad \rho_v<1 \qquad (2.9)$$

$$\nabla^2 \theta_t = 0 \qquad for \rho_a \geq 1, \quad \rho_v \geq 1 \qquad (2.10)$$

where the Laplacian operator is used to describe the conduction terms.

2.3. Single Vessel Solution

In this section, two solutions for the single vessel case are presented: a non-conformal mapping analytic solution which is exact only when $\bar{k}=1$ and a bicylindrical solution based on conformal mapping which is valid for all values of $\bar{k}$. The former will be used in a superposition scheme to construct the solution for two or more vessels while the latter will be used to examine the accuracy of the approximate solution when $\bar{k} \neq 1$. The geometry of the cross-sectional plane and the bicylindrical coordinates for the single vessel analysis are illustrated in Fig.3.

2.3.1. Non-conformal Mapping Solution

The governing equations for the vessel and embedded material (tissue) are given in (2.8) and (2.10) respectively. The corresponding boundary conditions are equations (2.4)-(2.6). The temperature solution can be decomposed into two parts $\theta = \theta_h + \theta_p$, where θ_h is the homogeneous solution and θ_p is the particular solution. The particular solutions for the vessel and tissue are:

$$\theta_{pa}=(\frac{1}{4}\rho_a^2-\frac{1}{16}\rho_a^4-\frac{3}{16})\frac{d\theta_{ab}}{dz} \qquad \rho_a<1 \qquad (2.11)$$

$$\theta_{pt}=\frac{1}{4}\bar{k}(\ln\rho_a)\frac{d\theta_{ab}}{dz} \qquad \rho_a\geq 1 \qquad (2.12)$$

and the homogeneous solution for the tissue, θ_h, takes the form

$$\theta_{ht}=(a_0+\sum_{n=1}^{\infty} a_n\rho^n\cos n\phi)\frac{d\theta_{ab}}{dz} \qquad (2.13)$$

Before adding the particular solution for the tissue (2.12) to the homogeneous solution (2.13), they must first be expressed in terms of common coordinates. Transforming the coordinates ρ_a, ϕ_a in the particular solution to ρ, ϕ and combining the resulting equation with the tissue homogeneous solution (2.13), we obtain

$$\theta_t=(a_0+\sum_{n=1}^{\infty} a_n\rho^n cosn\phi)\frac{d\theta_{ab}}{dz}+ \frac{1}{8}\bar{k}\ln(\rho^2+\bar{s}_a^{-2}-2\rho\bar{s}_a^{-2}\cos\phi)\frac{d\theta_{ab}}{dz} \qquad (2.14)$$

The coefficients a_0 and a_n in (2.14) are determined from boundary condition (2.6); however their evaluation is not straightforward. (2.14) is substituted in (2.6) and integral expressions for the a_n are then obtained from orthogonality. These integrals can be converted into contour integrals in the complex plane and then evaluated using residue theory. This elegant analysis,

which is described in the Appendix A, leads to the expressions,

$$a_0 = -\frac{\bar{k}}{4}\left(\frac{1}{Bi} + \ln\rho_R\right) \tag{2.15}$$

$$a_n = \frac{\bar{k}}{4(n+Bi)\rho_R^n}\left(\frac{Bi}{n} - 1\right)\left(\frac{\bar{s}_a}{\rho_R}\right)^n \tag{2.16}$$

A homogeneous solution to the vessel equation (2.8) is also required to satisfy boundary condition (2.5). A series solution of the form (2.13) cannot be used for $\bar{k} \neq 1$ since there is a singularity in the vessel region $\rho \leq 1$. Although an alternate infinite series solution can be constructed, the determination of the coefficients in this infinite series would require a cumbersome numerical evaluation. However, one notes that if $\bar{k} = 1$ the solution (2.13) will satisfy this boundary conditions (2.4) and (2.5) and the vessel equation (2.8) exactly. When $\bar{k} \neq 1$, the homogeneous solution (2.13) satisfies boundary condition (2.4), but not (2.5) and the solution (2.14) is only approximate, but, nevertheless, as we shall show shortly, highly accurate for most conditions of interest. This approximate analytic solution to the single vessel-tissue problem given by (2.14), (2.15) and (2.16) can be superposed to construct the solution to two or more vessels embedded at any location in a cylinder. The error due to this approximation for $\bar{k} \neq 1$ is examined in detail in section 2.5. Our approximate solution to the vessel temperature is thus obtained by adding (2.11) and (2.13)

$$\theta_a = \left(a_0 + \sum_{n=1}^{\infty} a_n \rho^n \cos n\phi\right)\frac{d\theta_{ab}}{dz} + \left(\frac{1}{4}\rho_a^2 - \frac{1}{16}\rho_a^4 - \frac{3}{16}\right)\frac{d\theta_{ab}}{dz} \tag{2.17}$$

Equations (2.14) and (2.17) reduce to the exact solutions for the limiting case s_a=0.

To complete the analysis, the bulk temperature θ_{ab} , shape factor σ_a and Nusselt number Nu_a are needed. Substituting (2.17) into (2.7) and evaluating the double integrals, we obtain an expression relating θ_{ab} and its gradient.

$$\theta_{ab}=(-\frac{11}{96}+a_0+\sum_{n=1}^{\infty} a_n \bar{s}_a^n)\frac{d\theta_{ab}}{dz} \tag{2.18}$$

The shape factor, σ_a , for heat transfer between the vessel and tissue cylinder is defined as:

$$\sigma_a=\frac{q_a}{2\pi k_t(T_{ab}-T_\infty)}=-\frac{\bar{k}}{4}\frac{\frac{d\theta_{ab}}{dz}}{\theta_{ab}} \tag{2.19}$$

where the q_a is the heat transfer per unit length of vessel which is equal to $-\rho_f c_f \pi a_a^2 \bar{V}_a (dT_{ab}/dZ)$. Equations (2.18) and (2.19) yield

$$\sigma_a=(\frac{11}{24}-4\sum_{n=0}^{\infty} a_n \bar{s}_a^n)^{-1} \tag{2.20}$$

The Nusselt number for the vessel is defined as

$$Nu_a=\frac{q_a}{\pi k_f(T_{ab}-T_{aw})}=-\frac{1}{2}\frac{\frac{d\theta_{ab}}{dz}}{\theta_{ab}-\theta_{aw}} \tag{2.21}$$

where θ_{aw} is the dimensionless mean wall temperature of the vessel which is defined as

$$\theta_{aw}=\frac{1}{2\pi}\int_0^{2\pi}\theta_a(1,\phi_a)d\phi_a \qquad at\ \rho_a=1 \tag{2.22}$$

Substituting (17) into (22) and introducing the resulting expression for θ_{aw} into (21) we obtain

$$Nu_a=48/11 \tag{2.23}$$

This result for the vessel Nusselt number is identical to that for a fully developed temperature distribution in a tube with constant surface heat flux. Examination of the vessel solution shows that the homogeneous part plays no role in the determination of Nusselt number.

2.3.2. Conformal Bicircular Mapping Solution for a Single Vessel for $\overline{k}\neq 1$

The single vessel solution presented above does not satisfy boundary condition (2.5) exactly when $\overline{k}\neq 1$. To examine the accuracy of this approximate solution an exact solution, valid for all values of $\overline{k}$, is developed in this section.

We introduce the bicylindrical transformation

$$x-iy=-\sinh\alpha_1\ \tanh\left(\frac{\alpha+i\beta}{2}\right) \qquad 0<\alpha<\infty,\ -\pi<\beta<\pi \tag{2.24}$$

where the coordinates α,β are shown in Fig.3. Constant α-coordinates are circles described by

$$(x+\sinh\alpha_1\coth\alpha)^2+y^2=\frac{\sinh^2\alpha_1}{\sinh^2\alpha} \tag{2.25}$$

$$\frac{a_a}{R}=\frac{\sinh\alpha_2}{\sinh\alpha_1} \tag{2.26}$$

with α_1 representing the vessel and α_2 the cylinder. Geometric relationships require that

and

$$\bar{s}_a=\sinh\alpha_1(\coth\alpha_2-\coth\alpha_1) \tag{2.27}$$

The governing equations for the vessel and tissue in the new coordinates are the same as (2.8) and (2.10) with the Laplacian terms expressed in terms of α and β.

The boundary conditions transform to

$$(\cosh\alpha_2+\cos\beta)\frac{\partial\theta_t}{\partial\alpha}=\sinh\alpha_2 Bi\theta_t \qquad for \quad \alpha=\alpha_2 \tag{2.28}$$

$$\theta_a(\alpha,\beta)=\theta_t(\alpha,\beta) \qquad for \quad \alpha=\alpha_1 \tag{2.29}$$

and

$$-k\frac{\partial\theta_a}{\partial\alpha}=\frac{\partial\theta_t}{\partial\alpha} \qquad for \quad \alpha=\alpha_1 \tag{2.30}$$

The solution to the vessel equation (2.8) is

$$\theta_a=(c_0+\sum_{n=1}^{\infty} c_n e^{-n\alpha}\cos n\beta)\frac{d\theta_{ab}}{dz}+(\frac{1}{4}\rho_a^2-\frac{1}{16}\rho_a^4-\frac{3}{16})\frac{d\theta_{ab}}{dz} \tag{2.31}$$

and the solution to the tissue equation (2.10) is

$$\theta_t=[\sum_{n=0}^{\infty}(A_n\sinh n\alpha+B_n\cosh n\alpha)\cos n\beta+A_0\alpha]\frac{d\theta_{ab}}{dz} \tag{2.32}$$

The coefficients A_n, B_n, C_n, are evaluated using boundary conditions (2.28)- (2.30). Boundary condition (2.28) yields a set of linear algebraic equations:

$$A_0(\cosh\alpha_2-\alpha_2 Bi\sinh\alpha_2)+\frac{1}{2}(A_1\cosh\alpha_2+B_1\sinh\alpha_2)-B_0 Bi\sinh\alpha_2=0 \tag{2.33}$$

$$\begin{aligned}&A_0+A_1(conh^2\alpha_2-Bi\sinh^2\alpha_2)+A_2 cosh2\alpha_2\\&+B_1(\cosh\alpha_2\sinh\alpha_2-Bi\sinh\alpha_2\cosh\alpha_2)+B_2 sinh2\alpha_2=0\end{aligned} \tag{2.34}$$

and

$$\begin{aligned}&A_{n-1}(\cosh\alpha_2-\tanh n\alpha_2\sinh\alpha_2)\frac{n-1}{2}+A_n(n\cosh\alpha_2-Bi\sinh\alpha_2\tanh n\alpha_2)\\&+A_{n+1}(\cosh\alpha_2+\tanh n\alpha_2\sinh\alpha_2)\frac{n+1}{2}+B_{n-1}(\tanh n\alpha_2\cosh\alpha_2-\sinh\alpha_2)\frac{n-1}{2}\\&+B_n(n\cosh\alpha_2\tanh n\alpha_2-Bi\sinh\alpha_2)+B_{n+1}(\tanh n\alpha_2\cosh\alpha_2+\sinh\alpha_2)\frac{n+1}{2}=0\\&\qquad for\quad n\geq 2\end{aligned} \tag{2.35}$$

Boundary condition equation (29) requires that

$$c_0 = A_0\alpha_1 + B_0 \tag{2.36}$$

and

$$c_n = e^{n\alpha_1}(A_n \sinh n\alpha_1 + B_n \cosh n\alpha_1) \qquad for\ n \geq 1 \tag{2.37}$$

Applying boundary condition equation (2.30), using orthogonality and evaluating the resulting integrals using residue theory, we obtain.

$$A_0 = -\frac{1}{4}\bar{k} \tag{2.38}$$

and

$$c_n = \frac{1}{2n}(-1)^{n+1} - \frac{1}{\bar{k}}e^{n\alpha_1}(A_n coshn\alpha_1 + B_n sinhn\alpha_1)\ for\ n \geq 1 \tag{2.39}$$

Equations (2.33)-(2.39) contain 3N+3 unknowns, whereas the number of equations is 3N+2. This set of equations is, therefore, not closed. Fortunately, $C_n\exp(-n\alpha_1)$ decreases as n is increased and thus it can be truncated at N terms. If we require that $C_{N+1}\exp(-(N+1)\alpha_1)=0$, then the above equations can be truncated and solved in closed form. Computations for $C_{N+1}\exp(-(N+1)\alpha_1)$ show that it decreases very rapidly. The criterion used to choose N in the sequence is

$$\left|\frac{A_j^{N+4}-A_j^N}{A_j^{N+4}}\right|+\left|\frac{B_j^{N+4}-B_j^N}{B_j^{N+4}}\right|+\left|\frac{C_j^{N+4}-C_j^N}{C_j^{N+4}}\right| \le 10^{-5} \qquad for \quad 0 \le j \le 10 \quad (2.40)$$

Using (2.19) as the definition for the shape factor, one obtains from (2.31)

$$\sigma_a = \left(\frac{11}{24} - 4\sum_{n=0}^{\infty}(-1)^n C_n e^{-2n\alpha_1}\right)^{-1} \qquad (2.41)$$

Result (2.41) is derived from a contour integration in the complex plane and residue theory. The Nusselt number for the vessel is again a constant equal to 48/11. This is the same as the value obtained from the approximate solution. This is not surprising since the homogeneous solution does not contribute to the Nusselt number.

2.4. Two-Vessel Solution: Countercurrent Heat Exchange

As an example of the superposition solution for multiple vessels, consider the problem of two embedded vessels with counterflow heat exchange. The solution to this problem is obtained by superposition of two single vessel solutions presented in section 2.3.1. The governing equations and boundary conditions are given by equations (2.4)-(2.6) and (2.8)-(2.10). The temperature solution is decomposed into two parts $\theta=\theta_h+\theta_p$ where θ_h and θ_p are the homogeneous and particular solution, respectively. The particular solutions for the artery, vein and tissue are:

$$\theta_{pa} = \left(\frac{1}{4}\rho_a^2 - \frac{1}{16}\rho_a^4 - \frac{3}{16}\right)\frac{d\theta_{ab}}{dz} - \bar{V}\,\bar{a}_v^2\left(\frac{1}{4}\bar{k}\ln\rho_v\right)\frac{d\theta_{vb}}{dz} \qquad (2.42)$$

$$\theta_{pv}=(\frac{1}{4}\bar{k}\ \ln\rho_a)\frac{d\theta_{ab}}{dz}-\bar{V}\ \bar{a}^{\,2}_{v}(\frac{1}{4}\rho_v^2-\frac{1}{16}\rho_v^4-\frac{3}{16})\frac{d\theta_{vb}}{dz} \tag{2.43}$$

$$\theta_{pt}=(\frac{1}{4}\bar{k}\ \ln\rho_a)\frac{d\theta_{ab}}{dz}-\bar{V}\ \bar{a}^{\,2}_{v}(\frac{1}{4}\bar{k}\ \ln\rho_v)\frac{d\theta_{vb}}{dz} \tag{2.44}$$

The homogeneous solution in the three regions that replaces (2.13), (2.15) and (2.16) is

$$\theta_h=(b_0+\sum_{n=1}^{\infty}b_n\rho^n cosn(\phi-\phi_{av}))\frac{d\theta_{ab}}{dz}+(c_0+\sum_{n=1}^{\infty}c_n\rho^n cosn\phi)\bar{V}\bar{a}^{\,2}_{v}\frac{d\theta_{vb}}{dz} \tag{2.45}$$

where

$$b_0=-\frac{\bar{k}}{4}(\frac{1}{Bi}+\ln\rho_R)\ , \tag{2.46}$$

$$b_n=\frac{\bar{k}}{4(n+Bi)\rho_R^N}(\frac{Bi}{n}-1)(\frac{\bar{s}_a}{\rho_R})^{n}\ , \tag{2.47}$$

$$c_0=\frac{\bar{k}}{4}(\frac{1}{Bi}+\ln\frac{\rho_R}{\bar{a}_v})\ , \tag{2.48}$$

and

$$c_n = -\frac{\bar{k}}{4(n+Bi)\rho_R^N}\left(\frac{Bi}{n}-1\right)\left(\frac{\bar{s}_v}{\rho_R}\right)^n \tag{2.49}$$

The temperature solutions in the artery and vein are used to determine the relationships for the bulk temperatures as defined by equation (2.7). The evaluation procedure of these double integrals is the same as that used in the single vessel case. Thus, the bulk temperature relationships for the interacting vessels that replaces (2.18) for a single vessel are,

$$\theta_{ab} = \left(\sum_{n=0}^{\infty} b_n \bar{s}_a^n - \frac{11}{96}\right)\frac{d\theta_{ab}}{dz} + \left(\sum_{n=0}^{\infty} c_n \bar{s}_a^n - \frac{\bar{k}\ \ln\left(\frac{\bar{sp}}{\bar{a}_v}\right)}{4}\right)\bar{V}\ \bar{a}_v^2 \frac{d\theta_{vb}}{dz} \tag{2.50}$$

$$\theta_{vb} = \left(\sum_{n=0}^{\infty} b_n \bar{s}_v^n + \frac{\bar{k}\ \ln\bar{sp}}{4}\right)\frac{d\theta_{ab}}{dz} + \left(\sum_{n=0}^{\infty} c_n \bar{s}_v^n + \frac{11}{96}\right)\bar{V}\ \bar{a}_v^2 \frac{d\theta_{vb}}{dz} \tag{2.51}$$

The coupled equations (2.50) (2.51) can be solved analytically if $\bar{a}_v$, $\bar{V}$, $\bar{s}_a$, $\bar{s}_v$ and $\bar{sp}$ are constant:

$$\theta_{ab} = \chi_1 \omega_{11} \exp(\lambda_1 z) + \chi_2 \omega_{12} \exp(\lambda_2 z) \tag{2.52}$$

$$\theta_{vb} = \chi_1 \omega_{21} \exp(\lambda_1 z) + \chi_2 \omega_{22} \exp(\lambda_2 z) \tag{2.53}$$

where eigenvalues $\lambda_{1,2}$ are given by

$$\lambda_{1,2}=\frac{-\eta\pm\sqrt{\eta^2-\xi}}{\xi} \tag{2.54}$$

where

$$\xi=\bar{V}\,\bar{a}_v^2\Big(\sum_{n=0}^{\infty} b_n \bar{s}_a^n-\frac{11}{96}\Big)\Big(\sum_{n=0}^{\infty} c_n \bar{s}_v^n+\frac{11}{96}\Big)- \bar{V}\,\bar{a}_v^2\Big(\sum_{n=0}^{\infty} b_n \bar{s}_v^n+\frac{\bar{k}\ln\bar{sp}}{4}\Big)\Big(\sum_{n=0}^{\infty} c_n \bar{s}_a^n-\frac{\bar{k}\ln(\frac{\bar{sp}}{\bar{a}_v})}{4}\Big) \tag{2.55}$$

and

$$\eta=-\frac{1}{2}\Big(\Big(\sum_{n=0}^{\infty} b_n \bar{s}_a^n-\frac{11}{96}\Big)+\bar{V}\bar{a}_v^2\Big(\sum_{n=0}^{\infty} c_n \bar{s}_v^n+\frac{11}{96}\Big)\Big) \tag{2.56}$$

ω_{ij} are the eigenvector coefficients in equations (2.50) and (2.51) and the χ and $_2\chi$ are integral constants which are determined by the bulk temperature at a reference position. For three or more vessels, relationships for θ_{ib}, i=1,2,3 ... N, analogous to (2.50) and (2.51) would be obtained.

2.5. Results And Discussion

2.5.1. Accuracy of the Approximate Solution: Single Embedded Vessel

Since boundary condition (2.5) is satisfied exactly only when the thermal conductivity ratio $\bar{k}$ is equal to unity, the solutions (2.14) and (2.17) are approximate for

all other values of $\overline{k}$. In this section we evaluate the error associated with this approximation by considering the single embedded vessel case for which an exact solution has been obtained in section 2.3.2 using conformal mapping. In particular, the shape factor σ_a is examined by evaluating the ratio of our approximate solution for σ_a, equation (2.20), with our exact solution for σ_a, equation (2.41). Comparisons are made for a wide range of the four governing parameters: the conductivity ratio $\overline{k}$, Biot number Bi, eccentricity $\overline{s}_a$ and the cylinder-vessel radius ratio ρ_R. The effect of conductivity ratio and Biot number on the accuracy of the shape factor for a configuration with large eccentricity defined by ρ_R=5 and $\overline{s}_a$ =3.5 is shown in Fig.4. Three Biot numbers are considered: Bi=0.1, 1.0, and 10. Values of Bi typical of the human upper limbs are 1.5 in air and 10 in water. The conductivity ratio is varied from 0 to 10. Since the approximate solution is exact for $\overline{k}$ =1, all curves intersect at a point corresponding to a shape factor ratio, $(\sigma_a)_{approximate}/(\sigma_a)_{exact}$, of unity. For Biot numbers of 0.1 and 1.0 the error in the shape factor is insignificant and at Bi=10 and $\overline{k}$ =10 the error is less than 3%. For blood vessels in tissue $1 \leq \overline{k} < 2$ and in engineering applications ranges from $6*10^{-5}$ (air-copper) to 12 (water-85% magnesia insulation). Fig.4 also shows that for $\overline{k} \leq 1$ the error in shape factor is less than 1%. This latter range of $\overline{k}$ includes fluids such as air, water and oil flowing through cylinders of materials such as glass, wood, metal, etc., which are common engineering applications.

The effect of eccentricity and Biot number on the accuracy of shape factor for $\overline{k}$ =10 and ρ_R=5 is shown in Fig.5. For the limiting case of concentric cylinders, i.e. $\overline{s}_a$ =0, the exact result for the shape factor ratio of unity is obtained for all Biot numbers regardless of the value of $\overline{k}$ since equations (2.14) and (2.17) reduce to the exact solutions. As the

eccentricity is increased the error increases monotonically reaching 7% at $\overline{s}_a$ =3.99 for Bi=10 but remaining small (less than 1%) for Bi=0.1 and 1.0. It should be noted that the maximum eccentricity for ρ_R=5 is 4.0, which corresponds to a vessel which is tangent to a cylinder. The effect of the cylinder-vessel diameter ratio ρ_R on the shape factor ratio for $\overline{k}$ =10 and $\overline{s}_a$ =3.5 is shown in Fig.6. Here the error in the shape factor increases as the cylinder radius ρ_R is decreased. Since $\overline{s}_a$ is constant, a decrease in ρ_R has the effect of increasing eccentricity. The minimum value of ρ_R representing the tangent configuration is obtained when ρ_R=4.5. On the other hand at large ρ_R ($\rho_R \geq 12$), the limiting case of concentric cylinders is approached and an exact value for the shape factor is obtained for all values of Bi and $\overline{k}$.

The results shown in Fig.4-6 indicate that even though boundary condition (2.5) is not satisfied exactly when $\overline{k} \neq 1$, the error associated with this approximation is minor especially for Bi or $\overline{k}$ less than unity. In particular, in biological applications where the value of $\overline{k}$ is approximately equal to unity, the error is indeed insignificant.

2.5.2. Two Embedded Vessels

The two-vessel solution is used to examine the Nusselt number, the artery-vein and matrix shape factors, the axial vessel bulk temperature distribution, the axial mean cylinder temperature distribution, and the surface temperature distribution of the artery, vein and cylinder.

Following the same procedure as for a single vessel, the Nusselt number for both artery and vein is found to be 48/11.

The two-vessel solution is used to obtain two heat transfer shape factors, σ_{av} and σ_m,

which describe, respectively, the heat transfer rate between the two vessels, and that between the vessels-tissue matrix and the environment. These factors are defined as

$$\sigma_{av} = \frac{q_a - q_v}{\pi k_t (T_{ab} - T_{vb})} \tag{2.57}$$

and

$$\sigma_m = \frac{q_a + q_v}{\pi k_m (T_m - T_\infty)} \tag{2.58}$$

where T_m is the mean matrix temperature (artery, vein and cylinder) given by

$$\frac{T_m - T_\infty}{T_0 - T_\infty} = \theta_m = \frac{1}{\pi \rho_R^2} \int_0^{\rho_R} \int_0^{2\pi} \theta(\rho,\phi) \rho d\rho d\phi \tag{2.59}$$

and k_m is the matrix conductivity given by

$$k_m = \frac{1 + \bar{a}_v^2}{\rho_R^2} k_f + (1 - \frac{1 + \bar{a}_v^2}{\rho_R^2}) k_t \tag{2.60}$$

Substituting the solutions for the bulk temperature of the artery and vein, (2.50) and (2.51), into the definition of σ_{av}, we obtain

$$\sigma_{av}=\frac{-\frac{1}{2}\bar{k}\left(\frac{d\theta_{ab}}{dz}+\bar{V}\,\bar{a}_v^{2}\frac{d\theta_{vb}}{dz}\right)}{\left[\sum_{n=0}^{\infty} b_n(\bar{s}_a^{n}-\bar{s}_v^{n})-\frac{11}{96}-\frac{\bar{k}}{4}\ln\bar{sp}\right]\frac{d\theta_{ab}}{dz}+\left[\sum_{n=0}^{\infty} c_n(\bar{s}_a^{n}-\bar{s}_v^{n})-\frac{\bar{k}}{4}\ln\left(\frac{\bar{sp}}{\bar{a}_v}\right)-\frac{11}{96}\right]\bar{V}\,\bar{a}_v^{2}\frac{d\theta_{vb}}{dz}} \tag{2.61}$$

For the general case σ_{av} depends on the local axial gradients of the vessel bulk temperatures. However, for the special case of two equal radii vessels embedded at equi-distance from the center of a cylinder, i.e. $\bar{a}_v=1$ and $\bar{s}_a=\bar{s}_v$, (2.61) simplifies to

$$\sigma_{av}=\frac{2\bar{k}}{\frac{11}{24}+\bar{k}\ln\bar{sp}} \tag{2.62}$$

This result shows that the shape factor σ_{av} for this special case depends only on the distance between the two vessels $\bar{sp}$. and is independent of eccentricity. It is interesting to note that if the radius of the embedding medium cylinder is infinite,then $\bar{s}_a$ is equal to $\bar{s}_v$. Setting $\bar{s}_a=\bar{s}_v$ and assuming equal flow rates in the two vessels, i.e. $\bar{V}\,\bar{a}_v^{\,2}=1$, equation (2.61) reduced to Wissler's [31] results for two vessels embedded in an infinite medium. Result (2.62) without the $\ln\bar{sp}$ term was also obtained to leading order in the perturbation of Zhu et al. [22] for small eccentricity. Expression (2.62) is especially useful in biological applications involving extremities such as a finger or tail where the artery-vein pair is symmetrically located relative to the skin surface.

Using the temperature solutions for the artery, vein and tissue to determine T_m from (2.59) and substituting the result into the definition of σ_m, we obtain

$$\sigma_m = \frac{4(\frac{d\theta_{ab}}{dz} - \bar{V}\,\bar{a}_v^2 \frac{d\theta_{vb}}{dz}) \frac{\rho_R^2}{(1+\bar{a}_v^2)\bar{k} + (\rho_R^2 - 1 - \bar{a}_v^2)}}{[\frac{Bi+2}{Bi} - (\frac{\bar{s}_a}{\rho_R})^2 - (\frac{1}{\rho_R})^2 + \frac{2}{3\bar{k}\rho_R^2}]\frac{d\theta_{ab}}{dz} - [\frac{Bi+2}{Bi} - (\frac{\bar{s}_v}{\rho_R})^2 - (\frac{\bar{a}_v}{\rho_R})^2 + \frac{2}{3\bar{k}}(\frac{\bar{a}_v}{\rho_R})^2]\bar{V}\,\bar{a}_v^2 \frac{d\theta_{vb}}{dz}} \tag{2.63}$$

Since the vessel area is small compared with the embedding medium area, the term $(1/\rho_R)^2$ in (2.63) is negligible. For $\bar{s}_a = \bar{s}_v$ and $\bar{k} \approx 1$ (2.63) simplifies to

$$\sigma_m = \frac{4}{\frac{Bi+2}{Bi} - (\frac{\bar{s}_a}{\rho_R})^2} \tag{2.64}$$

The dependence of the shape factor σ_m on $\bar{s}_a/\rho_R$ for various Biot numbers (0.1, 1.0, 10) is shown in Fig. 7. For Bi <1 the matrix shape factor is essentially constant independent of the vessels' location in the cylinder. However, at Bi=10, σ_m increases sharply as the vessels move closer to the cylinder surface. When the eccentricity is small, $\bar{s}_a/\rho_R \ll 1$, expression (2.64) reduces to the perturbation solution of Zhu et al [22] in which the $(\bar{s}_a/\rho_R)^2$ term does not appear.

Finally, the two-vessel solution is applied to the human arm to determine the artery-vein and matrix shape factors and the bulk and surface temperature distribution of the artery, vein and arm. The configuration examined models the arm as a constant radius ρ_R=12. The artery and vein are assumed to be symmetrically embedded in the tissue cylinder at $\bar{s}_a = \bar{s}_v$ =8 with $\bar{sp}$ = 3 and $\bar{a}_v$=1. The conductivity ratio $\bar{k}$ is equal to unity and thus boundary

condition (2.5) is satisfied exactly. Using (2.62) the artery-vein shape factor σ_{av} is found to be 1.28.

From (2.64) the corresponding matrix shape factors σ_m at Biot numbers 0.1, 1 and 10 for this model of the arm are 0.195, 1.565 and 5.294, respectively.

To determine the axial variation of bulk temperatures and the distribution of surface temperatures, it is necessary to first specify the boundary conditions on the bulk temperatures. Two conditions are needed to evaluate the constants of integration in (2.50) and (2.51). From the definition of the dimensionless artery bulk temperature, θ_{ab}, the first boundary condition is

$$\theta_{ab}=1, \quad z=0 \tag{2.65}$$

where z=0 is the shoulder end of the arm. The second boundary condition is obtained from the experimental data of Bazett [11] who measured the median basilic vein temperature at two ambient air temperatures of 21 °C and 34.5 °C. Thus:

$$\theta_{vb}=0.56, \quad Z/L=0.22, \quad at \quad T_\infty=21 \ ^oC \tag{2.66a}$$

$$\theta_{vb}=0.15, \quad Z/L=0.22, \quad at \quad T_\infty=34.5 \ ^oC \tag{2.66b}$$

These data are for the arm at rest where the Peclet number at the shoulder is approximately 3500 at normal ambient temperatures. The Biot number, which accounts for both convection and radiation, is 1.48. Based on boundary conditions (2.65) and (2.66) the results for the axial variation of the artery, vein and tissue temperatures, θ_{ab}, θ_{vb}, θ_{tm}, are shown in Fig.8 for

both ambient temperatures. The monotonic variation of these temperatures along the arm is unrealistic due to the simplified model used which neglects three key factor; cross sectional area variation of the arm, the axial decrease in the Peclet number due to the bleed-off from the axial vessels to the muscle and cutaneous circulations and the enhancement in tissue conductivity due to blood perfusion described by the Weinbaum-Jiji bioheat equation. Blood bleed off from the artery acts to warm the arm towards the wrist. These factors can be accounted for following the theoretical approach developed in Song et al. [36] and Zhu et al. [37].

Peripheral variations of surface temperature at Z/L=0.5 for the artery, vein and arm at T_∞=21 °C and T_∞=34.5 °C are shown in Figs. 9 and 10, respectively. These plots show that peripheral variation of surface temperature is moderate for the artery and more pronounced for the vein and arm. At both ambient temperatures the arm surface temperature peaks in the vicinity of the artery-vein pair. This single peak form is due to the fact that the distance between the artery and vein is smaller than their distance from the arm surface and thus they act as a single source.

Although the artery loses heat to the tissue and vein at both ambient temperatures, heat interchange between tissue and vein is strongly influenced by ambient temperature. Fig.9 shows that at T_∞ = 21 °C the vein heats the tissue while at T_∞ =34.5 °C, Fig.10, the direction of heat flow is reversed along the vein circumference. Thus at a given section along the arm, heat can flow from the tissue to the vein and from the vein to the tissue along the vein periphery.

2.6. Concluding Remarks

(1) Although the continuity of flux boundary condition at the vessel's surface is not exactly satisfied for $\overline{k} \neq 1$, the error in the new approximate analytic solution derived herein is small for very wide range of $\overline{k}$ values. In biological applications where $\overline{k}$ is approximately equal to unity and in many engineering applications where $\overline{k} \leq 1$, the error in the solution is of order one percent or less. Although this conclusion is based on a detailed study of the single embedded vessel case, the error associated with two or more embedded vessels can be expected to be of the same order since the multi-vessel solution is constructed by superposition of single vessel solutions.

(2) The approximate solution presented in section 2.4 for two vessels embedded anywhere in a cylinder can be easily extended to applications where the number of vessels is more than two. Indeed, this is the case of the human forearm where the major artery-vein pair in the upper arm bifurcates at the elbow to form two countercurrent pairs.

(3) The assumption of constant artery, vein and arm cross-sectional area used to obtain a solution for the axial temperature distribution in the simplified model for the arm in this paper can be relaxed. Axial variation of the three cross-sectional areas can be taken into consideration using a numerical integration of equations (2.50) and (2.51) along the length of the arm.

(4) With minor modification the method of solution can be applied to the case of two dissimilar fluids. Such applications are common in engineering systems.

Chapter 3. Experimental Study

In this chapter the vascular anatomy of the rat tail is examined experimentally to analyze the crucial vascular elements for the blood flow regulation and heat transfer modeling of the rat tail. Experimental study of the rat tail is conducted to investigate the thermoregulatory function of the rat tail blood flow. Tail blood flow rate at the tail base (BF_{base}) or tail middle (BF_{mid}) has often served, without justification, as an index of total tail blood flow (BF_{tot}), We sought to clarify the relationship between temperature, blood flow rate at the tail base, middle (BF_{mid}) and tip (BF_{tip}). Both unanaesthetized and anaesthetized rats were studied in a two-zone, temperature-controlled chamber for independent control of air temperature surrounding the tail (T_{loc}) and torso (T_{cent}). BF_{base} and BF_{mid} were measured by strain gauge plethysmography. BF_{tip} was measured by a new computerized balance technique. Tail surface temperatures were measured by the infra-red camera and calibrated thermocouples, and rectal temperature was measured by calibrated thermocouple. Transient tail blood flow, tip temperature (T_{tip}), lateral vein temperature (T_{lv}) and BF_{tip} were measured as T_{cent} changed from neutral to high. The results of this study will be used in chapter 4 to develop a new theoretical model of rat tail heat transfer.

3.1. Introduction

The rat tail has frequently been used for the study of blood flow control with regard to central and local thermoregulation. It is both an easily accessible preparation and a good model for the human digit because of the morphological similarities between the vascularity

of the rat tail and that of the human digit [24,25]. The tail can lose little or up to 40% of the rat's heat production through the regulation of its blood flow [27].

The thermoregulatory function of the tail blood flow has been inferred from blood flow measurements [15,26,27,28] and temperature measurement [29]. Rand et al. [27] investigated the change of the tail blood flow when rats were exposed to warm air. They found that the blood flow increased in response to high air temperatures, and suggested the flow responded as if it were controlled in an on-off manner. Young and Dawson [29] measured the temperature difference between the ventral and lateral surface o f the rat tail at various temperatures between 25 and 35 °C . They also suggested that the regulation of the tail blood flow is best described as on-off control. In contrast to Rand et al. and Young and Dawson, Hellström [26] found that the tail blood flow regulation is not of on-off type, but rather an effector response which increases proportionally with elevated rat core temperature. Raman et al. [15] have further suggested that the tail blood flow is linearly related to core temperature when the rat is warmed. They have also proposed that in additional to regulation of blood flow, the venous blood shunting between the "superficial" lateral veins and the "deep" ventral vein plays a major role in the determining heat transfer rate of the tail. One of the objectives of our present experiments is to determine what type of model best describes the tail blood flow regulation.

To answer the question whether there is a significant venous blood shunting between "superficial' and 'deep' veins, we need to analyzed the tail vascular elements and their arrangement to find out where are the "superficial" and "deep" veins. The detailed vascular anatomy of the rat tail were examined in the present study.

Angiographic data [29] revealed that there was no venous blood shunting during heat-induced vasodilation or cold-induced vasoconstriction. Since the high density of arteriovenous anastomose, AVA's, occurs at the distal end of the tail [9], it appears that a very high blood flow can be maintained there. It is possible that in the tip the range of blood flow may very high and that regulation of the flow to the tip may be more significant for tail heat transfer than the shunting of the venous blood within the tail. This generates an hypothesis that heat loss from the tail would be directly related to this axial redistribution of blood flow. There would be a greater blood flow increase in the distal tail region than in the proximal region when the rat is exposed to warm air. For geometrical reasons it is more efficient for a rat to increase the heat loss from the tail by increasing the tail blood flow at the distal region than at the proximal region.

To test the hypothesis that blood flow regulation is axial, we needed to measure the blood flow change in successively distal regions of the tail during a rat heat stress. However, there was no available method to measure the blood flow near the tail tip. The diameter of the tail near the tip is so small that the conventional mercury-in-silastic strain gauge could not be used there. To overcome this difficulty a new computerized micro-balance technique was used to measure the blood flow of the tail tip.

Previous studies of the tail blood flow regulation [15, 26,27,28] have only measured the blood flow at one location, either near the base [15,27,28] or near the middle [26] of the tail. They used the measured local blood flow as an index of total tail blood flow (BF_{tot}) without clear justification. Since the blood flow may change differently at different locations in the tail in response to the same change of thermal conditions,

measuring blood flow at one or another location may result in a different control model of the tail blood flow regulation depending on which blood flow is used. In this study, we sought to clarify the relationship between temperature and blood flow rate at the tail base, middle and tip under a range of thermal conditions. With these data we hoped to evaluate the prevailing hypotheses of on-off regulation of BF_{tot} and of venous shunting, to find an easily measured parameter for the description of the tail blood flow regulation, and to provide input parameters for a new mathematical model of rat tail heat transfer.

3.2. Experimental Studies on the Vascular Anatomy of the Rat Tail.

Although the vascular anatomy of the rat tail has been previously examined [25], further anatomical studies were performed to analyze vascular elements which we believe are critical in modeling heat transfer. Latex injected rats were chosen as the specimens for dissections. The rat tail was cut at different cross sections to investigate the cross-sectional structure of rat tail. This is schematically shown in Fig.11. The rat tail can be characterized as being composed of three different layers; bone, tendon and cutaneous, in which three major axial artery-vein pairs, one ventral and two lateral, which are embedded in the tendon at the interface with the cutaneous layer. In the specimens examined the two lateral arteries are very small compared with the ventral artery, and the ventral vein is small compared with the lateral veins. In order to investigate the axial vasculature variation and the microvessels supplies from the major vessels to the cutaneous layer, the cutaneous layer of the rat tail was cut along the entire tail length on the ventral side. The cutaneous layer was then peeled off and spread flat. The vasculature was examined with a stereo-microscope and

extensively photographed. Fig. 12 is a tracing of a photograph showing the ventral artery, lateral veins, bone and the inner surface of the cutaneous layer with its network of microvessels. The key findings in Fig. 12 which are crucial to tail thermoregulation and heat transfer modeling are: (1) The small lateral arteries are actually arcades connecting the first generation of branchings of the ventral artery. They arise from the ventral artery by short radial vessels at the mid-point of each vertebrae and do not appear to serve as conduits for axial flow down the tail, but rather as inter-arterial connections at each vertebral segment. (2) As the ventral artery approaches the tail tip, its diameter remains almost constant even though the cross-section area of the tail is greatly reduced. This structure suggests that high blood flow is maintained in the ventral artery near the tail tip. The tail volumetric flow is not uniform along the tail. The ventral artery at midtail is 300-600 μm depending on rat size. (3) The tail tip has a very high density of arteriovenous anastomoses (AVA's) and the AVA's allow a far higher blood perfusion at the tip than at any other tail region. This latter finding was supported by the first more detailed experimental measurements of the axial distribution of cutaneous flow described in section 3.3-3.5. (4) The dimensions of the deeper ventral vein are typically 1/4 to 1/3 the more superficial lateral veins, which are 300-600 μm at the midtail. Simple Poiseuille flow considerations, flow proportional to the 4^{th} power of the diameter, suggest that the flow in the ventral vein is of the order of one percent of that in the lateral veins. These results suggest that the venous blood shunting between the ventral and lateral veins is not as important in altering tail heat transfer as suggested by Ramon et al. [15].

3.3. Methods

Measurement of the axial variation of surface temperatures and blood flow were made in the tail of male Sprague-Dawley rats with weights 398 ± 27 g (SD). The rats were placed in a standard rat restraint chamber which was housed in a temperature controlled enclosure (see Fig. 13). The tail of the rat was passed through a membrane at one end of the chamber so that it could be kept at a temperature different from the torso. The temperature of the chamber was maintained by a continuous flow of air which passed through a coil in a temperature controlled bath. The chamber, which was mounted on a vertically adjustable platform, and was housed in a larger enclosure in which the temperature could also be independently set. By setting the temperature of the outer enclosure in which the tail resided and the chamber containing the rat torso, it was possible to independently control the torso and tail temperatures. There was a sliding port on the top of the outer enclosure for the introduction of the infra-red camera for thermal imaging of the tail. The vertically adjustable platform inside the large enclosure was used to keep the tail at an appropriate height so that it was in-focus for the infra-red camera.

Protocols for both conscious and unconscious rats were used in our experiments. Sodium pentobarbital (40 mg/kg) was used to induce anesthesia for the unconscious rats. Supplemental doses were administered as needed. Rats for the conscious experiments were trained over a two week period to stay in a standard rat restraint chamber prior to experiments. Tail surface temperatures, and base and mid tail blood flow were measured under a series of combinations of torso and tail temperature. Tail base measurements were made 2 cm from the extreme proximal end of the tail. Mid-tail measurements were

made at the mid-point of the tail. Tail surface temperatures were measured by the infra-red camera and calibrated thermocouples, and rectal temperature was measured by calibrated thermocouple. Tail base and mid blood flow were measured by venous occlusion plethysmography using a mercury-in-silastic strain gauge.

The rat tip blood flow was measured by venous occlusion plethysmography using a computerized electronic balance to measure tip weight change per unit time. The orientation of the tip on the balance is shown in Fig. 14. The tip was a region 2.5 cm long as measured from the distal end of the tail. After experiments were completed the tip was severed and weighed for comparison to the weight measured during the experiment. The in vivo measured weight may slightly underestimate the actual blood flow to the tip since some of the weight due to blood flow would be born by the proximal, supported portion of the tail. However, since this would be true before and after cuff inflation, we think that most of the weight change after occlusion was measured by the balance. If blood weighs roughly 1gm/ml then equivalency between weight change and blood volume change can be reasonably inferred. Errors in blood flow estimation by this technique would likely result in values lower than the true value.

3.4. Results

Figure 15 (a) shows the base and mid tail blood flow for conscious rats at tail enclosure temperatures (T_{loc}) of 17.1, 25.9 and 36.1 °C. The rat torso chamber temperature (T_{cent}) was maintained at 26 °C. Figure 15 (b) shows the blood flow changes at the tail base and middle comparing neutral to low and to high temperatures. Both the

base and mid tail blood flow increased in response to the elevated tail enclosure temperature. The change of the blood flow at the tail base was similar to that at the tail middle. This suggests that there is no axial redistribution of the tail blood flow in response to local tail thermal conditions.

Figure 16 (a) and Figure 16 (b) show how the rat torso chamber temperature influences the tail blood flow at the tail base and middle. Changing the rat torso chamber temperature from neutral to low results in a similar decrease in the tail blood flow: 48% at base and 49% at middle. However, heating the rat torso chamber from T_{cent} =25.8 °C to 36.6 °C causes the tail blood flow to increase 313% at the base and 742% at the middle. The much higher tail blood flow increase at the tail middle than that at the tail base indicates that, under thermal stress, the tail not only vasodilates its microvessels to increase the entire tail blood flow but also does this disproportionately in favor of the mid-tail.

Figure 17 shows the blood flow at the tail base and tip for unconscious rats under various torso chamber temperatures. The tail was in thermoneutral condition. The tip had a high blood flow even in thermoneutral and cool conditions. The blood flow of the tail tip was 10 to 11-fold higher than that at the tail base. The increase in the blood flow at the tip was 9 times as much as that at the tail base when the rat torso chamber temperature increased from neutral to high temperature. This suggests that the rats reapportion their total tail blood flow from the base to the tip region in response to the change of the torso thermal conditions from neutral to high.

Figure 18 and 19 show the infra-red thermal images and axial surface temperature

profiles along the top of the tail for an unconscious rat at torso chamber temperatures of 25 and 36 °C, and a tail chamber temperature of 22.5 °C. In a thermoneutral environment, T_{cent} =25 °C, the axial surface temperature is higher at the base of the tail, declining markedly toward the tip. However, under thermal stress, T_{cent} =36 °C, the axial surface temperature changes insignificantly along the tail length. The entire tail temperature is elevated, and the highest surface temperature is reached near the tip of the tail. The mean excess tail surface temperature at T_{cent} =36 °C is about three times as much as that at T_{cent} =25 °C.

Figures 20 and 21 show the time course of the change in blood flow at the tail base, middle and tip, and the tail base, tip and rectal temperatures in an unconscious rat following increases in the torso chamber temperature with the tail in the thermoneutral condition. The tail base temperature (T_{lv}) was measured on the lateral surface, which approximates the blood temperature within the underlying lateral vein. The tail tip temperature (T_{tip}) was measured at the top of the tail tip. The rat rectal temperature rose steadily during torso heating. The tail base blood flow increases proportionally to the increase in the rat rectal temperature. However, the blood flow at the tail middle and tip increases very slightly during the initial torso heating period. At a critical torso chamber temperature, between 34 °C and 38 °C , the blood flow at the tail middle and tip simultaneously jump, followed closely by a transient drop in the lateral tail base temperature and an abrupt increase in the tail tip temperature.

3.5. Discussion

The dominant thermoregulatory function of the rat tail is to increase heat loss under conditions of body heating. The present results concur with the results of previous studies which showed that the rat can significantly increase its heat dissipation by the regulation of the tail blood flow. Unfortunately, a single control model has not emerged from the past work on the rat tail blood flow and instead competing models have been proposed. One of the goals of the present study was to reconcile the different tail blood flow control models that have been proposed. The time course of lateral tail base, middle and tip temperature in the present study, in fact, supports a regionally mixed mode of tail blood flow regulation. The sudden onset of middle and tip vasodilation shown in Figs. 20 and 21 strongly suggests that when a critical core temperature is reached the distal regions of the tail are mobilized for heat loss in an on-off manner. Tail base flow, however, did not suddenly increase, but rather rose steadily as core temperature rose, appearing to respond in a manner proportional to body core temperature. From these results we conclude that the control mode for tail blood flow regulation is of the on-off type in the middle to distal region of the tail, and of the proportional type in the proximal region.

The probable reason that previous investigators supported one or the other model for the entire tail is that they based their conclusions on measurements from only one of these regions. Raman et al [15] measured the base tail blood flow and suggested that the total tail flow rises as a linear function of the rat rectal temperature. Hellström [26] also hypothesized a proportional control model even though his measurements were distal to the base region. A possible reason for the disagreement between his findings and the present study is the measurement methods used. He drilled through the tail to insert a 0.6mm stainless steel wire

where the strain gauge was placed; a procedure which may have altered the hemodynamics of the tail in that region.

Rand et al. [27] suggested an on-off control model for tail blood flow regulation based on their measurement of tail middle and base blood flow. They reported an abrupt increase or decrease in the tail middle temperature when a critical environmental temperature was reached. Young and Dawson [29] also suggested that rat tail blood flow regulation is of an on-off type, basing their conclusions on thermal rather than blood flow data. They measured ventral and lateral surface temperatures, inferring ventral artery and lateral vein temperatures. They reasoned that a large difference between these two temperatures, T_{AV}, suggested tail vasodilation while a small difference suggested vasoconstriction. They also measured heat transfer from the tail in two regions, and also based their conclusions about the mode of blood flow control on these data. Although the lateral surface temperature is a good approximation of the lateral venous temperature, the ventral surface temperature may at times be a poor index of the ventral arterial temperature. Model predictions in chapter 4 strongly suggest that there is a significant difference between the ventral artery and ventral surface temperature in neutral to hot ambient conditions because of a significant non-equilibration between the artery and surrounding tissue. The model also predicts that T_{AV} near the tip becomes negligible because of the extremely short distance between the arteries and veins and the high density of AVA's which permit rapid transfer of blood from the arterial to the venous sides of the circulation. Despite these potential problems with the quantitative aspects of their study, the qualitative findings of Young and Dawson support the notion of on-off blood flow control for the majority of the tail.

Although we do not know precisely where in the proximal region the mode of control changes from proportional to on-off, the thermal image data for steady-state surface conditions suggest that in thermoneutral conditions blood flow remains relatively high only in the first few cm distal to the tail base. We think that this is the region that is under proportional control. During body heating, the blood flow in this region steadily rose but never increased in a step-wise fashion. The rest of the tail, had a surface temperature barely above ambient when conditions were thermoneutral or lower, suggesting vasoconstriction over this part of the tail. We hypothesize that this vasoconstricted region is under on-off control, dilating only when core temperature reaches a critical level. Further studies where flow in the regions between our proximal and mid-tail measurement sites could delineate more precisely the place where the control mode changes. We predict the results would show that the transition from proportional to on-off control occurs where the sharp decrease in surface temperature occurs in the IR image in Fig. 18. Based on this we predict that 70-80% of the tail is regulated via the on-off mode of control.

Another reason that the base of the tail is a poor index of total tail heat transfer is that the magnitude of the blood flow change there is small relative to the distal tail. As Figures 16b and 17 show, the increase in flow in the distal regions following core heating is double that of the base region. If we are correct in hypothesizing that the region of on-off control includes most of the tail, then it would follow that the major variability in heat transfer derives from this mid to distal region. The relatively small area in the tail base that exhibits proportional control and the smaller maximal blood flow there would contribute in only a minor way to total tail heat transfer variability. If this is correct then mid-tail flow is

preferable to base blood flow as an index of total flow because it is more representative of total tail thermoregulatory blood flow.

When the mid to distal tail blood flow suddenly increases, the heat transfer from the core quickly reaches a maximum rate. Most of the heat entering via the arterial inflow is initially absorbed as heat storage in the cool distal tail. The transient drop in lateral tail base temperature during the initial vasodilatory phase occurred because the distal regions were previously almost as cool as the surrounding environment, and the blood stored in those regions was also cool. When the rate of return of this cool blood to the base was suddenly increased, it cooled the proximal regions of the tail as indicated by the transient drop in lateral vein temperature. Since the flow rate was extremely high, the distal tail temperature quickly rose to equal the base temperature. In the steady-state when the distal tail had been warmed, the additional heat was lost from the surface where the temperature was ultimately elevated by 10°C above its previous level. The transient drop in base temperature would actually reduce heat loss from the base region, indicating why heat loss from this region would not be a reliable index of total tail heat transfer.

Another objective of this study was to evaluate the "venous shunting" hypothesis proposed by Raman et al. [15]. They suggested that the rat can significantly alter its heat transfer by shunting blood from the lateral venous pathway to the ventral route. There are, however, a number of problems with the shunting hypothesis. First, Raman et al termed the lateral venous return route "superficial" and the later ventral route "deep", implying a significant difference in the distance between the vessel and the surface. These vessels are, in fact, both superficial though the ventral vein is a countercurrent vessel to the ventral artery

which is the main blood supply to the tail. Second, as already mentioned, they used blood flow at the base of the tail to infer total tail blood flow and then developed a model to fit the observed relationship between heat transfer and blood flow. It is unlikely that the base blood flow accurately reflected the total tail blood flow even though the measured heat transfer was for the entire tail. Third, one of the complicating factors in reaching a clear interpretation of their experiments is their use of a water immersion environment. Water has a far greater thermal conductivity than air and Chapman [38] estimated that the heat loss from the tail in water is more than 10 times as great as that in air under similar conditions. Hales [39] also suggested that the mode of regulation itself may be altered in a high conductivity environment. In warm T_{cent} the degree of vasodilation should be reduced in water, and in a cool T_{cent} the need to reduce heat loss would be much greater. Finally, their evidence for venous shunting depended upon a questionable assumption that the arterial blood entering the tail was the same as the rectal temperature. Bazett (11) showed by direct measurement that when the human extremity is exposed to the cold, the inlet arterial temperature may be several degrees lower than rectal temperature, presumably because of precooling of the slow arterial inflow. If this were true of the rat tail, then the segments of the plots of Raman (16) which show the same heat transfer at two different T_{cent} could superimpose and would then show that heat transfer relates only to blood flow.

The final point to make about the shunting hypothesis is that even if it is partially correct, the phenomenon is of minor importance since the tail is primarily a heat loss organ, and in neutral to cool environments it has a low blood flow, low surface temperature and consequently low heat loss. Heat conservation under these conditions is due almost entirely

to mid and distal blood flow reduction. The small amount of heat conservation achieved by venous shunting would be limited to a small region at the proximal part of the tail; the only region where blood flow remains elevated.

Our steady-state and transient studies lead to the conclusion that the rat tail becomes a thermoregulatory effector in warm to hot conditions when its blood flow rises in step-wise fashion after a critical core temperature is reached. When this vasodilation occurs, blood rushes along the ventral artery at approximately the same volumetric rate all the way to the tip, distributing radially via the arcading arterial branches which were formerly called the lateral arteries. The entire tail surface temperature rapidly rises, though the proximal lateral regions surface temperature transiently falls due to the return of precooled blood from the distal tail. Following the warming of the tail, the augmentation of total heat transfer is achieved by maintaining a uniformly high surface temperature. The proximal region of the tail does not contribute significantly to the increase in total heat transfer.

One of the interesting and novel findings of this study was the unusually high blood flow to the tail tip during warm thermal conditions. To our knowledge tip blood flow has not been previously measured. Anatomical studies in section 3.2 prior to our experiments suggested to us that the tip must sustain a high flow because the supply arteries are almost as large there as in the proximal tail, and the arcading vessels that branch from the supply vessels are exceedingly dense. The volume of tissue supplied by these arteries is one fourth as much per unit length compared to the proximal tail. Histological studies (3) also found most rat tail AVA's in this region. We were surprised, however, by the magnitude with which these predictions were correct. The maximal flow of 800 ml/ 100ml min^{-1} is one of

the highest tissue blood flows reported. One would be tempted to attribute these high values to an unknown bias in the measuring technique developed in these experiments. However, we believe that the errors in the measurement method are most likely to lead to an underestimation of the blood flow. This is because the change in tail weight following venous occlusion is probably partially born by the proximal supported part of the tip and not by the balance. We think that this error is probably small, and did not find a way to accurately estimate it. Overestimation of tip flow rate could occur during the inflation due to shifting of the tail by the inflation cuff, but beyond the period when this artifact might occur, the slope of weight of change vs. time can only be related to the inflow of blood. A valid criticism of the tip flow measurements is that they were only obtained in anesthetized rats. This condition no doubt altered the blood flow leading to higher flows particularly in thermoneutral conditions, but it was unfortunately unavoidable. Conscious rats constantly move their tail tips very slightly, and given the sensitivity of the measurement itself, this movement artifact obscured the weight change due to blood flow. It is reasonable, however, to assume that during heat stress, the flow rate in the unconscious rat is similar to that in the conscious rat. This is supported by the comparison of mid- and base blood flow data from the experiments on conscious and unconscious rats.

3. 6. Conclusions

In this study we have reached the following conclusions: 1) the blood flow at the proximal region of the tail is a poor indicator of total tail blood flow, 2) the mode of control of tail blood flow in reference to body temperature is not the same in all tail regions, being

proportional in the most proximal region, and on-off in the remaining regions, 3) mid to tip blood flow is the best indicator of the regulation of heat transfer from the tail, 4) venous shunting, if it occurs, is of minor importance in reducing tail heat transfer in cold environments, 5) in hot environmental conditions, tail tip blood flow is the highest of any tissue in the body.

Chapter 4. A Non-Uniform Three-Dimensional Perfusion Model of Rat Tail Heat Transfer

4.1. Abstract

Previous models of rat tail heat transfer have assumed that the tail is uniformly perfused along its length and have introduced questionable assumptions about the heat transfer role of the major axial arteries and the venous blood shunting between the superficial and deep veins. The recent experiments in chapter 3 have shown that (1) perfusion of the tail tip is more than 10-fold higher than that in the tail base, and (2) the perfusion of the middle region of the tail increases 8-fold during heat stress compared to 3-4-fold in the base and tip. Our anatomical studies have shown that the lateral arteries are a series of radially arcading connections from the ventral artery which probably do not serve as major axial conduit vessels. These observations indicate that current views and models for the blood flow distribution and heat transfer in the major axial arteries and veins and in the rat tail cutaneous circulation need substantial revision. Based on these new experimental findings a new three-dimensional model is developed to determine the heat transfer function of the rat tail at different local and central temperatures. The predictions of the model show good agreement for the axial surface temperature distribution in the rat tail presented in chapter 3. These results when combined with our anatomical studies in chapter 4 indicate that there is very little shunting of blood between the superficial lateral veins and the deep ventral vein as proposed by Raman et al. [15]. Although this model is based on the rat tail anatomy, it can be modified to treat the human limb and digit.

4.2. Introduction

This study was motivated by the need to develop a model to describe the heat transfer of a rat tail and a human digit. In the rat the tail is a vital heat transfer organ rejecting about 40 percent of the total body heat under conditions of thermal stress. A mathematical model for the human extremity and the rat tail was developed by Raman and co-workers [13,14]. They introduced three conduction shape factors and a blood flow distribution parameter that divides the venous return circulation between a deep vessel and a superficial vessel. These four parametric constants were determined by curve fitting their experimental data in Raman et al. [15,16] rather than a fundamental theory to predict these constants from measurements of the vascular anatomy of the major axial vessels. Thus the model does not provide a theoretical prediction of the heat transfer and temperature distribution in the rat tail and the human digit, for conditions other than their experiment. The central assumption of model in Raman et al. [14] is that the rat tail will dissipate or save heat by redistributing the venous blood returning via either the superficial lateral veins or deep ventral vein. The existence and the heat transfer role of this venous shunting will be examined in the present study using experimental input data , in chapter 3, for the axial distribution of blood flow in the tail and detailed observation of the vascular anatomy.

Previous models [18-21] for the human limb have either been based on a simple one-dimensional representation for countercurrent heat exchange [18,19], or on multi-layers using the Pennes equation [20,21] Mitchell and Myers [18] treated the central artery and vein as a one-dimensional countercurrent heat exchanger with constant radius. The perfusion or bleed-off was neglected and the heat loss from the extremity was not considered.

Therefore the arterial and venous temperatures were assumed to be equal at the end of the limb. Wissler [20] and Keller and Seiler [21] treated the limb as concentric cylindrical layers. Each layer was modeled by a Pennes equation with different blood perfusion rates. However, to properly model heat transfer in the human limb, digit or the rat tail, one must take into consideration countercurrent blood flow through the major axial arteries and veins, blood perfusion in the microvascular network, axial variation in tissue anatomy and thermal interaction with the external environment. Major aspects of this complex, coupled, multi- domain, three dimensional problem were dealt with by Zhu and his co-workers [22,23]. In Zhu et al. [22] a three-dimensional approximate analytic solution was developed for treating unequal countercurrent heat transfer between parallel paired vessels of non-uniform temperature asymmetrically embedded in a constant radius cylinder of uniform thermal conductivity with surface convection. This basic model was used to describe the unequal countercurrent heat exchange in the core region of the whole limb model in Zhu et al. [23]. The major limitation of the models in Zhu et al. [22,23] is that they require small eccentricity of the major axial arteries and veins, whereas these vessels can be highly asymmetric in the limb and run close to the surface in the human digit and rat tail. This limitation is removed in the recent theory developed in chapter 2, where the vessels can be arbitrarily positioned in the cross-section of the limb.

A solution for the heat transfer between multiply embedded axial vessels in a tissue cylinder may be obtained by the superposition of single vessel solutions provided that both the governing equations and boundary conditions are linear and the solutions for the different individual vessels can be expressed in common coordinates. Various heat transfer

problems for a single vessel embedded in a homogeneous semi-infinite or finite cylindrical medium were examined in [30, 32, 33] and chapter 2 . Chato [30] and Bau and Sadhal [32] considered a single vessel embedded in a semi-infinite medium. The boundary conditions on the free surface were convective in Chato [30] and isothermal in Bau and Sadhal [32]. Defelice and Bau [33] analyzed a single vessel eccentrically embedded in a cylinder using a conformal mapping method. Convective boundary conditions were considered on the vessel and cylinder surface. Although conformal mapping methods can be applied for a single vessel, the form of the solution precludes superposition since solutions for more than one vessel in a cylinder can not be transformed to common bicylindrical coordinates. An infinite series solution for one or more vessels arbitrarily positioned in a cylinder with surface convection was presented in chapter 2. This solution is exact when the thermal conductivity of the fluid is equal to that of the cylinder material and is a very good approximation when these conductivities are not equal. The major limitations of the solution in chapter 2 are that it treats the cylinder material as a uniform region and does not take into account the blood perfusion in the cutaneous layer.

The highly perfused cutaneous layer, which characterizes the rat tail and human digit, plays a major role in heat transfer in the extremities. The blood perfusion in the tail cutaneous layer is not uniform, and the pattern of the blood flow distribution to the tail changes corresponding to different local and central temperatures. In addition, the tail and digit have a relatively large bone region. These factors which are critical in heat transfer modeling of the extremity will be addressed in the new model for the rat tail developed in this study. In the present model, an exact two-dimensional temperature distribution in the

tail's cross- section was first obtained subject to the assumption that the ratio of the blood to tendon thermal conductivity $\overline{k}$ is equal to unity and an approximate solution is obtained for $\overline{k} \neq 1$. This basic solution will be used in the development of the model for the axial thermal interaction in the rat tail, following the procedure described in chapter 2. Although the present model is based on the rat tail anatomy, it can be readily modified to treat the human limb and digit.

4.3. Anatomical Background and Tail Blood Flow

The anatomical studies of the rat tail [25,29] have shown that the rat tail consists of three different layers; bone, tendon and cutaneous, with different thermal properties. The tail has three major axial artery-vein pairs, one ventral and two lateral, which are embedded in the tendon at the interface with the cutaneous layer. Fig.11 is a schematic diagram of this axial vascular anatomy. In chapter 3, efforts have been made to more carefully analyze the vascular elements which are crucial in modeling rat tail heat transfer. We have investigated the axial vascular variation of the three major artery-vein pairs and the microvessels supplying the cutaneous layer from the major axial vessels using rat tail specimens injected with latex. Fig. 12 is a tracing of a photograph showing the ventral artery, lateral arteries, bone and the inner surface of the cutaneous layer with its network of microvessels.

The anatomical study results in chapter 3 show that the tail has only one major supply artery, the ventral artery. The small lateral arteries are actually arcades connecting the first generation of the branching of the ventral artery. As the ventral artery approaches

the tail tip, its diameter remains relatively large even though the cross-sectional area of the tail is greatly reduced. The high density of arteriovenous anastomose, AVA's, occurs at the distal end of the tail. The dimensions of the deeper ventral vein is typically 1/4 to 1/3 the more superficial lateral veins, which are 300-600 μm at the midtail. These tail vascular structures suggest that: (1.) The ventral vein is not a major conduit for axially returning blood, thus the shunting of the blood to a deep vein as proposed in [14] is highly unlikely. (2.) The tail volumetric flow is not uniform along the tail. A very high blood flow can be maintained in the tip region.

In chapter 3 the local perfusion at the base and the middle of the tail is measured using a strain gauge plethysmography, and the mean blood perfusion of the tail tip (distal 2.5 cm region) is measured using a new computerized balance technique. The experimental results have shown that: (1) the perfusion of the tail tip is 10-fold higher than that in the tail base; (2) the perfusion of the middle region of the tail increases 8-fold during heat stress compared to 4-fold in the base and 3-fold in the tip and (3) central (body) temperature affects blood flow perfusion in the base of the tail differently from the middle and tip; a steady rise in rectal temperature produces a steady rise in blood flow perfusion at the base of the tail, but produces an abrupt rise in the tip and mid-tail perfusion. This abrupt rise of the perfusion is referred to as an on-off control of the perfusion. The shunting of blood to a "deep" ventral vein proposed by Raman et al. [15] is highly unlikely. Rather, the on-off control of cutaneous perfusion serves as the major element of the rat tail thermoregulation. This conclusion is further supported by our anatomical observation that the small ventral vein does not play a major role in the heat transfer of the rat tail since it is

not a major conduit for axially returning blood.

4.4. Formulation and Solution

4.4.1. Decomposition of the Multi-Vessel Problem

The geometry of the cross- sectional plane of the rat tail used in our simplified vascular model is shown in Fig. 22 (a). The model considers three concentric layers; bone, tendon and cutaneous (skin), having different conductivities. The Pennes bioheat equation is used to model blood perfusion in the cutaneous layer and a Laplace equation is employed in the tendon layer and bone region. In addition, one ventral artery and two lateral veins are considered in the model. The small lateral arteries and ventral vein are neglected in the present model since our anatomical and experimental studies, discussed in section 2, have shown that the former are a series of radially arcading connections from the ventral artery and the latter does not play a major role in the heat transfer of the rat tail. We assume that the flow in the vessels is laminar with a parabolic velocity profile. The tail is long and axial conduction can be neglected.

The non-dimensional parameters and variables are defined as follows:

$$\bar{a}_i=\frac{a_i}{a_a},\qquad \bar{sp}_{ij}=\frac{sp_{ij}}{a_a},\qquad \bar{s}_i=\frac{s_i}{a_a},\qquad \rho=\frac{r}{a_a}$$
$$\rho_i=\frac{r_i}{a_i},\qquad \rho_R=\frac{R}{a_a},\qquad \rho_t=\frac{R_t}{a_a},\qquad \rho_b=\frac{R_b}{a_a} \tag{4.1}$$
$$z=\frac{Z}{a_a\,p_e},\qquad \bar{V}_i=\frac{V_i}{V_0},\qquad \theta=\frac{T-T_\infty}{T_0-T_\infty},\qquad \bar{k}=\frac{k_f}{k_t}$$
$$k_1=\frac{k_t}{k_c},\qquad k_2=\frac{k_t}{k_b},\qquad Bi=\frac{hR}{k_t},\qquad p_e=\frac{2\rho_f c_f a_a V_0}{k_f}$$

where the geometric variables are defined in Figs.22 (a, b) and a_a is the ventral artery radius at the tail entrance. The dimensionless governing equations for the cutaneous layer (4.2), tendon (4.3), vessels (4.4), and bone (4.5) are:

$$\frac{1}{\rho}\frac{\partial}{\partial\rho}(\rho\frac{\partial\theta_c}{\partial\rho})+\frac{1}{\rho^2}\frac{\partial^2\theta_c}{\partial\phi^2}-\beta_c^2(\theta_c-\theta_{1b})=0, \quad \beta_c^2=\frac{w_c\rho_f c_f a_a^2}{k_c} \tag{4.2}$$

$$\frac{1}{\rho}\frac{\partial}{\partial\rho}(\rho\frac{\partial\theta_t}{\partial\rho})+\frac{1}{\rho^2}\frac{\partial^2\theta_t}{\partial\phi^2}=0 \qquad for \quad tendon \tag{4.3}$$

$$\frac{1}{\rho}\frac{\partial}{\partial\rho}(\rho\frac{\partial\theta_i}{\partial\rho})+\frac{1}{\rho^2}\frac{\partial^2\theta_i}{\partial\phi^2}=\mp\bar{V}_i(1-\rho_i^2)\frac{d\theta_{ib}}{dz} \tag{4.4}$$

$$\frac{1}{\rho}\frac{\partial}{\partial\rho}(\rho\frac{\partial\theta_b}{\partial\rho})+\frac{1}{\rho^2}\frac{\partial^2\theta_b}{\partial\phi^2}=0 \tag{4.5}$$

The minus sign in (4.4) is used to describe the countercurrent flow of the veins and the positive sign is used to describe the flow of the artery. The subscript *i* in (4.4) denotes any one of the three vessels; for the ventral artery *i*=1, for the lateral veins *i*=2,3. The dimensionless boundary conditions on the interfaces between the bone and the tendon, tendon and vessels, tendon and cutaneous layer are continuity of temperature and heat flux. The boundary condition at the external cutaneous surface is

$$\frac{\partial \theta_c}{\partial \rho} = -\frac{Bi}{\rho_R}\theta_c \quad for \quad \rho=\rho_R \tag{4.6}$$

where $\rho_R=R/a_a$ with $R=R(z)$ and $\rho_R=\rho_R(z)$.

In order to use the superposition method to solve this multi-vessel heat transfer problem, we consider first the heat transfer from a single vessel embedded in a tendon annulus, which is shown schematically in Fig. 22 (b). It is convenient mathematically to split the total source term $\beta_c^2\theta_{1b}$ in (4.2) into N equal contributions $\beta_c^2\theta_{1b}/N$, one for each vessel, and rewrite (4.2) as:

$$\frac{1}{\rho}\frac{\partial}{\partial \rho}(\rho\frac{\partial \theta_c}{\partial \rho})+\frac{1}{\rho^2}\frac{\partial^2 \theta_c}{\partial \phi^2}=\beta_c^2(\theta_c-\frac{\theta_{1b}}{N}) \tag{4.7}$$

The source terms in the overall boundary value problem for each vessel, Fig.22 (b), thus include the vessel source term, right hand side of (4.4), and a Pennes perfusion source term in the cutaneous layer, right hand side of (4.7), which is 1/N times the total source strength for these layers. This splitting of the particular solution for θ_c is arbitrary and has no physical meaning. The only requirement is that the sum of the particular solutions for θ_c be equal to θ_{1b}. When the solutions to equations (4.3), (4.4), (4.5) and (4.7) are superposed for the three vessels, one obtains the solution to the multi-vessel heat transfer problem without changing the boundary conditions, since the latter are homogeneous.

4.4.2. Single Vessel Solution

We decomposed the vessel and tendon solution into two parts $\theta=\theta_h+\theta_p$, where θ_h

is the homogeneous solution and θ_p is the particular solution. The particular solutions for the vessel and tendon are:

$$\theta_{pi}=(\frac{1}{4}\rho_i^2-\frac{1}{16}\rho_i^4-\frac{3}{16})Q_i \qquad \rho_i<1 \tag{4.8}$$

$$\theta_{pt}=\frac{1}{4}\bar{k}(\ln\rho_i)Q_i \qquad \rho_i\geq 1 \tag{4.9}$$

where

$$Q_i=\pm\bar{V}_i\bar{a}_i^2\frac{d\theta_{ib}}{dz} \tag{4.10}$$

is an axially varying source strength for each vessel. The homogeneous solution for the tendon, θ_h, takes the form:

$$\theta_{ht}=c_0+\sum_{n=1}^{\infty}(c_n\rho^n+d_n\rho^{-n})cosn\phi \tag{4.11}$$

Note that while the particular solution about each vessel axis is radically symmetric the homogeneous solution varies with ϕ so that vessel wall temperature is non-uniform. The temperature solutions for the cutaneous layer and bone are respectively:

$$\theta_c-\frac{\theta_{1b}}{N}=a_0I_0(\beta_c\rho)+b_0K_0(\beta_c\rho)+\sum_{n=1}^{\infty}[a_nI_n(\beta_c\rho)+b_nK_n(\beta_c\rho)]cosn\phi \tag{4.12}$$

and

$$\theta_b = e_0 + \sum_{n=1}^{\infty} e_n \rho^n cosn\phi \qquad (4.13)$$

The temperature solutions for the bone, tendon and cutaneous layer must satisfy the heat flux and temperature continuity boundary conditions on their interfaces and the convection condition on the tail surface. Substituting the bone, tendon and cutaneous temperature solutions into these boundary conditions, one obtains infinite series expressions for the temperature in each region. Applying orthogonal and contour integrals on these equations and using residue theory, we obtain the expressions for all the coefficients a_n, b_n, c_n, d_n, e_n in equations (4.11-4.13), see Appendix. The series solutions (4.11)-(4.13) converge rapidly. Typically eight terms are required for the convergence of the solutions to within five significant digits.

A homogeneous solution for vessel equation (4.4) is required to exactly satisfy the temperature and heat flux continuity on the interface between the vessels and the tendon. Although an infinite series solution can be constructed for equation (4.4) for the vessels, the determination of the coefficients in this series requires a tedious numerical evaluation. However, one notes that when $\overline{k}$ =1, the homogeneous solution (4.11) satisfies the vessel boundary conditions and energy equation exactly. We, therefore, choose the homogeneous solution for the vessels to be of the same form as the homogeneous solution for the tendon (4.11). When $\overline{k} \neq 1$, this homogeneous solution satisfies temperature continuity exactly, but introduces small errors in the local continuity of heat flux on the vessel surface. Therefore, the solution is approximate when $\overline{k} \neq 1$. However, as shown in chapter 2, the error introduced for $\overline{k} \neq 1$ is insignificant, if the integral of the total flux associated with the

particular solution (4.8) is satisfied exactly.

4.4.3. Model for the Axial Variation of the Temperature and Heat Transfer in the Rat Tail.

The single vessel solution described in section 4.4.2 is used to construct the solution for the two-dimensional temperature field in the three layer model for the rat tail cross-section shown in Fig.22(a), where there are three primary axial vessels, N=3 in (4.12). The two-dimensional solution by superposition is:

$$\theta = \sum_{j=1}^{3} \theta_{s,j} \tag{4.14}$$

where $\theta_{s,j}$ is the single vessel solution for vessel j. The superposed temperature solution for vessel i is :

$$\theta_i = \sum_{j=1}^{3} [\theta_{p,ij} + \theta_{h,ij}], \qquad i=1 \ artery, \quad 2,3 \ vein \tag{4.15}$$

where

$$\theta_{p,ij} = \begin{cases} (\frac{1}{4}\rho_j^2 + \frac{1}{16}\rho_j^4 - \frac{3}{16})Q_j & i=j \\ \frac{\bar{k}}{4}\ln(\rho_j)Q_j & i\neq j \end{cases} \tag{4.16}$$

and

$$\theta_{h,ij} = [c_0]_j + \sum_{n=1}^{\infty} [c_n\rho^n + d_n\rho^{-n}]_j \cos n(\phi - \phi_{v,j}) \tag{4.17}$$

The subscript *j* in (4.17) denotes that the coefficients c_n and d_n are determined by the single vessel solution of vessel *j*, and ϕ_{vj} is the angle of the vessel *j* shown in Fig.22 (a).

Substituting the temperature solutions for the three vessels into the definition of the bulk temperature θ_{ib}:

$$\theta_{ib} = \frac{2}{\pi} \int_0^{2\pi} \int_0^1 \theta_i (1-\rho_i^2) \rho_i d\rho_i d\phi_i \ , \tag{4.18}$$

and evaluating the resulting integrals using residue theory as described in chapter 2, one obtains:

$$\theta_{ib} - c_{0l}\theta_{1b} = \sum_{j=1}^{3} (A_{ij} + Ap_{ij})(\pm \bar{V}_j \bar{a}_j^2 \frac{d\theta_{jb}}{dz}) \tag{4.19}$$

i=1 *artery*, 2, 3 *vein*

where

$$A_{ij} = [c_0^*]_j + \sum_{n=1}^{\infty} [c_n^* \bar{s}_i^n + d_n^* \bar{s}_i^{-n}]_j \tag{4.20}$$

$$c_0 = c_{0l} \frac{\theta_{1b}}{N} + c_0^* Q_j \tag{4.21}$$

and

$$Ap_{ij} = \begin{cases} -\frac{1}{2} Nu & i=j \\ \frac{\bar{k}}{4} \ln \frac{\overline{sp}_{ij}}{\bar{a}_j} & i \neq j \end{cases} \tag{4.22}$$

Nu, the Nusselt number, has the value of 48/11. This is the solution for a radially symmetric heat flux in fully developed pipe flow, see result (2.23) in chapter 2. The coefficients c_n*, d_n* in (4.20) are c_n and d_n (see B(10) and B(11)) scaled by Q_j respectively.

The Runge-Kutta-Verner fifth-order and sixth-order method are used to integrate the system of ordinary differential equations (4.19). The tolerance for the global error control of the integration is 0.0005. Due to the symmetry of vessels 2 and 3, we need only two boundary conditions to solve the coupled equations (4.19). From the definition of the dimensionless artery bulk temperature, θ_{1b}, the first boundary condition is θ_{1b} =1 at Z=0. The second condition is obtained by assuming that the temperature of the tail tip, the distal 2.5 cm, is uniform. Quasisteady tail tip energy conservation requires that the convective energy flux entering the tip be equal to the energy loss at the tip surface

$$\rho_f c_f W_{tip} V_{tip} (\theta_{1b} - \theta_{2b}) = A_{tip} h_{tip} \theta_{tip} \tag{4.23}$$

Here V_{tip} and A_{tip} are tip cutaneous volume and tip surface area, respectively, W_{tip} is the tip blood perfusion rate and θ_{tip} is the mean tip dimensionless surface temperature. An iteration method is used to determine the value of $\theta_{2b,}$ at Z=0. A value for vein temperature $\theta_{2b,}$ at Z=0, is assumed, and (4.19) is integrated to determine θ_{tip} and (θ_{1b}-θ_{2b}) at the tip.

This solution must satisfy (4.23). To integrate the equations (4.19), one needs to know the axial variation of the perfusion in the cutaneous layer, the axial geometry of the three layers and the axial flow M_i in the three major vessels. The tail cutaneous perfusion in the tail base and middle region was assumed to vary linearly along the axis. It is determined from the experimentally measured local perfusion rate at the tail base and middle. In the tail tip , the experimentally measured cutaneous perfusion is the mean value over the distal 2.5 cm of the tail. Based on our anatomical studies, we assume that the thickness of the cutaneous layer is constant along the tail and equal to 0.8 mm. The tapered tail cross-section is assumed to vary linearly with Z with a radius of 5.5 mm at Z=0 and 1.8 mm at Z=L. Blood is supplied from the ventral artery to the cutaneous layer through the microvascular network. The axially varying artery flow rate, M_1, can be related to the local cutaneous perfusion W_c, and the cutaneous cross-sectional area G_c using a continuity of flow condition:

$$M_1 = \int_Z^L G_c W_c \, dZ \tag{4.24}$$

which requires that all the flow leaving the ventral artery enters the cutaneous layer through the local radial supply vessels and lateral artery arcade shown in Fig.12. It is reasonable to treat the vessels as elastic with adjustable radius that changes with flow. From Murray's law and the requirement that the fluid shear stress be constant along the vessel axis, Kamiya et al. [40],

$$\frac{M_i}{a_i^3} = constant \qquad i=1\ artery,\ \ 2,3\ vein \tag{4.25}$$

(4.25) can be used to relate the local blood vessel radius to the local blood flow determined from (4.24).

Using equations (4.24, 4.25), one obtains the local average axial velocity in the vessels:

$$\overline{V_1} = \frac{V_1}{V_o} = \frac{(\int_Z^L G_c\ W_c\ dZ)^{1/3}}{(\int_0^L G_c\ W_c\ dZ)^{1/3}} \qquad for\ artery \tag{4.26}$$

$$\overline{V_2} = \overline{V_3} = \frac{V_2}{V_o} = \frac{1}{2}\frac{a_1^2}{a_2^2}\overline{V_1} = \frac{1}{2}\frac{a_1^2}{a_2^2}\frac{(\int_Z^L G_c\ W_c\ dZ)^{1/3}}{(\int_0^L G_c\ W_c\ dZ)^{1/3}} \qquad for\ vein \tag{4.27}$$

4.5. Parameters Values

The values of several of the parameters used herein are the same as those proposed in Zhu et al. [23]. The Biot number, Bi , which includes both convective and radiative contributions is 0.116. The thermal conductivities of the blood, bone, tendon and

cutaneous tissue are assumed, for a first approximation, to be the same. For this approximation the temperature and heat flux continuity is satisfied exactly on their interfaces. The tail surface, tendon and bone radius are 5.5, 4.7 and 2.5 mm respectively at the tail base Z=0, and the tail surface radius is 1.8 mm at the tip, Z=L=225 mm. The artery and veins are embedded in the tendon annulus at $s_1=s_2=s_3=3.6$ mm with $a_1=a_2=a_3=0.3$ mm at the tail base Z=0. The experimentally measured cutaneous perfusion, used in the calculation, at base, middle and tip are 60.2, 60.7 (ml/100ml min.) and 572.3 (ml/100ml min.) respectively at T_{cent}= 36 ^{0}C, and 13.4, 7.2 (ml/100ml min.) and 208.4 (ml/100ml min.) respectively at T_{cent}= 25 ^{0}C.

5. RESULTS

Fig.23 shows the comparison of the axial surface temperature profile along the top of the tail ($\phi=\pi/2$), predicted by the present model using the measured blood flow rate, with experimental data for a rat at body chamber temperatures (T_{cent}) of 36 ^{0}C and 25 ^{0}C, and tail chamber at 22.5 ^{0}C. Reasonable agreement between the model and the experiment is obtained except that the axial profile is slightly underpredicted at T_{cent}=36 ^{0}C. One possible reason for this underestimation is that there is a small dorsal vein that runs close to the top of the cutaneous layer which, for simplicity, is not considered in the present model. For the thermal stress condition, the dorsal vein may drain some blood back to the tail base. Heat conduction between the dorsal vein and the top cutaneous layer may cause the tail top temperature to be closer to the local vein temperature. This explanation is supported by the fact that the predicted local vein temperature at the tail tip, as shown in Fig.24, is

closer to the measured tail top temperature in Fig.23 at T_{cent}=36 ^{0}C. One observes in Fig.23 that the tail maintains a much higher surface temperature for the conditions of thermal stress, T_{cent} = 36 ^{0}C, than for thermal neutral condition, T_{cent}= 25 ^{0}C, to allow more heat to be dissipated to the environment. It can be estimated from the tail surface temperature profile Fig. 23 that the tail loses about three times as much heat, at T_{cent} =36 ^{0}C, as at T_{cent} =25 ^{0}C. There is a large axial decrease in tail temperature at T_{cent} =25 ^{0}C, whereas at T_{cent} =36 ^{0}C the tail temperature is nearly uniform. This difference is caused mainly by the difference in the axial bulk temperature profile of the ventral supply artery at T_{cent}=25 ^{0}C and T_{cent}=36 ^{0}C, which we discuss next.

Fig.24 shows the axial bulk temperature profiles for the ventral artery and lateral vein predicted by the present model using the measured blood flow rates for a rat at T_{cent} =25 ^{0}C and 36 ^{0}C, and tail chamber at 22.5 ^{0}C. The blood flow in the ventral supply artery functions as a heat source for the rat tail. For the case of thermal stress, T_{cent} =36 ^{0}C, the tail vasodilates its capillaries and the AVA's in its tip and mid regions. This vasodilation causes a large increase (3 to 8-fold) in mid and tip region cutaneous blood perfusion and a large increase in flow in the ventral artery. As observed in Fig.24, the artery bulk temperature decreases very little at these elevated flow rates. However, when the rat is at thermal neutral condition, T_{cent}=25 ^{0}C, no vasodilation occurs. The flow in the ventral artery is very low and there is a dramatic decrease in the axial artery bulk temperature. For these conditions the blood in the ventral artery nearly achieves thermal equilibration with the tail chamber temperature by the time it reaches the tip.

Fig.25 shows the peripheral surface temperature variation, and the artery and vein

bulk temperatures at Z/L=0.5 as predicted by the present model for the same flow conditions as Fig. 24. The peripheral surface temperature reaches a maximum below the ventral artery and a minimum near the lateral veins. The predicted surface temperature difference between the ventral and lateral sites, at T_{cent} =36 ^{0}C, is similar to that at T_{cent} =25 ^{0}C . This temperature difference was used by Young and Dawson [29] as the temperature difference between the ventral artery and lateral veins to investigate the tail vasodilation and vasoconstriction for a rat at various thermal conditions. The validation of this approach was questioned by Raman et al. [15] in their experimental studies. As shown in Fig. 25, there is a significant difference in temperature between the ventral artery bulk temperature and the ventral surface temperature for a rat at both thermal stress and thermal neutral conditions. This variation is mainly due to the significant thermal nonequilibration between the artery and the surrounding tissue. Therefore, the ventral surface temperature is not a good index of the ventral artery temperature.

6. Discussion

The results in Figs. 23 and 25 indicate a significant axial and peripheral tail surface temperature variation. This variation was not treated in the simple rat tail model of Raman et al. [14]. Their model assumes that the whole tail is at a uniform temperature, which is equal to the water temperature in which the tail was immersed in their experiment. Their model, therefore, applies only to the conditions of their experiment, which is physiological non-realistic for a non-aquatic mammal. Raman et al. also assume that the blood flow along the ventral artery to the tip without bleed-off and then is shunted via a valve to either

a deep or superficial vein. Three thermal conductances and a blood distribution parameter were introduced, and then determined by curve fitting their experimental data. The major limitations and questions that arise from these assumptions and approach are: (1) The model can not be used to describe rat tail heat transfer under common thermal conditions, a tail in air, where the tail surface temperature is variable as shown in Fig. 23 and Fig. 25. It can been estimated from Chapman [38] that the heat loss of a tail in water is more than 10 times as great as that in air under similar conditions. (2) The ventral vein was treated as a deep vein in their model and served a major role in the tail thermoregulation. However, the anatomical and experimental studies of Thorington [32], Young and Dawson [29] and chapter 3 have shown that the small ventral vein is not a major conduit for axially returning blood. The good agreement between the tail axial surface temperature profile measured by our experiment and the one predicted by the present model, where this vein is neglected, provides further evidence that the small ventral vein does not play a major role in the tail heat transfer. Physiologically, for a rat subject to thermal stress, it is more efficient for the rat to vasodilate its tail capillaries and AVA's to allow a higher blood perfusion in its cutaneous layer and thus more heat to be dissipated to the environment, instead of shunting its blood from its ventral vein to the lateral veins. As shown in Fig. 23 the axial uniformity of the surface temperature under conditions of thermal stress is due to the ventral artery supply and there is little countercurrent exchange, as also predicted by Raman et al. [14] for the rat tail in water. (3) Their model did not consider the microcirculation in the perfused cutaneous layer. Blood can only reach the large axial veins by first passing through the microcirculation. Weinbaum et al. [41] have shown that the most significant heat

transfer occurs in vessels that are smaller than 200 μm in size. Since the blood must first pass through the microcirculation, it has to equilibrate thermally with the local cutaneous layer before it reaches the large axial veins. If one follows this reasoning to its logical conclusion, it is evident that the only way a deep venous return path could conserve heat is if the blood in the vein, which first lost its heat in passage through the microcirculation, picked up heat from countercurrent exchange with the blood supply in the ventral artery. This disagrees, however, with one of the major conclusions of the model in Raman et al. [14], which predicts that such countercurrent exchange is so small as to be insignificant. All these arguments indicate that the shunting of blood to a "deep" ventral vein does not occur in the rat tail.

Figure 6 shows that there is a significant difference between θ_c and θ_{1b} compared to the small difference between θ_c and θ_{2b}. In principle the source term $\beta_c^2(\theta_c - \theta_{1b})$ in the Pennes equation (4.2) should be replaced by $\beta_c^2(\theta_{2b} - \theta_{1b})$. Since the temperature difference between the θ_c and θ_{2b} is small, the error caused by the assumption in the Pennes equation (4.2) that the blood equilibrate to the local tissue before it returns to the vein is minor. However for other applications of the model, such as the human limb, the temperature difference between the flow back of the blood and the venous blood should be considered.

4.8. Conclusions

(1) The model developed herein takes into account the axial variations in tail anatomy and our experimental observations of the axial blood flow distribution in the tail at different local and central temperatures. The predictions of the model show good

agreement with the axial surface temperature distribution in the rat tail reported in chapter 3. (2) A new approach is presented to treat the multi-vessel heat transfer problem as the superposition of single vessel solutions by constructing a new governing equation (4.7) to describe the heat transfer in the blood perfused cutaneous layer. (3) Because of the anatomical similarity of the rat tail and the human digit: long tapered cylinder, blood perfused cutaneous layer, large center bone region, axial parallel vessels embedded in the tendon tissue and high density of AVA's at the tip, the rat tail model can be readily extended to describe the heat transfer in the human digit. This multi-vessel solution approach can also be used to improve the human limb model proposed in Zhu et al. [23] by eliminating the limitation of small vessel eccentricity in the core region and providing a better description of the heat transfer in the blood perfused cutaneous layer. (4) Since the new solution approach allows the vessel number and location to be arbitrary, the general approach can also be used to resolve the long standing controversy as to whether there is a significant shunting of venous blood between the superficial and deep veins in the human limb and digit. This question does not arise in the rat tail since our anatomical studies show that the major axial veins are superficial and located near the tendon interface with the cutaneous layer.

Chapter 5. Conclusion

An approximate three-dimensional analytic solution is presented in chapter 2 for describing the heat transfer from a cylinder with two or more axially interacting eccentrically embedded vessels. The cylinder exchanges heat by convection with the environment and has a non-uniform surface temperature due to the vessel eccentricity. The flow in the vessels can be either countercurrent or unidirectional. The primary objective in obtaining this new solution is to develop a three dimensional variable geometry non-uniform perfusion model for rat tail heat transfer. This fundamental configuration can also be used as a building block for modeling heat transfer in the human limb and digit. The solution is constructed by superposition of a new solution for a single embedded vessel which exactly satisfies the boundary conditions when the thermal conductivity of the fluid is equal to that of the cylinder material and is a very good approximation when these conductivities are not equal. The solution allows for an arbitrary location of the embedding vessels. This is of special interest in the heat transfer modeling of the human limb, digit and the rat tail, where the major blood vessels are located far away from the axis. The theory can be readily extended to applications where the number of the vessels is more than two. Axial variation of the vessels and the embedding medium can also be taken into consideration in this solution as well as axial bleed off. With minor modification the method of solution can be applied to the case of two dissimilar fluids. Such applications are common in engineering systems.

The tail anatomical structure and the thermoregulatory function of tail blood flow have been investigated in chapter 3. The tail has only one major supply artery, the ventral

artery. As the ventral artery approaches the tail tip, its diameter remains relatively large even though the cross-sectional area of the tail is greatly reduced. The high density of arteriovenous anastomose, AVA's, occurs at the distal end of the tail. The dimensions of the deeper ventral vein is typically 1/4 to 1/3 the more superficial lateral veins, which are 300-600 μm at the midtail. These tail vascular structures suggest that: (1.) The ventral vein is not a major conduit for axially returning blood, thus the shunting of the blood to a deep vein as proposed in [14] is highly unlikely. (2.) The tail volumetric flow is not uniform along the tail. A very high blood flow can be maintained in the tip region.

The blood flow within the tail changes as a function of the air temperatures surrounding the tail T_{loc} and the torso T_{cent}. Changing the rat tail thermal conditions results in similar changes of the tail blood flow at the tail base and middle. The major thermoregulatory function of the tail is to increase the tail heat loss for a rat subject to body heating. The tail can lose about three times as much heat at T_{cent}=36 °C, as T_{cent} =25 °C. This significant increase in tail heat loss is achieved through the regulation of the tail's cutaneous circulation. The control model for tail blood flow regulation differs depending on the axial location: there is an on-off control in the tail mid and tip regions, whereas there is a proportional increase in local perfusion with the rat core temperature in the tail base region for rats under body heating. Changing T_{cent} from neutral to high caused BF_{mid} to increase 742% while BF_{base} increased only 313%; All BF increases were similar (163% and 136%) when T_{loc} was changed from neutral to high. The blood flow in the tail tip is more than 10 to 11-fold higher than that in the tail middle and base. This is in accordance with the tail's anatomical structure which shows that the tail has its highest density AVA's

in its tip region. The experimental results suggest that shunting of blood to "deep " veins proposed by Raman et al [14]. probably does not occur. Rather, the blood perfusion in the middle and distal regions of the tail is abruptly increased or decreased to control heat loss.

Our experimental studies in chapter 3 indicated that current views of the blood flow distribution pattern in the major axial arteries and veins and in the microcirculation need revision. In chapter 4, a new analytical three-dimensional rat tail heat transfer model is presented to determine the axial temperature distribution and the heat transfer which considers these important new experimental observations. The model also takes into account the pattern of blood flow distribution to the tail at different local and central temperatures. The model considers three concentric layers; bone, tendon and cutaneous (skin), having different conductivities. The Pennes bioheat equation is used to model blood perfusion in the cutaneous layer and a Laplace equation is employed in the tendon layer. In addition, the rat tail has three major axial vessel pairs, one ventral and two lateral, which are embedded in the tendon at the interface with the cutaneous layer. The predictions of the model show good agreement with the experimentally measured axial surface temperature distribution in the rat tail. A new approach is presented to treat the multi-vessel heat transfer problem as the superposition of single vessel solutions, by constructing a new governing equation to describe the heat transfer in the blood perfused cutaneous layer. Because of the anatomical similarity of the rat tail and the human digit: long tapered cylinder, blood perfused cutaneous layer, large center bone region, axial parallel vessels embedded in the tendon tissue and high density of AVA's at the tip, the rat tail model can be readily extended to describe the heat transfer of the human digit. The multi-vessel solution can also

be used to improve the human limb model [23] by eliminating the limitation of small vessel eccentricity in the core region and providing a better description of the heat transfer in the blood perfused cutaneous layer. Since the new solution approach allows the vessel number and location to be arbitrary, the general approach can be used to investigate the long standing controversy as to whether there is a significant shunting of venous blood between the superficial and deep veins in the human limb and digit. This question does not arise in the rat tail since our anatomical studies show that the major axial veins are superficial and located near the tendon interface

In conclusion, the present research has led to a better understanding of the fundamental mechanism of the rat tail thermoregulation and its microvascular heat transfer. Similar experimental studies can be carried out for the human limb and human digit to investigate the axial distribution of the blood flow and its thermoregulatory function. The theoretical model has provided a much more accurate description of the temperature profiles and the macro and microvascular heat transfer mechanisms in the rat tail than previous studies and new insight into the thermoregulatory structure-function relation of the tail.

Appendix A

The purpose of this appendix is to show how the coefficients a_0 and a_n in equation (2.14) can be analytically evaluated. Substituting (2.14) into boundary condition (2.6) yields

$$\sum_{n=1}^{\infty} a_n n\rho_R^{n-1}\cos n\phi+\frac{\bar{k}}{4}\frac{\rho_R-\bar{s}_a\cos\phi}{\rho_R^2+\bar{s}_a^2-2\rho_R\bar{s}_a\cos\phi} = -\frac{B_i}{\rho_R}(a_0+\sum_{n=1}^{\infty} a_n\rho_R^n cosn\phi+\frac{\bar{k}}{8}\ln(\rho_R^2+\bar{s}_a^2-2\rho_R\bar{s}_a\cos\phi)) \tag{A1}$$

If (A1) is integrated over ϕ from 0 to 2π all the a_n terms vanish except a_0 and one obtains

$$a_0=-\frac{\bar{k}}{4}(\frac{1}{B_i}+\ln\rho_R) \tag{A2}$$

If one multiplies equation (A1) by cosmϕ and then integrates term by term over the interval $0\le\phi\le2\pi$, one obtains for each of the terms on the right hand side of (A1)

$$\int_{-\pi}^{\pi} a_0 cosm\phi d\phi=0 \tag{A3}$$

$$\int_{-\pi}^{\pi}(\sum_{n=1}^{\infty} a_n n\rho_R^n cosn\phi)cosm\phi d\phi=ma_m\rho_R^m\pi \tag{A4}$$

and

$$\int_{-\pi}^{\pi} \frac{\bar{k}}{8} \ln(\rho_R^2 + \bar{s}_a^2 - 2\rho_a \bar{s}_a \cos\phi) \cos m\phi \, d\phi = -\frac{\bar{k}\rho_a \bar{s}_a}{4m} \int_{-\pi}^{\pi} \frac{\sin\phi \sin m\phi}{\rho_R^2 + \bar{s}_a^2 - 2\rho_R \bar{s}_a \cos\phi} d\phi \tag{A5}$$

where the right hand side of (A5) is obtained after integration by parts. We define the integral I_1 by

$$I_1 = \int_{-\pi}^{\pi} \frac{\sin\phi \cos m\phi}{\rho_R^2 + \bar{s}_a^2 - 2\rho_R \bar{s}_a \cos\phi} d\phi \tag{A6}$$

and denote the integral in (A5) by

$$I_2 = \int_{-\pi}^{\pi} \frac{\sin\phi \sin m\phi}{\rho_R^2 + \bar{s}_a^2 - 2\rho_R \bar{s}_a \cos\phi} d\phi \tag{A7}$$

so that their sum

$$I_1 + iI_2 = \int_{-\pi}^{\pi} \frac{\sin\phi (\cos m\phi + i \sin m\phi)}{\rho_R^2 + \bar{s}_a^2 - 2\rho_R \bar{s}_a \cos\phi} d\phi \tag{A8}$$

can be treated by a contour integration in the complex plane.

Introducing the complex variable $\Omega = Re^{i\phi}$, when $d\phi = -id\Omega/\Omega$ on the unit circle R=1, the integral (A8) can be written as a contour integration around the unit circle in the complex plane

$$I_1+iI_2=\oint\frac{1}{2\rho_R\bar{s}_a}\frac{(\Omega^2-1)\Omega^{m-1}}{\Omega^2+\frac{\rho_R^2+\bar{s}_a^2}{\rho_R+\bar{s}_a}\Omega+1}d\Omega \tag{A9}$$

Using residue theory, the integral (A9) can be evaluated as

$$I_1+iI_2=\frac{\pi i}{\rho_R\bar{s}_a}\left(\frac{\bar{s}_a}{\rho_R}\right)^m \tag{A10}$$

$$\int_{-\pi}^{\pi}\frac{\bar{k}}{8}\ln(\rho_R^2+\bar{s}_a^2-2\rho_a\bar{s}_a\cos\phi)cosm\phi d\phi=-\frac{\bar{k}\pi}{4m}\left(\frac{\bar{s}_a}{\rho_R}\right)^m \tag{A11}$$

The integral obtained from the second term on the left hand side (A1) can be evaluated by a similar procedure. The contour integration on the unit circle in the Ω plane in this case leads to

$$\int_{-\pi}^{\pi}\frac{\bar{k}}{4}\frac{\rho_R-\bar{s}_a\cos\phi}{\rho_R^2+\bar{s}_a^2-2\rho_R\bar{s}_a\cos\phi}cosm\phi d\phi=\frac{\bar{k}\pi}{4\rho_R}\left(\frac{\bar{s}_a}{\rho_R}\right)^m \tag{A12}$$

Combining results (A4), (A11), and (A12), one obtains the following expression for the coefficient a_n

$$a_n=\frac{\bar{k}}{4(n+B_i)\rho_R^n}\left(\frac{B_i}{n}-1\right)\left(\frac{\bar{s}_a}{\rho_R}\right)^n \tag{A13}$$

APPENDIX B

The purpose of this appendix is to show how the coefficients a_0, b_0, c_0, e_0, a_n, b_n, c_n, d_n and e_n in equations (4.11- 4.13) can be analytically evaluated. After transforming the local vessel coordinates ρ_i, ϕ_i in the tendon particular solution (4.9) to the bone centered coordinates ρ, ϕ and combining the resulting equation with the tendon homogeneous solution (4.10), we obtain:

$$\theta_t = [c_o + \sum_{n=1}^{\infty} (c_n \rho^n + d_n \rho^{-n}) cosn\phi] + \frac{\bar{k}}{4}[\frac{1}{2}\ln(\rho^2 + \bar{s}_i^2 - 2\rho \bar{s}_i \cos\phi) - \ln \bar{a}_i^2] Q_i \qquad \text{(B1)}$$

for the tendon. The boundary condition on the outside cutaneous surface is equation (4.6) and the boundary conditions on the interface between the bone, tendon and cutaneous layer are temperature and heat flux continuity. Substituting the cutaneous layer temperature solution (4.12) into boundary condition (4.6), one obtains:

$$\begin{aligned} & a_0 I_1(\beta_c \rho_R) - b_0 K_1(\beta_c \rho_R) + \sum_{n=1}^{\infty} [a_n \frac{I_{n-1}(\beta_c \rho_R) + I_{n+1}(\beta_c \rho_R)}{2} - b_n \frac{K_{n-1}(\beta_c \rho_R) + K_{n+1}(\beta_c \rho_R)}{2}] \cos n\phi \\ & = -\frac{Bi}{\beta_c \rho_R}[a_0 I_0(\beta_c \rho_R) + b_0 K_0(\beta_c \rho_R) + \sum_{n=1}^{\infty} (a_n I_n(\beta \rho_R) + b_n K_n(\beta \rho_R)) \cos n\phi + \frac{\theta_{1b}}{N}] \end{aligned} \qquad \text{(B2)}$$

Applying orthogonal integration to (B2), converting the resulting integrals into contour integrals in the complex plane and then using the residue theory, one obtains the following equations for the coefficients:

$$a_0[I_1(\beta_c \rho_R) + \frac{Bi}{\beta_c \rho_R} I_o(\beta_c \rho_R)] - b_o[K_1(\beta_c \rho_R) - \frac{Bi}{\beta_c \rho_R} K_o(\beta_c \rho_R)] = -\frac{Bi}{\beta_c \rho_R} \frac{\theta_{1b}}{N} \qquad \text{(B3)}$$

and

$$a_n\left[\frac{I_{n-1}(\beta_c\rho_R)+I_{n+1}(\beta_c\rho_R)}{2}+\frac{Bi}{\beta_c\rho_R}I_n(\beta_c\rho_R)\right]- b_n\left[\frac{K_{n-1}(\beta_c\rho_R)+K_{n+1}(\beta_c\rho_R)}{2}-\frac{Bi}{\beta_c\rho_R}K_n(\beta_c\rho_R)\right]=0 \tag{B4}$$

Substituting the infinite series expressions for the temperature in the bone, tendon and cutaneous layer, equations (B1) and (4.12, 4.13), into boundary conditions for the continuity of temperature and heat flux, one obtains an infinite series of algebraic expressions for the coefficients. Applying orthogonal integration to these resulting equations, and evaluating these integrals in the same manner as described for (B2), one obtains the equivalent expressions to (B3, B4) for the remaining coefficients. The final expressions for the coefficients a_0, b_0, c_0, e_0 a_n, b_n, c_n, d_n and e_n in equations (4.11-4.13) are:

$$a_0=\frac{\frac{Bi}{\beta_c\rho_R}K_1(\beta_c\rho_t)\frac{\theta_{1b}}{N}+\frac{k_1}{\beta_c\rho_t}\left[K_1(\beta_c\rho_R)-\frac{Bi}{\beta_c\rho_R}K_0(\beta_c\rho_R)\right]\frac{\bar{k}}{4}Q_i}{\Delta_0} \tag{B5}$$

$$b_0=\frac{\frac{Bi}{\beta_c\rho_R}I_1(\beta_c\rho_t)\frac{\theta_{1b}}{N}+\frac{k_1}{\beta_c\rho_t}\left[I_1(\beta_c\rho_R)+\frac{Bi}{\beta_c\rho_R}I_0(\beta_c\rho_R)\right]\frac{\bar{k}}{4}Q_i}{\Delta_0} \tag{B6}$$

$$\begin{aligned}c_0 &= a_0 I_0(\beta_c\rho_t)+b_0 K_0(\beta_c\rho_t)+\frac{\theta_{1b}}{N}-\frac{\bar{k}}{4}\ln\frac{\rho_t}{\bar{a}_i}Q_i \\ &= c_{0l}\frac{\theta_{1b}}{N}+c_0^{*}Q_i\end{aligned} \tag{B7}$$

and

$$e_0 = c_0 + \frac{\bar{k}}{4} \ln \frac{\bar{s}_i}{\bar{a}_i} Q_i \tag{B8}$$

where

$$\Delta_0 = I_1(\beta_c \rho_t)[K_1(\beta_c \rho_R) - \frac{Bi}{\beta_c \rho_R} K_0(\beta_c \rho_R)] + K_1(\beta_c \rho_t)\ [I_1(\beta_c \rho_R) + \frac{Bi}{\beta_c \rho_R} I_0(\beta_c \rho_R)] \tag{B9}$$

and

$$c_n = \frac{\frac{\bar{k}}{4n} Q_i [\rho_t^n (\frac{\bar{s}_i}{\rho_t})^n - \frac{1-k_2}{1+k_2} \rho_b^n (\frac{\rho_b}{\bar{s}_i})]}{\frac{1-\Delta_n}{1+\Delta_n} \rho_t^{2n} - \frac{1-k_2}{1+k_2} \rho_b^{2n}} = c_n^* Q_i \tag{B10}$$

$$d_n = \rho_b^n [\frac{\bar{k}}{4n} Q_i (\frac{\rho_b}{\bar{s}_a})^n - c_n \rho_b^n] \frac{1-k_2}{1+k_2} = d_n^* Q_i \tag{B11}$$

$$b_n = \frac{c_n \rho_t^{\ n} + d_n \rho_t^{\ -n} - \frac{\bar{k}}{4n} (\frac{\bar{s}_i}{\rho_t})^n\ Q_i}{\Delta_{1n} I_n(\beta_c \rho_t) + K_n(\beta_c \rho_t)} \tag{B12}$$

$$a_n = \Delta_{1n} b_n \tag{B13}$$

$$e_n = \rho_b^{-n} \left[c_n \rho_b{}^n + d_n \rho_b{}^{-n} - \frac{\bar{k}}{4n} \left(\frac{\rho_b}{\bar{s}_i} \right)^n Q_i \right] \tag{B14}$$

where

$$\Delta_n = \frac{\dfrac{n k_1}{\beta_c \rho_c} \left[\Delta_{1n} I_n(\beta_c \rho_t) + K_n(\beta_c \rho_t) \right]}{\Delta_{1n} \dfrac{I_{n-1}(\beta_c \rho_t) + I_{n+1}(\beta_c \rho_t)}{2} - \dfrac{K_{n-1}(\beta_c \rho_t) + K_{n+1}(\beta_c \rho_t)}{2}} \tag{B15}$$

and

$$\Delta_{1n} = \frac{\dfrac{K_{n-1}(\beta_c \rho_R) + K_{n+1}(\beta_c \rho_R)}{2} - \dfrac{Bi}{\beta_c \rho_R} K_n(\beta_c \rho_R)}{\dfrac{I_{n-1}(\beta_c \rho_R) + I_{n+1}(\beta_c \rho_R)}{2} + \dfrac{Bi}{\beta_c \rho_R} I_n(\beta_c \rho_R)} \; . \tag{B16}$$

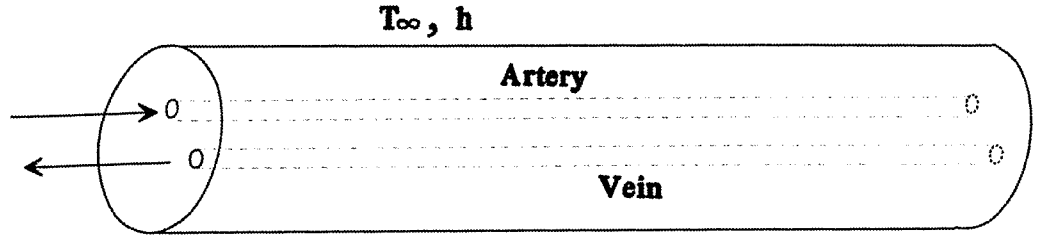

1. Schematic of countercurrent vessels embedded in surrounding medium cylinder.

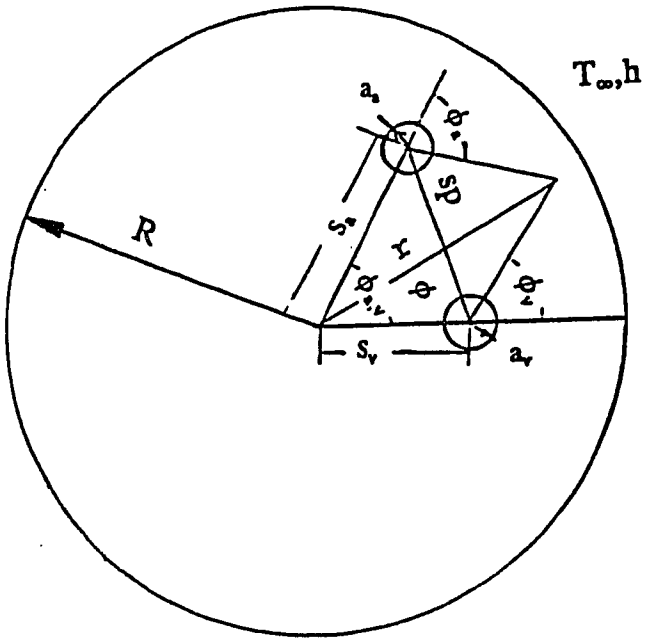

2. The geometry of the cross-sectional plane and coordinate system.

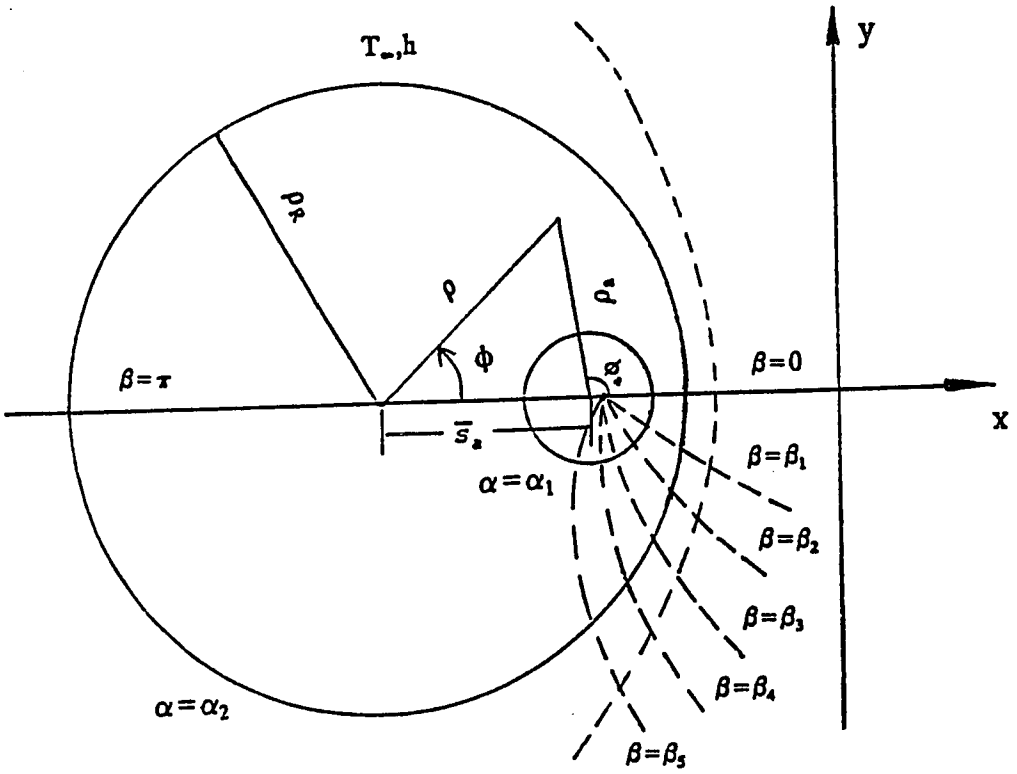

3. Radial coordinate and bicylindrical coordinate system for single vessel.

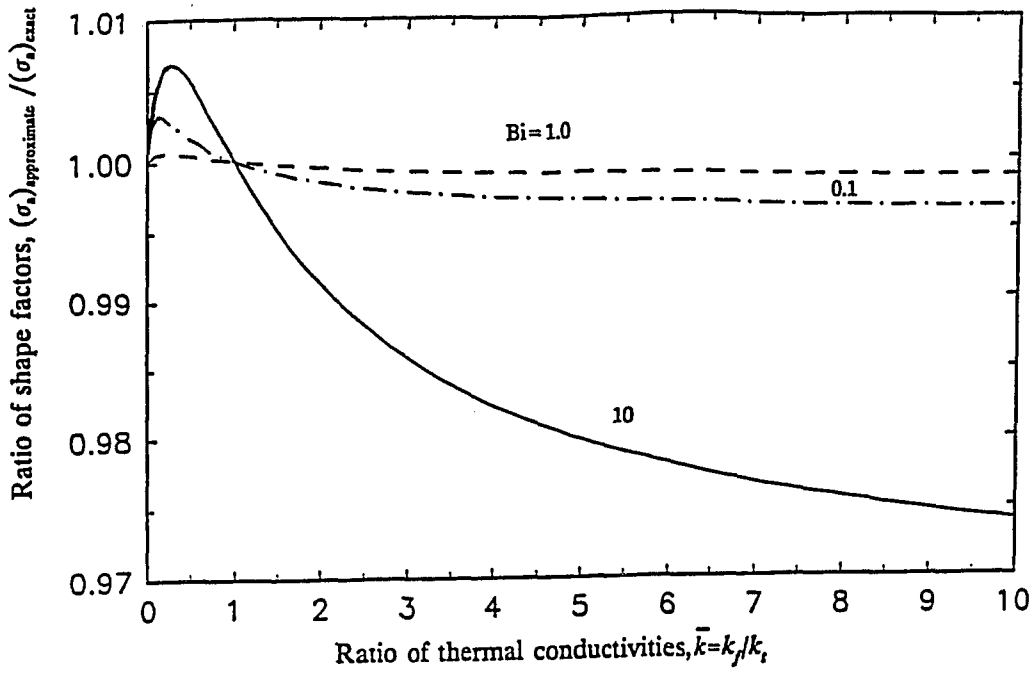

4. Effect of conductivity ratio $\overline{k}$ on the accuracy of single vessel shape factor. Comparison between approximate and exact (conformal mapping) results for $\rho_R=5$ and $\overline{s}_a=3.5$.

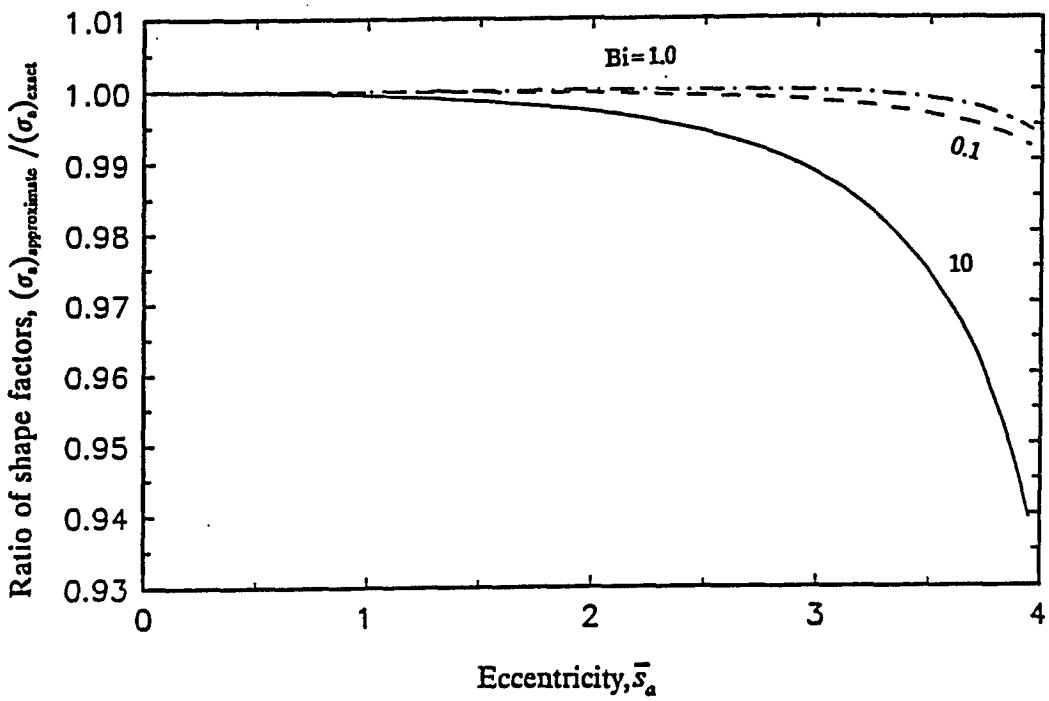

5. Effect of eccentricity $\bar{s}_a$ on the accuracy of single vessel shape factor. Comparison between approximate and exact (conformal mapping) results for $\rho_R=5$ and $\bar{k}=10$.

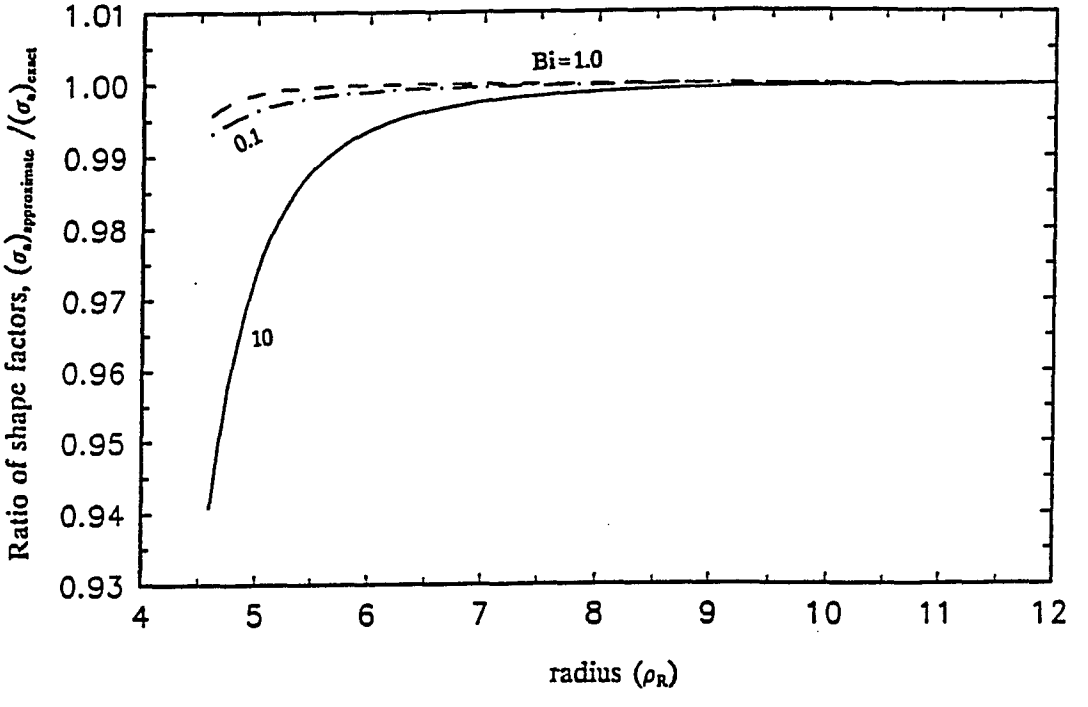

6. Effect of cylinder size ρ_R on the accuracy of single vessel shape factor. Comparison between approximate and exact (conformal mapping) results for $\overline{s}_a=3.5$ and $\overline{k}=10$.

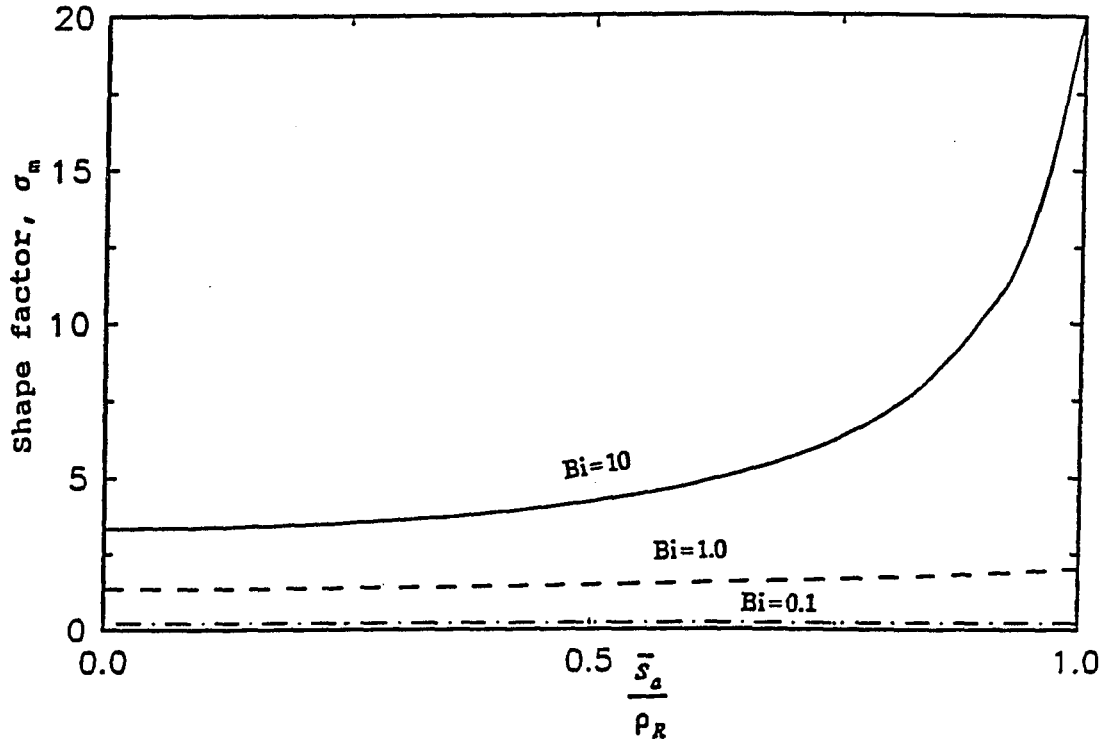

7. Matrix shape factor for countercurrent vessels for $\bar{s}_a = \bar{s}_v$ and $\bar{k} = 1$.

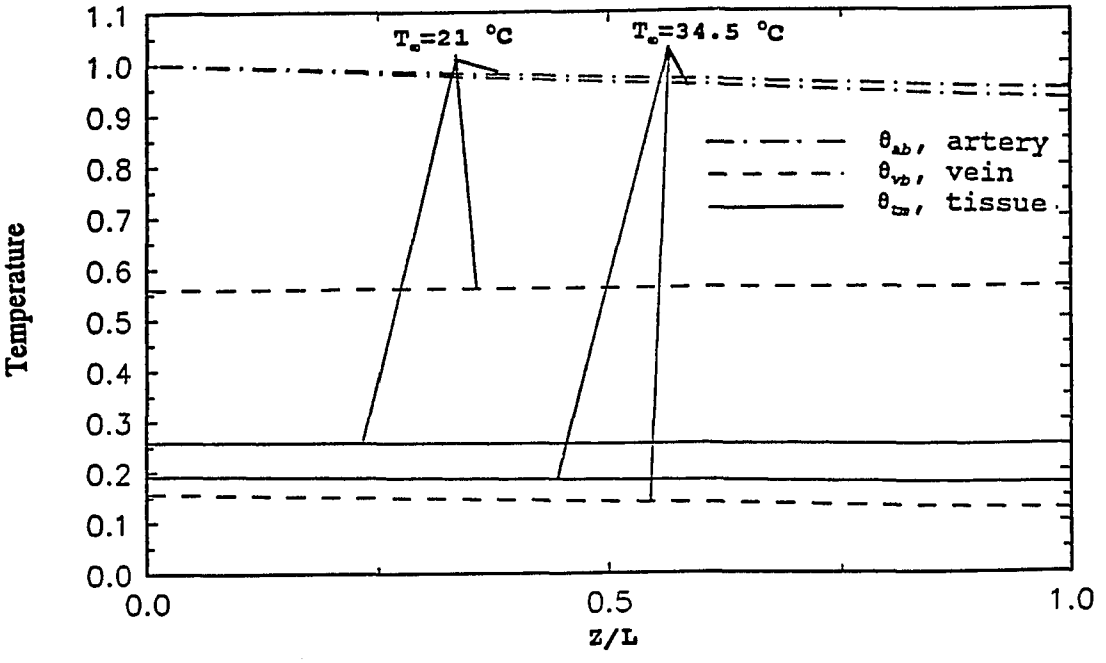

8. Effect of environment temperature on the axial variation of the artery and vein bulk temperature and the tissue mean temperature for countercurrent heat exchange for $\rho_R=12$, $\overline{s}_a=\overline{s}_v=8$, $\overline{sp}=3$, $\overline{V}=1$, $\overline{a}_v=1$, $\overline{k}=1$, Pe=3500 and Bi=1.48.

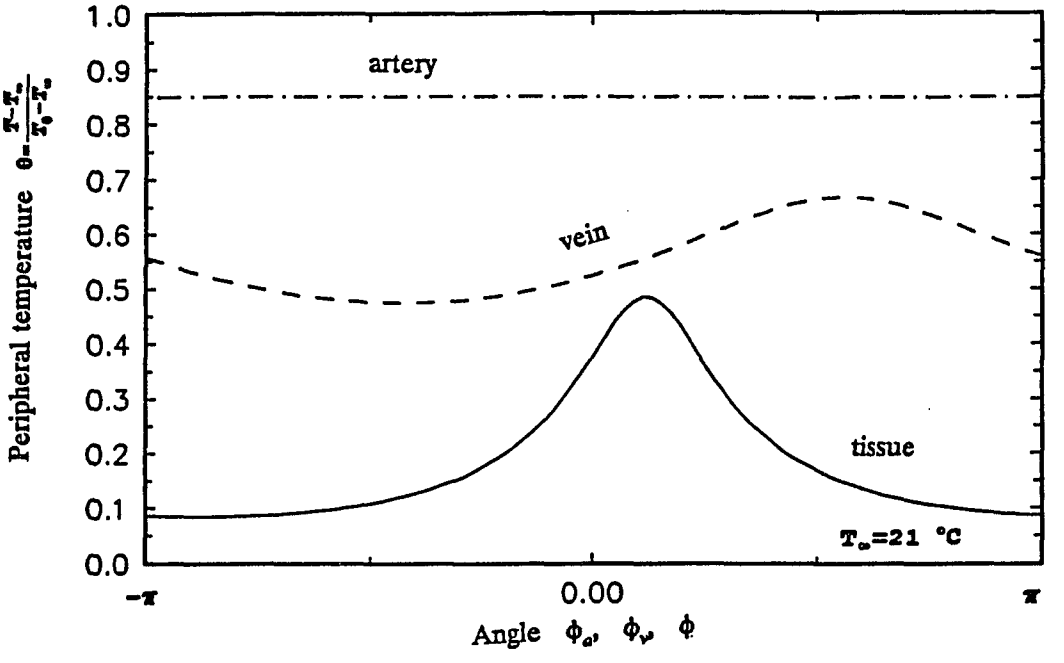

9. Peripheral surface temperature variation for the artery, vein and arm at cross-section Z/L=0.5, for Bi=1.48, ρ_R=12, $\overline{s}_a=\overline{s}_v$=8, $\overline{sp}$=3, $\overline{V}$=1, $\overline{a}_v$=1, $\overline{k}$=1, Pe=3500 and T_∞=21 °C.

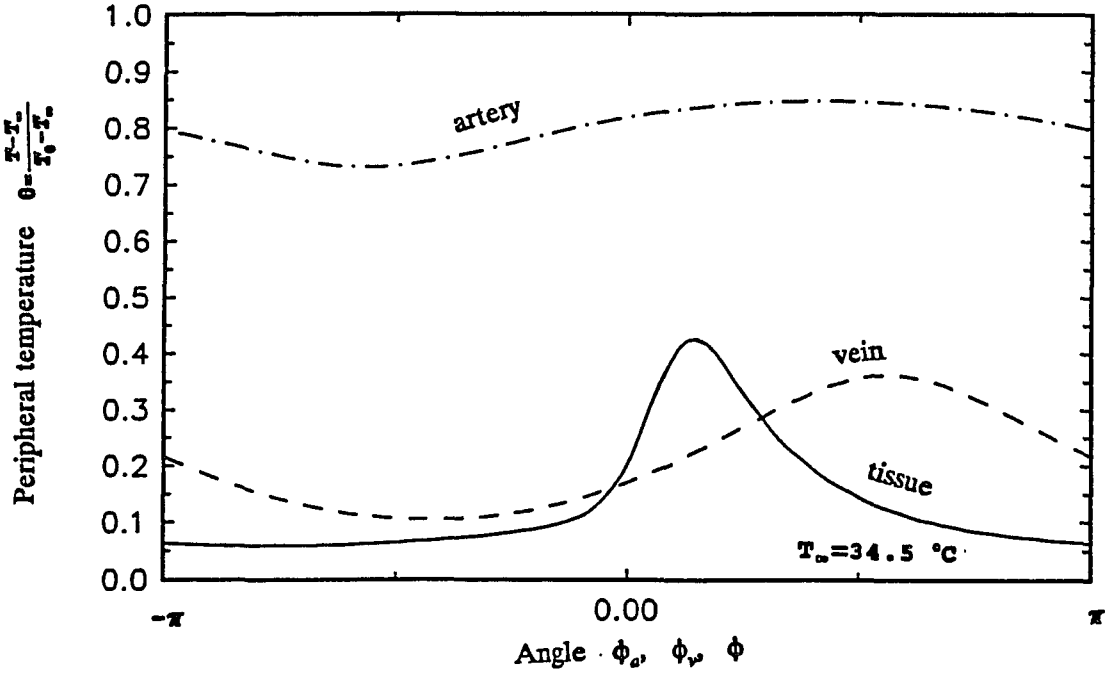

10. Peripheral surface temperature variation for the artery, vein and arm at cross-section Z/L=0.5, for Bi=1.48 , ρ_R=12, $\overline{s}_a=\overline{s}_v$=8, $\overline{sp}$=3, $\overline{V}$=1, $\overline{a}_v$=1, $\overline{k}$=1, Pe=3500 and T_∞=34.5 °C.

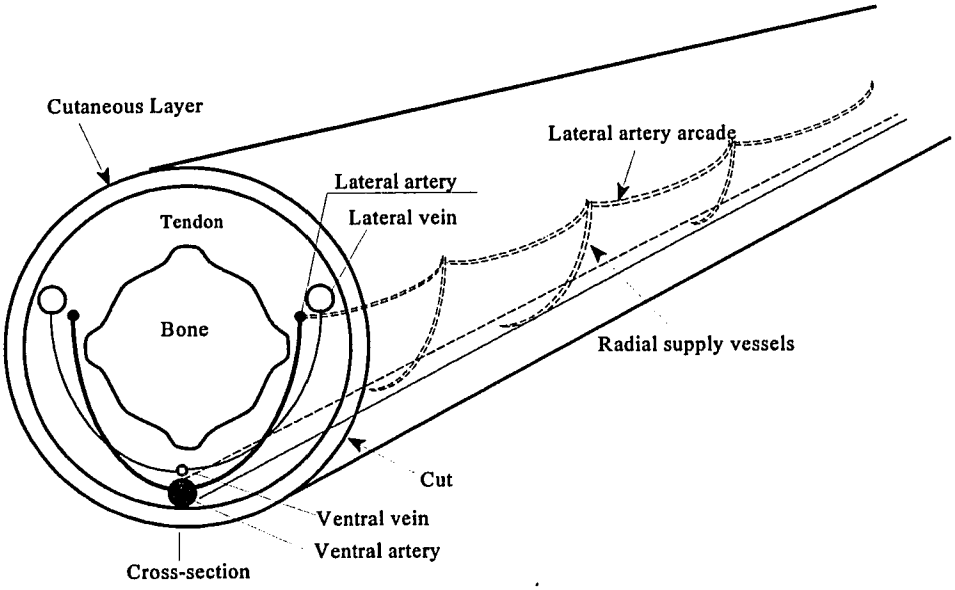

11. Schematic diagram of the rat tail.

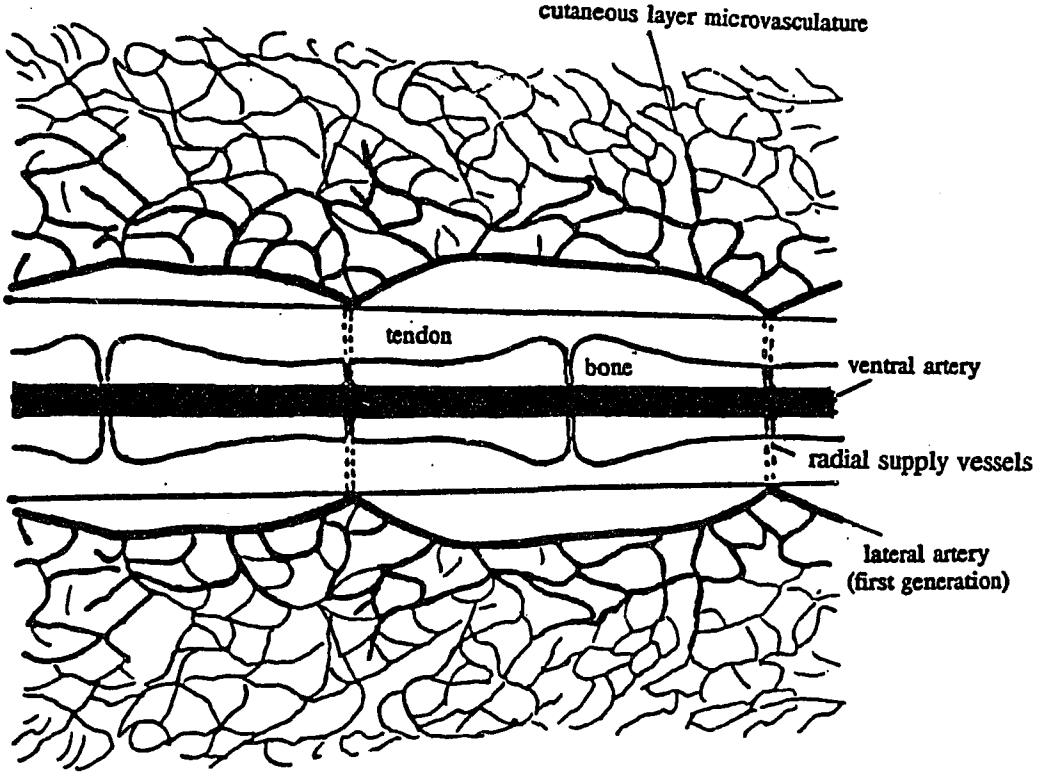

12. Ventral view of the vascular structure of the rat tail.

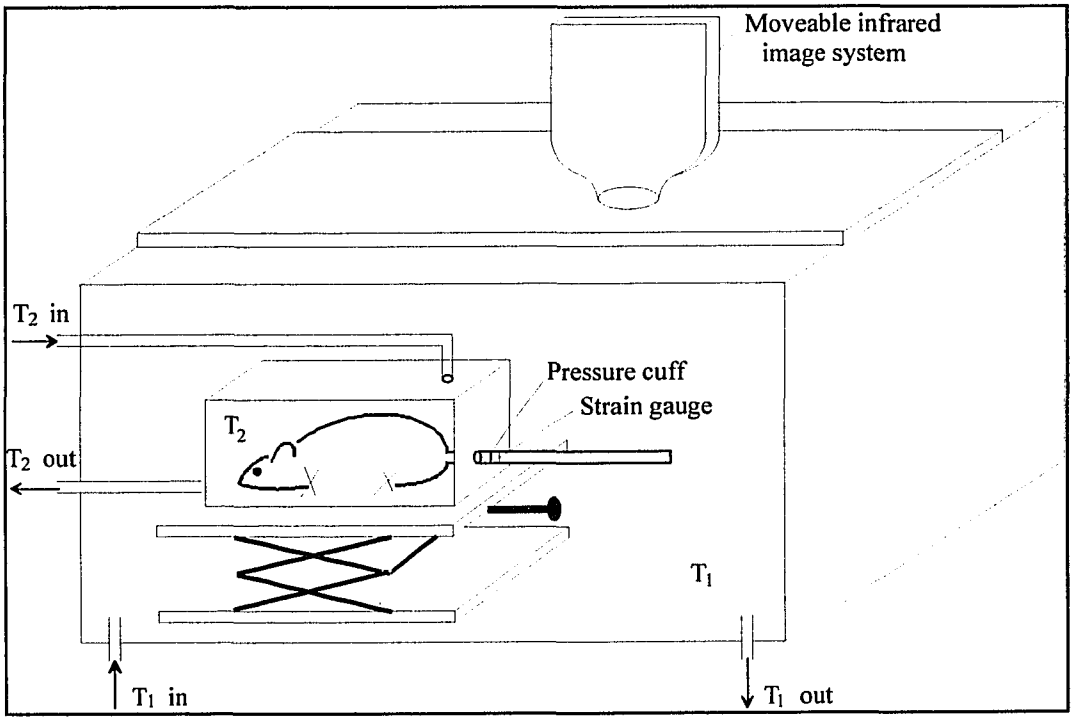

13. Apparatus for the temperature and blood flow measurement of the rat tail.

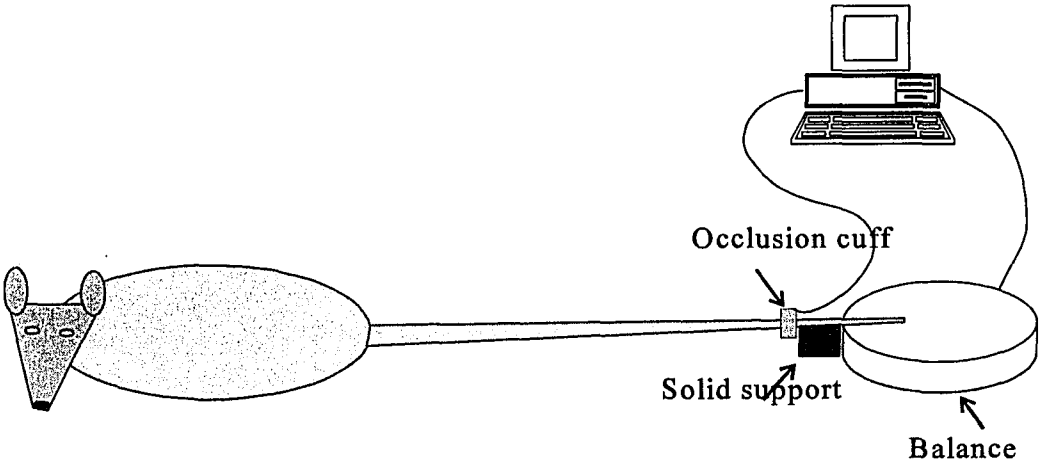

14. Technique for measuring tail tip blood flow. The tail is stabilized by a solid block that is flush with the top of the balance. The balance is connected to a computer which collects the data and controls the cuff inflation.

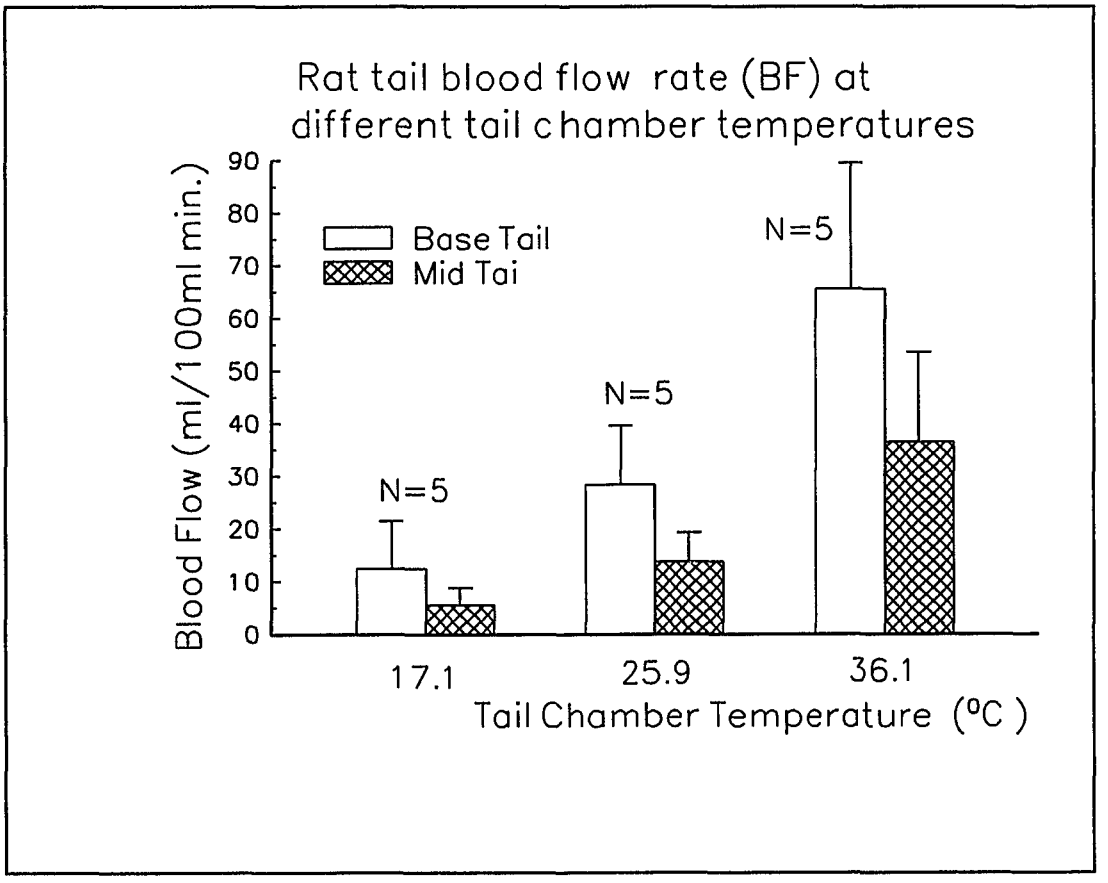

15.a Base and mid tail blood flow rates (BF) at different tail chamber (outer enclosure) temperatures for conscious rats. Rat torso chamber temperature was 26 °C. Error bars are ±1 STD.

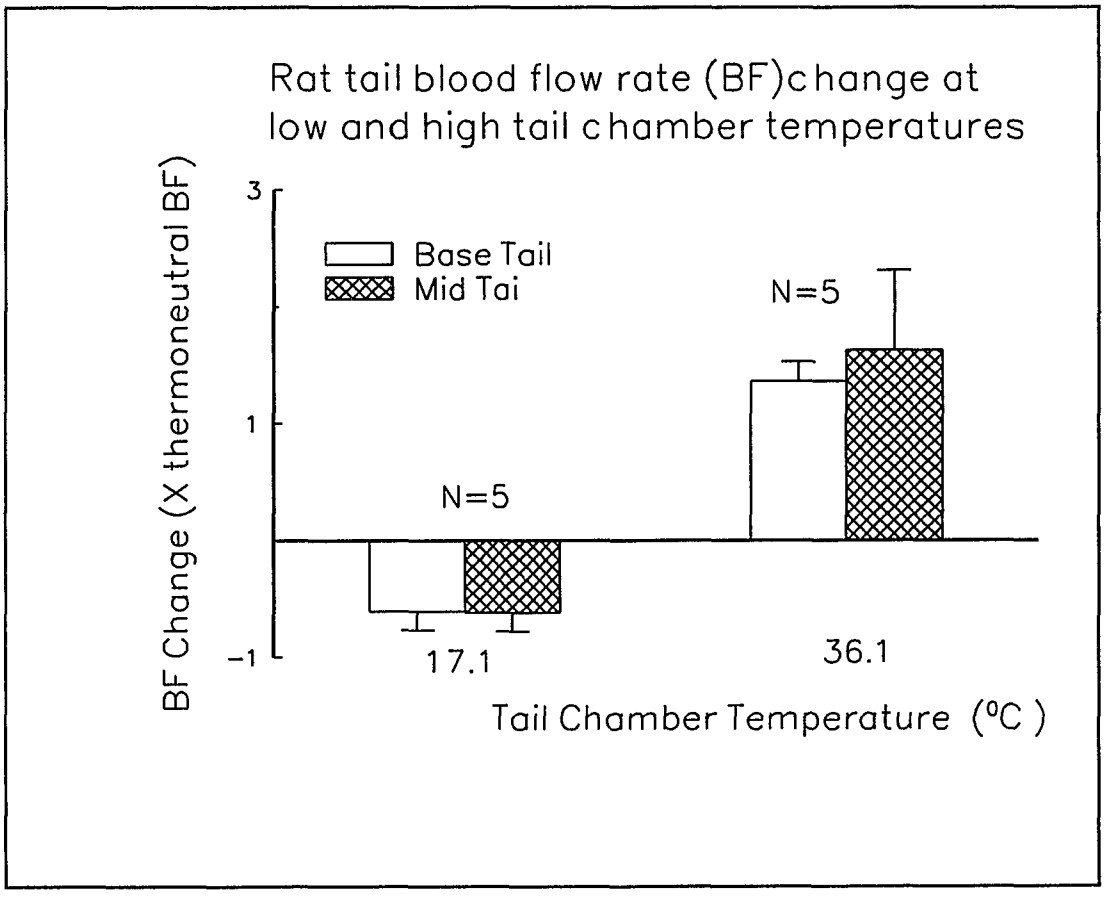

15.b Base and mid tail blood flow rate(BF) changes from thermoneutral (25.9 ^{0}C) BF to high and low tail chamber (outer enclosure) temperatures for conscious rats. Torso chamber temperature was 26 ^{0}C. Error bars are ± 1 STD.

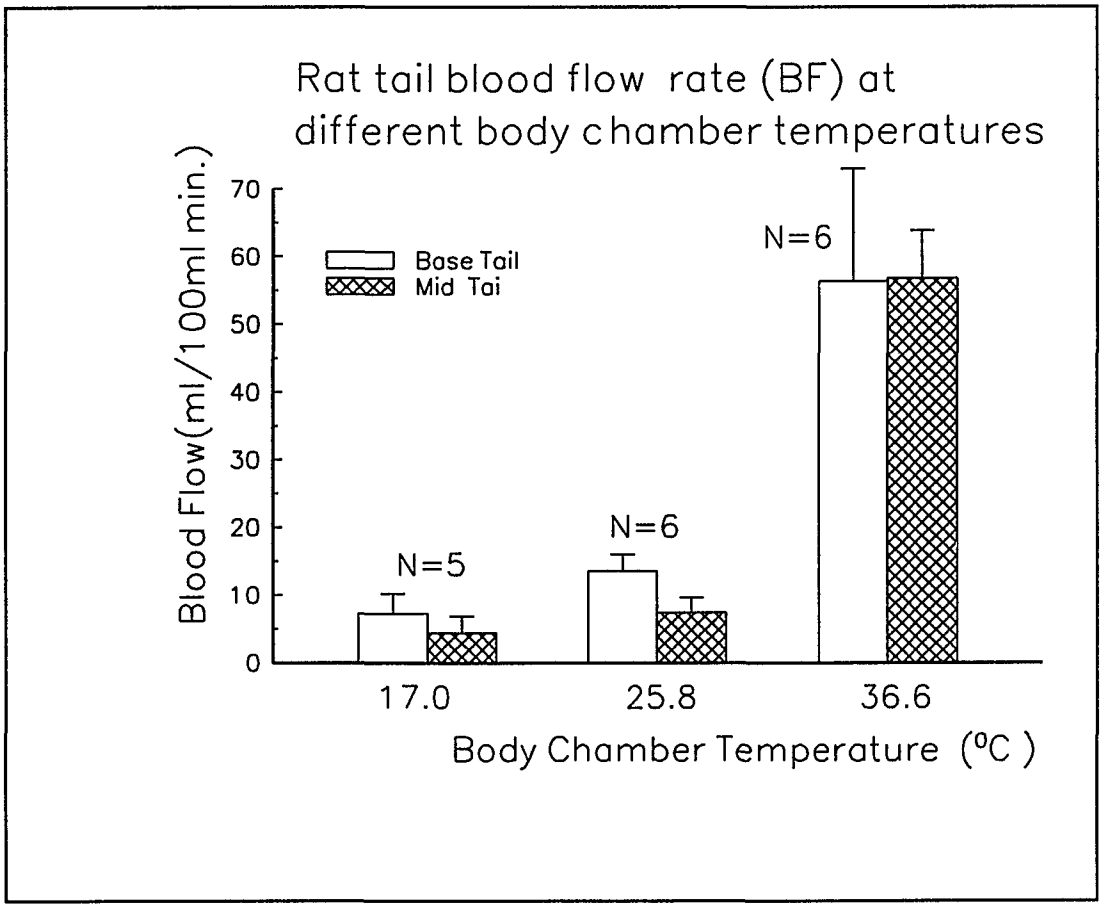

16.a Base and mid tail blood flow rate(BF) at different torso chamber temperatures for conscious rats. Tail enclosure temperature was 25.5 ^{0}C. Error bars are ± 1 STD.

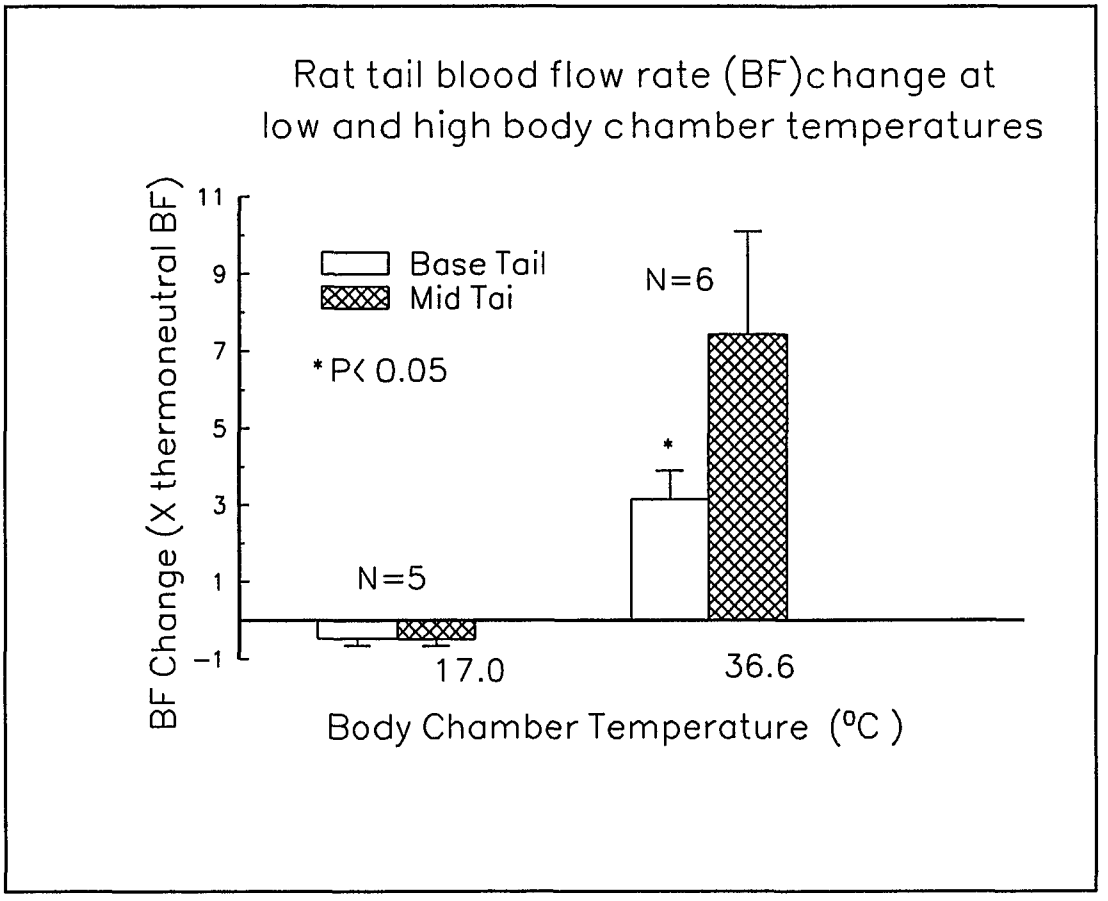

16.b Base and mid tail blood flow rate(BF) change from thermoneutral (25.8 ^{0} C) BF to high and low torso chamber temperatures for conscious rats. Tail enclosure temperature was 25.5 ^{0}C. Error bars are $\pm$1 STD. * indicates statistical significance of the 0.05 level.

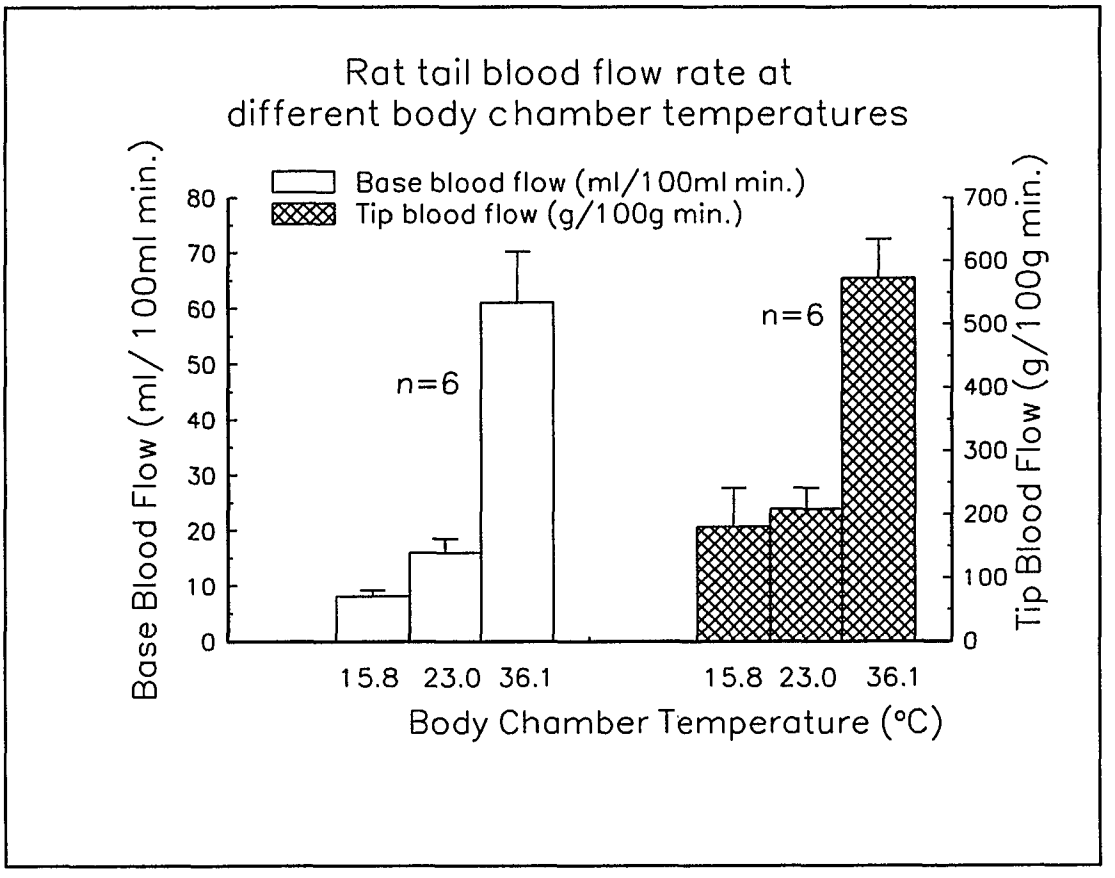

17. Base and tip blood flow rates (BF) at different torso chamber temperatures for unconscious rats. Tail enclosure temperature was 25 ^{0}C. Error bars are 1 STD. Tip blood flow was measured by venous occlusion plethysmography using an electronic balance to measure weight change per unit time following occlusion. Note factor of 10 difference between base and tip blood flow scales.

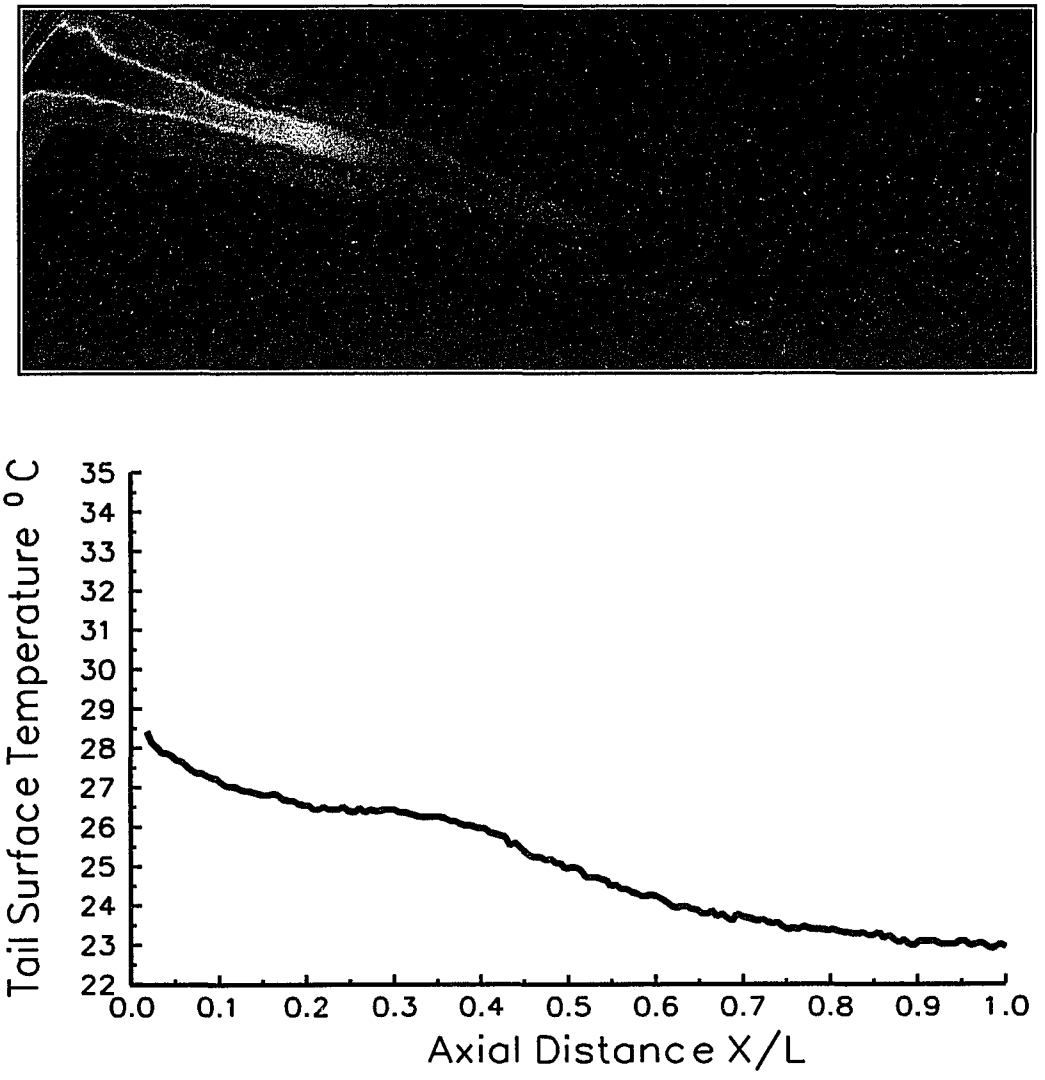

18. Infra-red thermal image and axial temperature profile of rat tail surface for an unconscious rat. Torso chamber temperature was at 25 ^{0}C and tail enclosure temperature was at 22.5 ^{0}C.

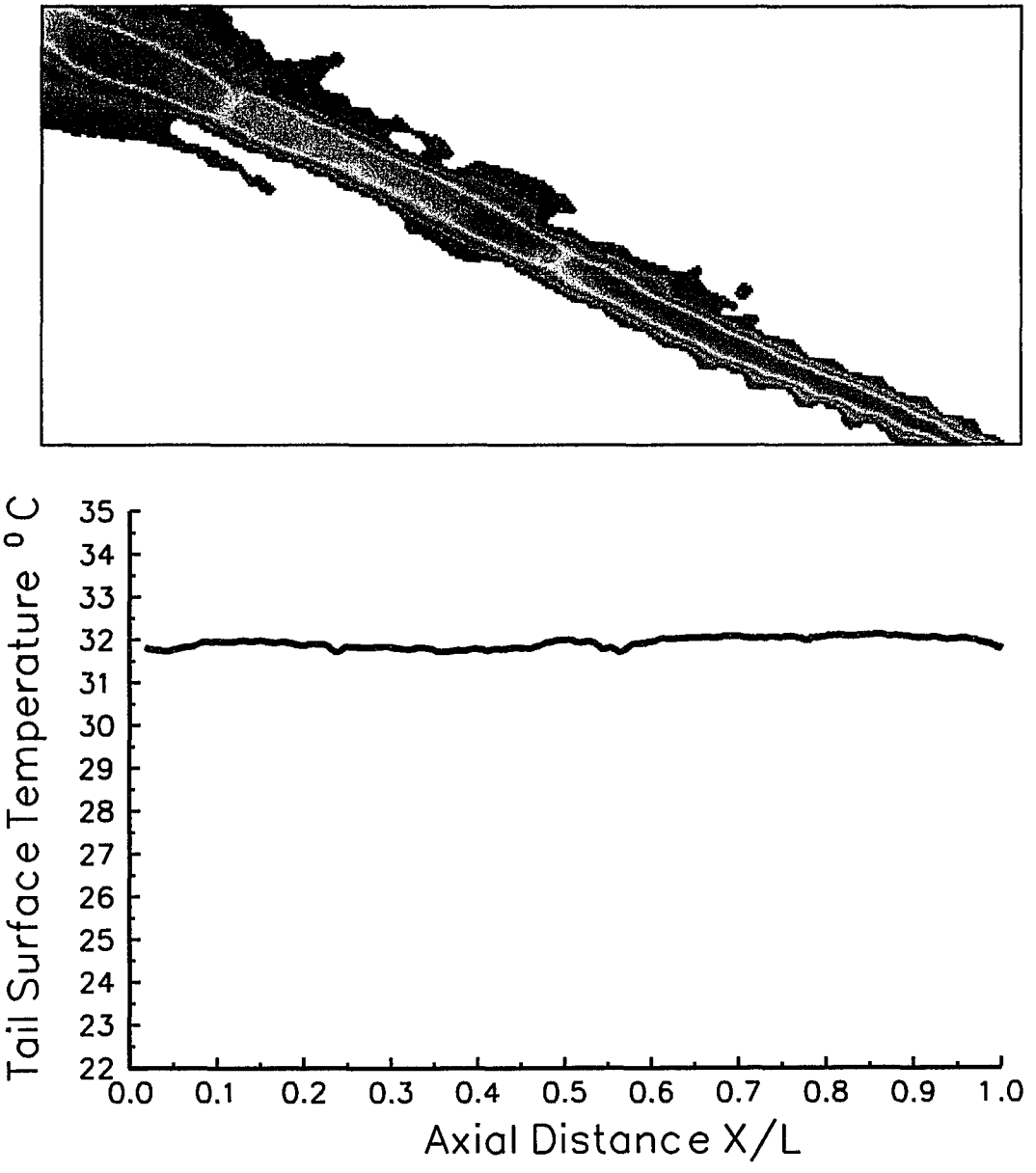

19. Infra-red thermal image and axial temperature profile of rat tail surface for an unconscious rat. Torso chamber temperature was at 36 ^{0}C and tail chamber temperature was at 22.5 ^{0}C.

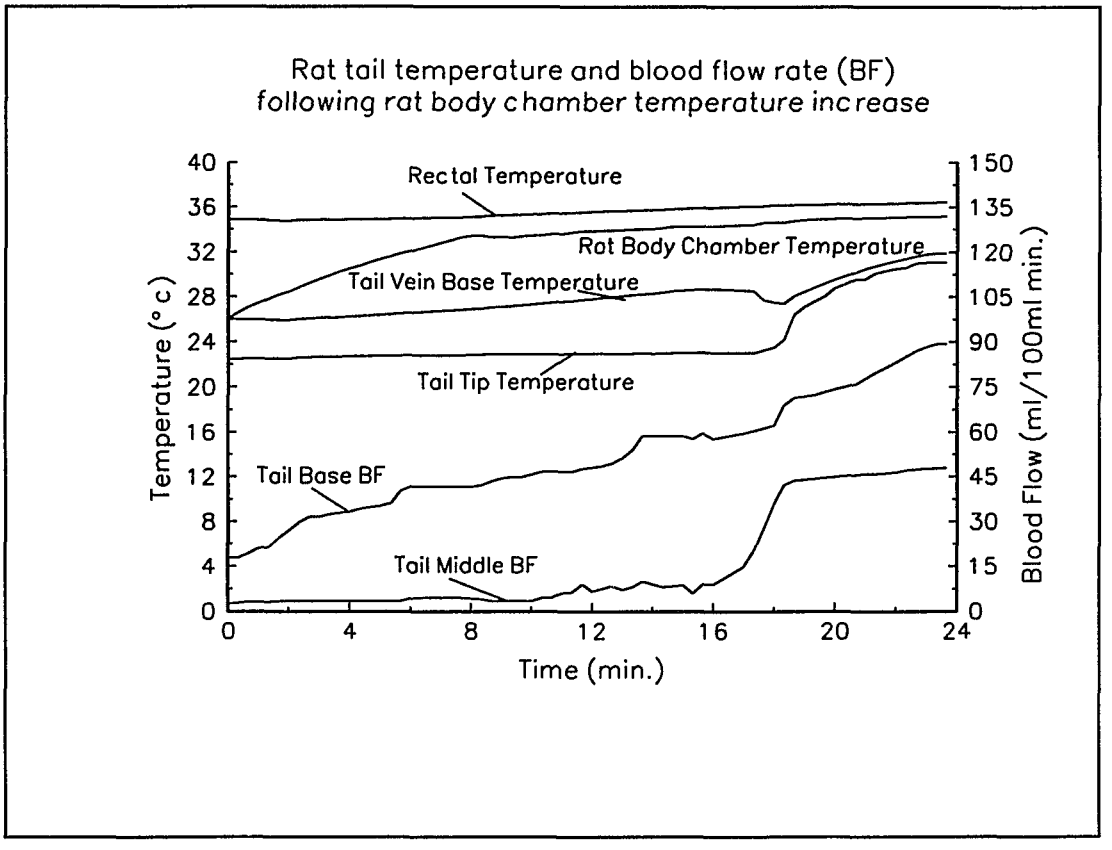

20. Transient base and mid tail BF, and tail surface temperature in an unconscious rat following an increase in the rat Torso chamber temperature at t=0 (min.).

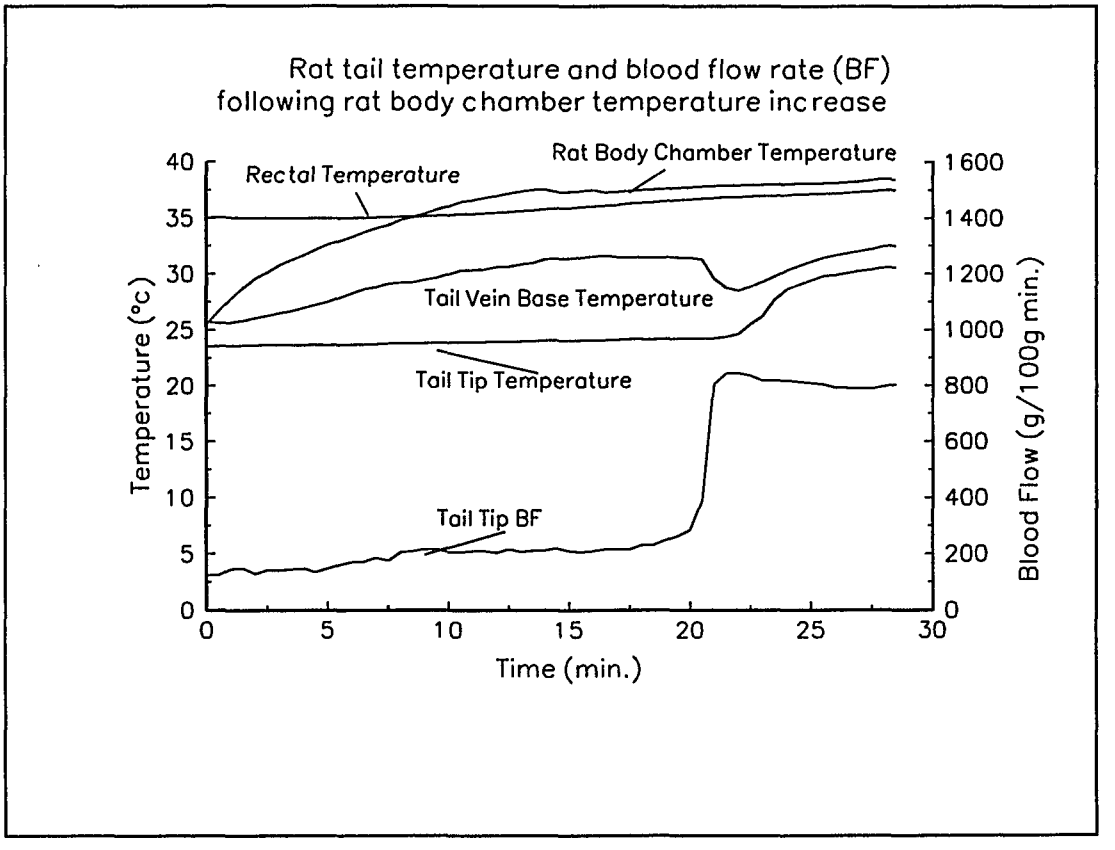

21. Transient tail tip BF and tail surface temperature in an unconscious rat following an increase in the rat body chamber temperature at t=0 (min.).

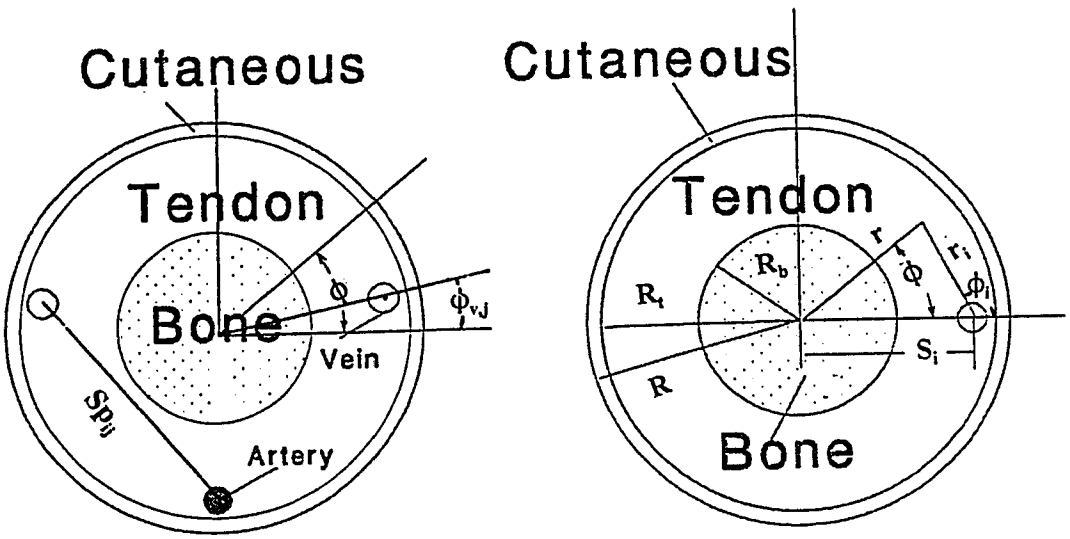

22. Schematic of the cross-sectional planes of (a) the rat tail prototype and (b) single vessel model.

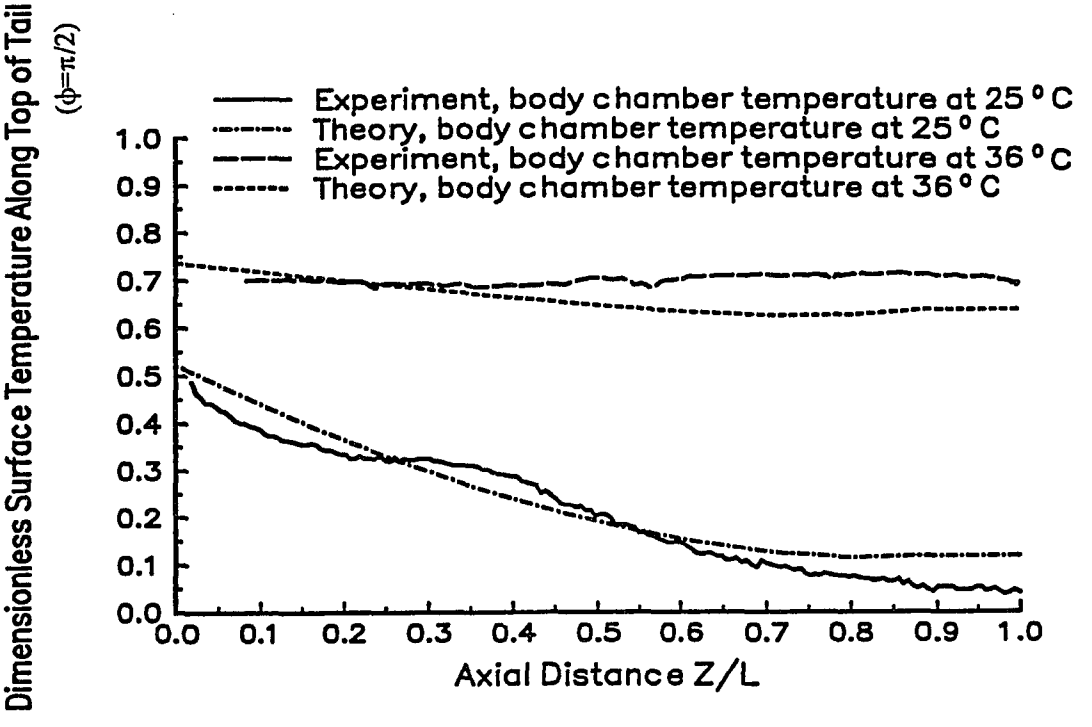

23. Comparison of tail axial temperature profile predicted by present model with experimental data for a rat at torso chamber temperatures of 36 ^{0}C and 25 ^{0}C, and tail enclosure temperature at 22.5 ^{0}C. $k_c=k_t=k_b=k_f$, at Z=0, R=5.5 mm, R_t=4.7mm, R_b=2.5mm, and Bi=0.116.

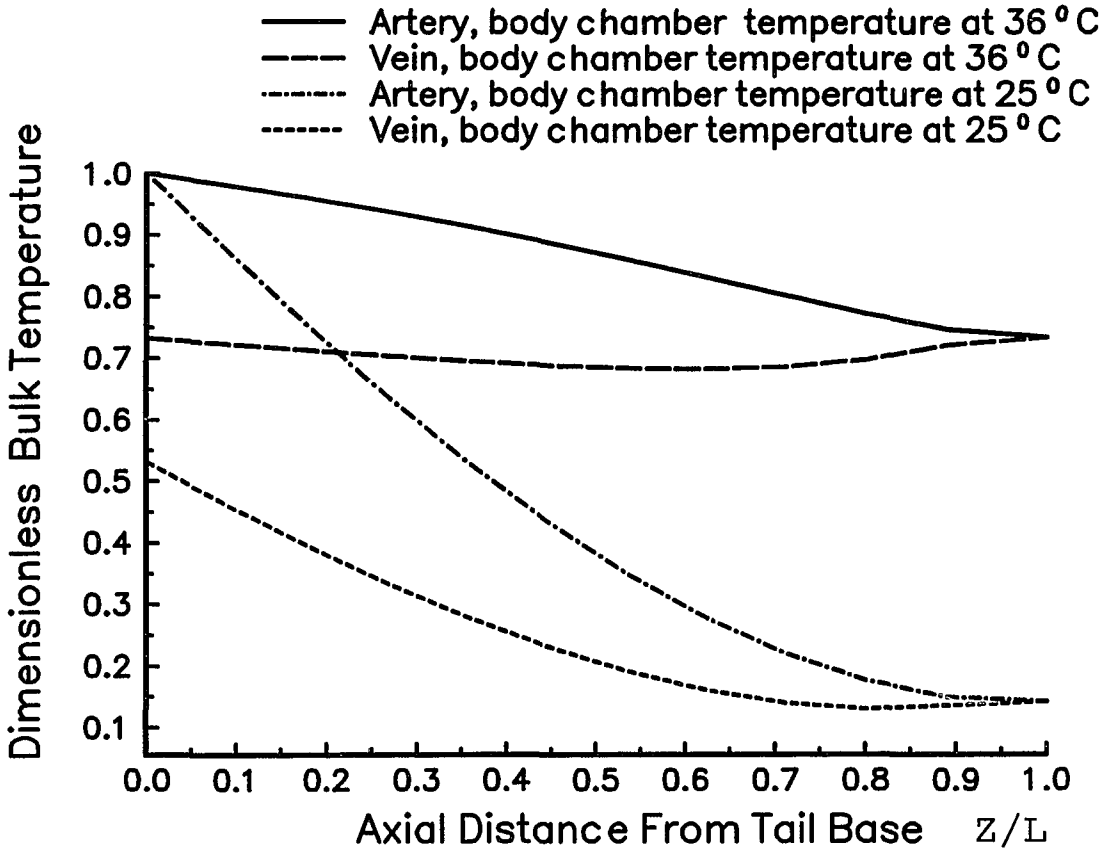

24. Axial bulk temperature variation of artery and vein predicted by present model using the measured blood flow rate for a rat at torso chamber temperatures of 36 ^{0}C and 25 ^{0}C, and tail enclosure temperature at 22.5 ^{0}C. $k_c=k_t=k_b=k_f$, at Z=0, R=5.5 mm, R_t=4.7mm, R_b=2.5mm, and Bi=0.116.

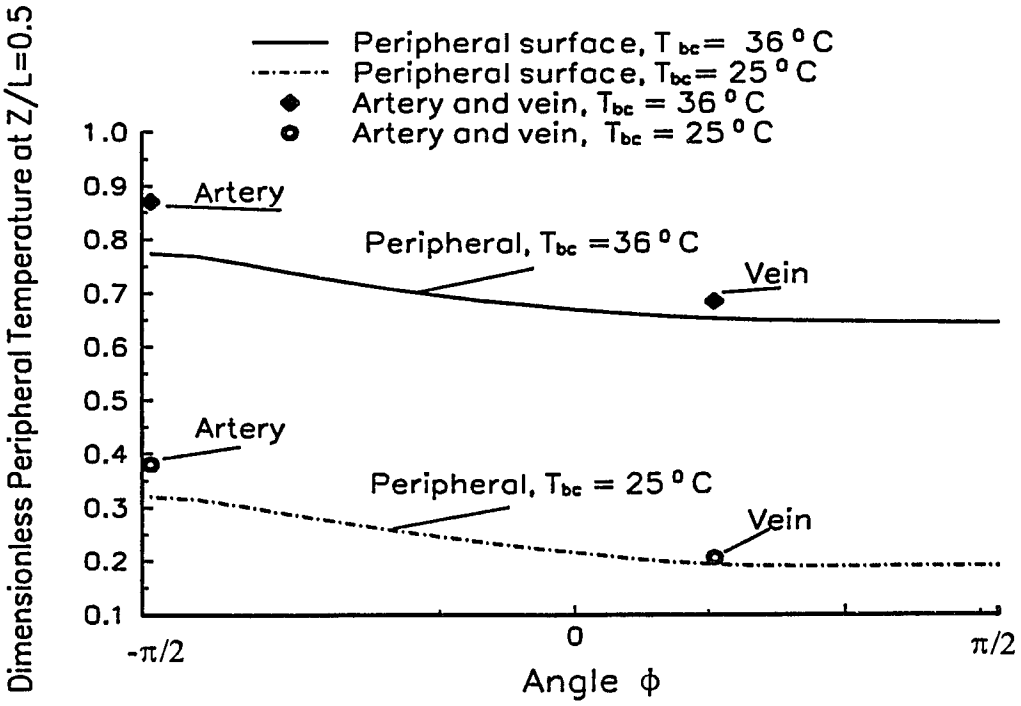

25. Peripheral surface temperature variation and artery, vein bulk temperature at Z/L=0.5, predicted by present model using the measured blood flow rate for a rat at torso chamber temperatures (T_{cent}) of 36 ^{0}C and 25^0 C, and tail enclosure temperature at 22.5 ^{0}C. $k_c=k_t=k_b=k_f$, at Z=0, R=5.5 mm, R_t=4.7mm, R_b=2.5mm, and Bi=0.116. The angle ϕ is shown in Fig. 22 a, for artery $\phi=-\pi/2$, and for vein $\phi=\pi/6$.

BIBLIOGRAPH

1. Rowell, L. B. Cardiovascular adjustments to thermal stress. In: *Handbook of Physiology Section 2: The Cardiovascular System, Vol III, Peripheral Circulation and Organ Blood Flow, Part 2*, edited by J. T. Shepherd and S. R. Abboud. Bethesda,Maryland: Waverly Press, Inc., 1983, p. 967-1023.

2. Wenger, C. B., M. F. Roberts, E. R. Nadel, and J. A. J. Stolwijk. Thermoregulatory control of finger blood flow. *J. Appl. Physiol.* 38(6): 1078-1082, 1975.

3. Nadel, E. R., E. Cafarelli, M. F. Roberts, and C. B. Wenger. Circulatory regulation during exercise in different ambient temperatures. *J. Appl. Physiol.* 46(3): 430-437, 1979.

4. Rowell, L. B. *Human Circulation.* New York: Oxford, 1986,

5. Nagasaka, T., T. Nunomura, and K. Hirata. Partitional measurement of finger circulation between blood vessels located deeply and those located superficially. *Microcirc.* 2: 507-508, 1987.

6. Stoner, H. B., P. Barker, G. S. G. Riding, D. E. Hazlehurst, L. Taylor, and R. W. Marcuson. Relationships between skin temperature and perfusion in the arm and leg. *Clin. Physiol.* 11: 27-40, 1991.

7. Kenney, W. L. and J. M. Johnson. Control of skin blood flow during exercise. *Med. Sci. Sports Exerc.* 24: 303-312, 1992.

8. Clark, E. R. Arterio-venous anastomoses. *Physiol. Rev.* 18: 229-247, 1938.

9. Gemmell, R. T. and J. R. S. Hales. Cutaneous arteriovenous anastomoses present in the tail but absent from the ear of the rat. *J. Anat.* 124(2): 355-358, 1977.

10. Bazett, H. C., B. Mcglone. Temperature gradients in the tissue in man. *Am. J. Physiol.* 82: 415-451, 1927.

11. Bazett, H. C., L. Love, M. Newton, L. Eisenberg, R. Day, and R. Forster. Temperature changes in blood flowing in the arteries and veins in man. *J. Appl. Physiol.* 1: 3-19, 1948.

12. Bazett, H. C., E.S. Mendelson, L. Love, B. Libet. Precooling of blood in the arteries effective heat capacity and evaporative cooling as factors modifying cooling of the extremities. *J. Appl. Physiol.* 1: 169-183, 1948.

13. Raman, E. R., and V. J. Vanhuyse. Analytical model for the temperature dependence of the circulation pattern in upper extremities. *Rad. Environ. Biophys.* 12: 257-269., 1975.

14. Raman, E. R., V. J. Vanhuyse, and M. F. Roberts. Mathematical circulation model for the blood-flow-heat-loss relationship in the rat tail. *Phys. Med. Biol.* 7: 859-875, 1987.

15. Raman, E. R., M. F. Roberts, and V. J. Vanhuyse. Body temperature control of rat tail blood flow. *Am. J. Physiol.* 245: R426-R432, 1983.

16. Raman, E. R., and V. J. Vanhuyse. Temperature dependence of the circulation pattern in the upper extremities. *J. Physiol. (London)* 249: 197-210., 1975.

17. Scholander, P. F., and Krog J. Countercurrent heat exchange and vascular bundles in sloths. *J. Appl. Physiol.* 10(3): 405-411, 1957.

18. Mitchell, J. W. and G. E. Myers. An analytical model of the counter-current heat exchange phenomena. *Biophys. J.* 8: 897-911, 1968.

19. Keller, K. H. and L. Seiler. An analysis of peripheral heat transfer in man. *J. Apple. Physiol.* 30: 779-786, 1971.

20. Wissler, E. H. A mathematical model of the human thermal system. *Bull. of Math. Biophys.* 26: 147-166, 1964.

21. Arkin, H. and A. Schitzer. A model of thermoregulation in the human body . *ASME Winter ann Meeting.* 84-WA/HT-66, 1984.

22. Zhu, M., S. Weinbaum, and L. M. Jiji. Heat exchange between unequal countercurrent vessels asymmetrically embedded in a cylinder with surface convection. *Int. J. Heat Mass Trans.* 33: 2275-2284, 1990.

23. Zhu, M., S. Weinbaum, and D. E. Lemons. A three-dimensional variable geometry countercurrent model for whole limb heat transfer. *ASME J. Biomech. Eng.* 114: 366-376, 1992.

24. Gry, Henry. Anatomy of the human body. C. M. Goss, ed. Philadelphia, *Lea and Febiger*, 1959.

25. Thorington, R. W. The biology of rodent tails. A study of form and function. *For Wainwright,AK,Arctic Aeromed. Lab.* 823: AAL-TR-65-8, 1966.

26. Hellström, B. Heat vasodilation of the rat tail. *CA.. J. Physiol. Pharmacol.* 53:202-206. 1975.

27. Rand, R. P., A.C. Burton, and T. Ing. The Tail of the rat, in temperature regulation and

acclimation. *Can. J. Physiol. Phamacol.* 43: 257-267, 1965.

28. O'Leary, D. S., J. M. Johnson, and W. F. Taylor. Mode of neural control mediating rat tail vasodilation during heating. *J. Appl. Physiol.* 59(5): 1533-1538, 1985.

29. Young, A. A. and N. J. Dawson. Evidence for on-off control of heat dissipation from the tail of the rat. *Canadian J. Phys. Pharm.* 60: 392-398, 1982.

30. Chato, J.C. Heat transfer to blood vessels, *ASME J. Biomech. Engng* 102, 110-118, 1980.

31. Wissler, E.H. An analytical solution for countercurrent heat transfer between parallel vessels with a linear axial temperature gradient, *ASME J. Biomech. Engng* 110, 254-256,1988.

32. Bau, H.H. and S.S. Sadhal, Heat losses from a fluid flowing in a buried pipe. *Int. J. Heat Mass Transfer* 25, 1621-1629, 1982.

33. Difelice, R.F. Jr. and H.H Bau, Conductive heat transfer between eccentric cylinders with boundary conditions of the third kind, *ASME J. Heat Transfer* 105, 678-680, 1983.

34. Baish, J.W., P.S. Ayyaswamy and K.R. Foster, Small-scale temperature fluctuations in perfused tissue during local hyperthermia, *ASME J. Biomech. Engng* 108, 246-250, 1986.

35. Zhu, M., S. Weinbaum, L. M. Jiji and D.E. Lemons, On the generalization of the Weinbaum-Jiji bioheat equation to microvessels of unequal size: the relation between the near field and local average tissue temperatures, *ASME J. Biomech. Engng* 110, 74-81, 1988.

36. Song, W. J., S. Weinbaum, L. M. Jiji and D. E. Lemons, A combined macro and microvascular model for whole limb heat transfer. *ASME J. of Biomech Engng* 110, 259-268, 1987.

37. Zhu, M. Generalization of the Weinbaum-Jiji bioheat equation and studies of whole limb heat transfer. *Ph.D. Dissertation*, The City University of New York, New York, 1990.

38. Chapman, J. A. Heat transfer. *Macmillan Publishing Company*, 4th Ed: pp 315-322, New York, 1984.

39. Hales, J. R. S., C. Jessen, A. A. Fawcett, and R. B. King. Skin AVA and capillary dilation and constriction induced by local skin heating. *Pflugers Arch.* 404: 203-207, 1985.

40. Kamiya, A.,R. Bukhari and T. Togawa. Adaptive regulation of wall shear stress optimizing vascular tree function. *Bulletin of Mathematical Biology.* 46: No.1 127-137,

1984.

41. Weinbaum, S. and L. M. Jiji. Effect of microvascular blood flow on surface tissue heat transfer. Part I: Anatomical background and model conceptualization. *ASME J. Biomech. Eng.* 106: 321-330, 1984.